SANDIA REPORT
SAND2010-5540
Unlimited Release
Printed August 2010

Polyamide Desalination Membrane Characterization and Surface Modification to Enhance Fouling Resistance

Elizabeth M. Van Wagner, Benny D. Freeman, Mukul M. Sharma, Michael A. Hickner, and Susan J. Altman

Prepared by
Sandia National Laboratories
Albuquerque, New Mexico 87185 and Livermore, California 94550

Sandia National Laboratories is a multi-program laboratory managed and operated by Sandia Corporation, a wholly owned subsidiary of Lockheed Martin Corporation, for the U.S. Department of Energy's National Nuclear Security Administration under contract DE-AC04-94AL85000.

Approved for public release; further dissemination unlimited.

Sandia National Laboratories

Issued by Sandia National Laboratories, operated for the United States Department of Energy by Sandia Corporation.

NOTICE: This report was prepared as an account of work sponsored by an agency of the United States Government. Neither the United States Government, nor any agency thereof, nor any of their employees, nor any of their contractors, subcontractors, or their employees, make any warranty, express or implied, or assume any legal liability or responsibility for the accuracy, completeness, or usefulness of any information, apparatus, product, or process disclosed, or represent that its use would not infringe privately owned rights. Reference herein to any specific commercial product, process, or service by trade name, trademark, manufacturer, or otherwise, does not necessarily constitute or imply its endorsement, recommendation, or favoring by the United States Government, any agency thereof, or any of their contractors or subcontractors. The views and opinions expressed herein do not necessarily state or reflect those of the United States Government, any agency thereof, or any of their contractors.

Printed in the United States of America. This report has been reproduced directly from the best available copy.

Available to DOE and DOE contractors from
U.S. Department of Energy
Office of Scientific and Technical Information
P.O. Box 62
Oak Ridge, TN 37831

Telephone: (865)576–8401
Facsimile: (865)576–5728
E–Mail: reports@adonis.osti.gov
Online ordering: http://www.doe.gov/bridge

Available to the public from
U.S. Department of Commerce
National Technical Information Service
5285 Port Royal Rd
Springfield, VA 22161

Telephone: (800)553–6847
Facsimile: (703)605–6900
E–Mail: orders@ntis.fedworld.gov
Online order: http://www.ntis.gov/ordering.htm

SAND2010-5540
Unlimited Release
Printed August 2010

Polyamide Desalination Membrane Characterization and Surface Modification to Enhance Fouling Resistance

Elizabeth M. Van Wagner[1], Benny D. Freeman[1], Mukul M. Sharma[2], Michael A. Hickner[3], and Susan J. Altman[4]

[1]Department of Chemical Engineering
Center for Energy and Environmental Resources
The Univeristy of Texas at Austin
Austin, TX 78758

[2]Department of Petroleum & Geosystems Engineering
The University of Texas at Austin
Austin, TX 78712

[3]Department of Materials Sciecne and Engineering
The Pennsylvania State University
University Park, PA 16802

[4]Geochemistry Department
Sandia National Laboratories
P.O. Box 5800
Albuquerque, NM 87185–0735

Abstract

The market for polyamide desalination membranes is expected to continue to grow during the coming decades. Purification of alternative water sources will also be necessary to meet growing water demands. Purification of produced water, a byproduct of oil and gas production, is of interest due to its dual potential to provide water for beneficial use as well as to reduce wastewater disposal costs. However, current polyamide membranes are prone to fouling, which decreases water flux and shortens membrane lifetime. This research explored surface modification using poly(ethylene glycol) diglycidyl ether (PEGDE) to improve the fouling resistance of commercial polyamide membranes.

Characterization of commercial polyamide membrane performance was a necessary first step before undertaking surface modification studies. Membrane performance was found to be sensitive to crossflow testing conditions. Concentration polarization and feed pH strongly influenced NaCl rejection, and the use of continuous feed filtration led to higher water flux and lower NaCl rejection than was observed for similar tests performed using unfiltered feed.

Two commercial polyamide membranes, including one reverse osmosis and one nanofiltration membrane, were modified by grafting PEGDE to their surfaces. Two different PEG molecular weights (200 and 1000) and treatment concentrations (1% (w/w) and 15% (w/w)) were studied. Water flux decreased and NaCl rejection increased with PEGDE graft density ($\mu g/cm^2$), although the largest changes were observed for low PEGDE graft densities. Surface properties including hydrophilicity, roughness and charge were minimally affected by surface modification.

The fouling resistance of modified and unmodified membranes was compared in crossflow filtration studies using model foulant solutions consisting of either a charged surfactant or an oil in water emulsion containing *n*-decane and a charged surfactant. Several PEGDE-modified membranes demonstrated improved fouling resistance compared to unmodified membranes of similar initial water flux, possibly due to steric hindrance imparted by the PEG chains. Fouling resistance was higher for membranes modified with higher molecular weight PEG. Fouling was more extensive for feeds containing the cationic surfactant, potentially due to electrostatic attraction with the negatively charged membranes. However, fouling was also observed in the presence of the anionic surfactant, indicating hydrodynamic forces are also responsible for fouling.

ACKNOWLEDGEMENTS

This work was originally published as a Ph. D. Thesis at the Department of Chemical Engineering at the University of Texas at Austin by Elizabeth M. Van Wagner[1]. The research that Elizabeth conducted was partially funded as a graduate research project through Sandia National Laboratories Laboratory Directed Research and Development (LDRD) program. Michael A. Hickner served as the Sandia mentor for Elizabeth for the first portion of the LDRD and Susan Altman for the latter portion. Professor Benny was Elizabeth's advisor at The University of Texas. Paula Staniulis is thanked from re-formatting this document into the SAND report format.

The acknowledgements in the original thesis were as follows:

I would like to thank my advisor, Professor Benny Freeman, for his support and guidance, as well as for the many experiences and opportunities I have been fortunate enough to have during my graduate studies. I would like to thank my co-advisor, Professor Mukul Sharma, for providing a unique perspective on my research. I also extend my gratitude to Dr. Bill Mickols for sharing his vast membrane expertise.

The Freeman group members deserve special recognition for countless fond memories of graduate school. Dr. Haiqing Lin, Dr. Scott Kelman, Dr. Scott Matteucci, Dr. Victor Kusuma, Dr. Ho Bum Park, Dr. Alyson Sagle, Dr. Bryan McCloskey, Dr. Yuan-Hsuan Wu, Hao Ju, Richard Li and Brandon Rowe all shared their knowledge and helped create a great camaraderie within the group. Newer group members have continued the tradition.

Finally, I would like to thank my family and friends. Old friends and new friends made in graduate school have made this experience more enjoyable. I am grateful to have met my friend and fiancé, Jason Dees, during graduate school, and I look forward to our future together. My family stands by me in everything I do, always ready to help in any way possible. I am very thankful for their constant love and support.

[1] Copyright of the thesis belongs to Elizabeth Marie Van Wagner. This report is published with Dr. Van Wagner's permission.

This page is intentionally left blank

CONTENTS

ABSTRACT 3

ACKNOWLEDGEMENTS 5

TABLE OF CONTENTS 7

LIST OF TABLES 11

List of Figures 13

1 INTRODUCTION 21
- 1.1 Water Shortage Issues Facing the World 21
- 1.2 Desalination 21
- 1.3 Produced Water 21
- 1.4 Types of Water Treatment Membranes 22
- 1.5 Membrane Fouling 23
- 1.6 Goals and Organization of the Dissertation 24
- 1.7 References 25

2 BACKGROUND AND THEORY 27
- 2.1 Osmosis and Reverse Osmosis 27
- 2.2 Membrane Transport Model 28
- 2.3 Concentration Polarization 34
- 2.4 Evolution of Reverse Osmosis Membranes 36
- 2.5 Membrane Performance as a Function of Test Conditions 38
- 2.6 Salt Rejection Mechanism 39
- 2.7 Surface Properties and Membrane Fouling 40
- 2.8 Fouling Resistance of Poly(ethylene glycol) 45
- 2.9 Surface Modification in the Literature 47
- 2.10 References 49

3 EXPERIMENTAL MATERIALS AND METHODS 55
- 3.1 Materials 55

3.1.1 Commercial Membranes 55
3.1.2 Poly(ethylene glycol) Diglycidyl Ether 56
3.1.3 Water 57
3.1.4 Foulants 57
3.2 Methods 59
3.2.1 Membrane Storage, Handling, and Pretreatment 59
3.2.2 Modification Methods 59
3.2.2.1 Dip Coating 59
3.2.2.2 Spin Coating 59
3.2.2.3 Top Surface Treatment 60
3.2.3 Dead End Testing 61
3.2.4 Crossflow Testing 62
3.2.4.1 Crossflow Apparatus 62
3.2.4.2 Cleaning Protocol 63
3.2.4.3 Fouling Test Procedure 63
3.2.4.4 Rejection Measurements 65
3.2.5 Surface Characterization 66
3.2.5.1 ATR-FTIR 66
3.2.5.2 XPS 66
3.2.5.3 Graft Density 66
3.2.5.4 Zeta Potential 68
3.2.5.5 AFM 68
3.2.5.6 Contact Angles 68
3.3 References 69

4 COMMERCIAL REVERSE OSMOSIS MEMBRANE PERFORMANCE CHARACTERIZATION 71
4.1 Abstract 71
4.2 Motivation 71
4.3 Detailed Measurement Protocol 75
4.4 Results and Discussion 77
4.4.1 Concentration Polarization 77
4.4.2 Effect of Feed pH on Membrane Performance 80
4.4.3 Performance at Manufacturer's Specified Conditions 81

4.4.4 Influence of Continuous Feed Filtration on Membrane Performance 86
4.4.5 Permeance/Salt Passage Tradeoff 87
4.5 Conclusions 88
4.6 Acknowledgements 88
4.7 References 89

5 SURFACE CHARACTERIZATION OF A COMMERCIAL REVERSE OSMOSIS MEMBRANE 93
5.1 Abstract 93
5.2 Results and Discussion 93
5.2.1 ATR-FTIR 93
5.2.2 XPS 94
5.2.3 Surface Roughness and Hydrophilicity 96
5.2.4 Surface Charge 96
5.3 Conclusions 102
5.4 References 102

6 SURFACE MODIFICATION USING POLY(ETHYLENE GLYCOL) DIGLYCIDYL ETHER TO ENHANCE MEMBRANE FOULING RESISTANCE 105
6.1 Abstract 105
6.2 Results and Discussion 105
6.2.1 Characterization of PEGDE on the Modified Membrane Surfaces via FTIR and XPS 105
6.2.2 Graft Density of PEGDE on the Modified Membrane Surface 107
6.2.3 Surface Charge, Hydrophilicity, and Roughness 109
6.2.4 Water Flux and NaCl Rejection of Modified Membranes 110
6.2.5 Fouling Resistance and Flux Recovery in Surfactant Fouling Tests 113
6.2.6 Fouling Resistance and Flux Recovery in Emulsion Fouling Tests 119
6.2.7 NaCl and Organic Rejection in Fouling Tests 122
6.3 Conclusions 125
6.4 Acknowledgements 126
6.5 References 126

7 CONCLUSIONS AND RECOMMENDATIONS 129
7.1 Conclusions 129

7.1.1 Reverse Osmosis Membrane Characterization 129
7.1.2 Surface Modification Using Poly(ethylene glycol) Diglycidyl Ether..... 129
7.1.3 Fouling Resistance 130
7.2 Recommendations 130
7.2.1 Surface Modification 130
7.2.2 Membrane Fouling 132
7.3 References 132

APPENDIX: ADDITIONAL SURFACE MODIFICATION METHODS, SURFACE CHARGE MEASUREMENTS, AND FOULING STUDIES 135
A.1 Additional Surface Modification Methods 136
A.1.1 Dip Coating 136
A.1.2 Spin Coating.....138
A.2 Surface Charge 139
A.3 Fouling 141
A.4 References 143

BIBLIOGRAPHY 145

LIST OF TABLES

Table 3.1. Water permeance, salt permeance, and NaCl rejection values specified by Dow Water & Process Solutions for the LE, XLE, and NF90 membranes. 56

Table 4.1. Comparison of reported membrane performance to manufacturer benchmark values for several commercial reverse osmosis membranes. 73

Table 4.2. Summary of experimental conditions for the LE and XLE characterization studies (24-25°C and 150 psig feed pressure (Δp = 10.3 bar) maintained for all experiments). 77

Table 4.3. Comparison of concentration polarization-corrected water permeance and salt permeance values[a] of LE and XLE membranes to manufacturer specifications.....79

Table 4.4. Comparison of measured membrane performance to manufacturer benchmark values (test conditions matching those of manufacturer).....86

Table 5.1. Theoretical and measured polyamide elemental composition (atomic concentration). 95

Table 6.1. XPS measurements of surface atomic concentration (%) of oxygen, nitrogen and carbon measured for an unmodified XLE membrane and XLE membranes modified with MW 1000 PEGDE.....107

Table 6.2. Surface properties (charge, hydrophilicity and roughness) of unmodified and PEGDE-modified membranes.....110

Table 6.3. Initial NaCl rejection and NaCl rejection in the presence of each foulant (measured at t = 24 hrs).[1] 123

Table 6.4. Initial NaCl rejection and final NaCl rejection (i.e., measured after fouling and cleaning, at t = 30 hrs).[1] 125

Table A1. Pure water flux (dead end, Δp = 10.3 bar) of XLE membranes treated with 10% (w/w) MW 200 PEGDE by submersion for different times (1 minute vs. 10 minutes) and at different temperatures (room temperature vs. 40°C). 137

Table A2. XPS measurements of surface atomic concentration (%) of oxygen, nitrogen, carbon, and sulfur for an unmodified XLE membrane and XLE membranes modified with 10% (w/w) MW 200 PEG and PEGDE. 137

Table A3. NaCl rejection measured at t = 1 hr ($R_{initial}$), t = 24 hours (R_{foul}) and t = 30 hours (R_{final}) for fouling in the absence of intentionally added foulant. 143

This page is intentionally left blank

LIST OF FIGURES

Figure 1.1. Sparation characteristics of the four major pressure-driven membrane separations [3]. 23

Figure 2.1. Direction of water flow and pressure difference for an osmotic membrane in (a) osmosis, (b) osmotic equilibrium and (c) reverse osmosis [1, 2]. The solute (i.e., salt) concentration is higher on the left hand side of each membrane in this figure. 27

Figure 2.2. Solvent electrochemical potential gradient and corresponding pressure and solvent activity profiles in a charged membrane according to the solution-diffusion and pore-flow models [2]. 28

Figure 2.3. Schematic of salt boundary layer profile for reverse osmosis membranes. Feed salt concentration at the membrane interface ($c_{so(m)}$) is greater than the bulk feed concentration (c_{so}) due to accumulation of rejected salt in a boundary layer at the membrane surface [7]. 35

Figure 2.4. Chemical structures of metaphenylene diamine, trimesoyl chloride, and resulting interfacially polymerized polyamide membrane, where n characterizes the degree of crosslinking [16]. 37

Figure 2.5. Composite reverse osmosis membrane structure. The reinforcing fabric base (~120 μm) is coated with a thin layer of microporous polysulfone (~40 μm) and the interfacially polymerized selective polyamide layer (~0.1 μm) [16]. 38

Figure 2.6. Influence of (a) feed pressure, (b) feed salt concentration, (c) feed temperature, and (d) feed pH on water flux and NaCl rejection of an FT-30 membrane [14]. 39

Figure 2.7. Contact angle, θ, measured using (a) the sessile drop method with a water droplet in air and (b) the captive bubble method with an oil droplet in water. A smaller contact angle indicates a more hydrophilic surface. 41

Figure 2.8. Structure of electric double layer, including Stern layer and diffuse layer, and potential as a function of distance from the membrane surface [6]. 43

Figure 2.9. Development of the streaming potential at the membrane-solution interface. (a) The electric double layer is at rest until (b) an applied pressure causes liquid flow, ion movement, and the development of a streaming current, I_s. (c) The accumulation of counterions leads to formation of a potential difference, E, and (d) a leak current, I_L. At equilibrium, I_s=I_L and the measured potential difference is the streaming potential [29]. 44

Figure 2.10. Chemical structure of poly(ethylene glycol) (PEG), where n is the number of repeat ethylene oxide units. 46

Figure 2.11. The configuration of PEG molecules grafted to a surface transitions from a mushroom to a brush structure as the attachment site density increases [33]. An attachment site is indicated by "x." 46

Figure 3.1. Chemical structure of poly(ethylene glycol) diglycidyl ether (PEGDE), where n is the number of repeat ethylene oxide units (n ≈ 4, 9, 13 and 22). 57

Figure 3.2. Predicted reaction between a primary amine chain end of the polyamide membrane with an epoxide molecule. Note that since the epoxide chosen for study is difunctional, reaction may occur at both epoxide endgroups, forming loops instead of the brush structure depicted in this figure.....58

Figure 3.3. Chemical structure of (a) dodecyltrimethylammonium bromide (DTAB) and (b) sodium dodecyl sulfate (SDS). 58

Figure 3.4. Top surface treatment method for membrane modification. 61

Figure 3.5. Schematic of dead end test cell. 61

Figure 3.6. Schematic of crossflow filtration system. 63

Figure 3.7. (a) Timeline and (b) typical observed water flux during a crossflow fouling experiment. 65

Figure 3.8. Schematic of the magnetic suspension balance, including zero point and measuring point positions. 67

Figure 3.9. Apparatus used for captive bubble measurements of oil-in-water contact angles. The oil droplet is released under water, below the active surface of the membrane (sample is loaded with active side facing down), and floats up to the membrane surface. 69

Figure 4.1. (a) Pure water flux, water flux in 2000 mg/L NaCl feed, and apparent NaCl rejection for the LE membrane as a function of feed flowrate. (b) Apparent NaCl rejection, concentration polarization modulus (M), and true NaCl rejection for the LE membrane as a function of feed flowrate. Experiment 1 conditions: T = 24 -25°C, Δp = 10.3 bar, feed passed continuously through a carbon and particle filter, feed pH 7.7. Error bars in the figure represent one standard deviation of the experimental results for the three samples tested in this experiment. 78

Figure 4.2. (a) Pure water flux, water flux in 2000 mg/L NaCl feed, and apparent NaCl rejection for the XLE membrane as a function of feed flowrate. (b) Apparent NaCl rejection, concentration polarization modulus (M), and true NaCl rejection for the XLE membrane as a function of feed flowrate. Experiment 2 conditions: T = 24-25°C, Δp = 10.3 bar, feed passed continuously through a carbon and particle filter, feed pH 7.8. Error bars in the figure represent one standard deviation of the experimental results for the three samples tested in this experiment. 78

Figure 4.3. Average water flux and true NaCl rejection as a function of feed pH (T = 24-25°C, Δp = 10.3 bar, flowrate = 4 L/min, feed passed continuously through a carbon and particle filter, feed pH adjusted using 1 M HCl or 5% NaOH). (a) LE membranes (M = 1.09-1.22, experiment 3). (b) XLE membranes (M = 1.16-1.29, experiment 4). Error bars in the figures represent one standard deviation of the experimental results for the three samples tested. Note: numbers 1-8 indicate the order of the measurements, and demonstrate the reversibility of the pH/rejection phenomenon. The lines were drawn to follow trends suggested by the data, and should be used to guide the eye. 81

Figure 4.4. (a) Average water flux, apparent NaCl rejection and true NaCl rejection as a function of time for three LE membranes tested at Dow Water & Process Solutions' specified conditions (T = 24-25°C, Δp = 10.3 bar, flowrate = 4 L/min, unfiltered feed, feed pH 7.9, M = 1.26, experiment 5). Note: uncertainty in water flux ~ 0.5-0.9 LMH, uncertainty in R_{app} ~ 0.2-0.4%, uncertainty in R_{true} ~ 0.1-0.3%. (b) Water flux and (c) Apparent and true NaCl rejection as a function of time for each of the three LE membranes. 83

Figure 4.5. Average water flux, apparent NaCl rejection and true NaCl rejection as a function of time for XLE membranes tested at Dow Water & Process Solutions' specified conditions (T = 24-25°C, Δp = 10.3 bar, flowrate = 4 L/min, unfiltered feed, feed pH 7.8, M = 1.31, experiment 6). Note: uncertainty in water flux ~ 2.4-3.8 LMH, uncertainty in R_{app} ~ 0.07-0.2%, uncertainty in R_{true} ~ 0.04-0.1%. 84

Figure 4.6. Comparison of average water flux and true NaCl rejection (T = 24-25°C, Δp = 10.3 bar, flowrate = 4 L/min) as a function of time. (a) LE membranes tested in unfiltered feed (experiment 5, feed pH 7.9, M = 1.26, unfilled symbols) and continuously filtered feed (experiment 7, feed pH 7.8, M = 1.14, filled symbols). Note: experiment 5 uncertainty given in Figure 4.4(a); experiment 7 uncertainty in water flux ~ 0.6-1.0 LMH, uncertainty in R_{true} ~ 0.07-0.1%. (b) XLE membranes tested in unfiltered feed (experiment 6, feed pH 7.8, M = 1.31, unfilled symbols) and continuously filtered feed (experiment 8, feed pH 7.8, M = 1.21, filled symbols). Note: experiment 6 uncertainty given in Figure 4.5; experiment 8 uncertainty in water flux ~ 2.2-2.5 LMH, uncertainty in R_{true} ~ 0.08-0.1%. 87

Figure 4.7. Permeance/selectivity tradeoff plot for LE and XLE membranes (experiments 1-8). Water and salt permeance values have been corrected for the effects of concentration polarization (osmotic pressure at the membrane surface, $\pi_{so(m)}$, used in place of bulk feed osmotic pressure, π_{so}). 88

Figure 5.1. ATR-FTIR spectrum of a Dow Water & Process Solutions XLE composite polyamide membrane. (a) mid-infrared region (500-4000 cm^{-1}) and (b) view of 1000-1800 cm^{-1} region, where peaks characteristic of composite aromatic polyamide membranes are labeled 1-4. 94

Figure 5.2. ATR-FTIR spectrum of MW 200 poly(ethylene glycol) diglycidyl ether.....95

Figure 5.3. Repeat chemical structures for (a) uncrosslinked ($C_{12}O_4N_2H_{10}$) and (b) crosslinked ($C_{18}O_3N_3H_{12}$) aromatic polyamides. 96

Figure 5.4. Image of an *n*-decane droplet on an inverted XLE membrane submerged in water, using the captive bubble method for contact angle measurement. 97

Figure 5.5. Zeta potential versus feed pH for an XLE membrane (0.01 M NaCl background electrolyte). 98

Figure 5.6. Apparent NaCl rejection as a function of feed pH for an XLE membrane. Overall rejection was determined from measuring solution conductivity, Na^+ rejection was determined using ICP-MS, and Cl^- rejection was determined using ion chromatography.....99

Figure 5.7. Surface concentration of charged sites as a function of feed pH, calculated from the model (Equation 5.13), with $[RNH_2]_{tot} = 0.650 \times 10^{-7}$ mol/m^2 and $[RCOOH]_{tot} = 1.03 \times 10^{-7}$ mol/m^2, and from Equation 5.2 (i.e., using experimental zeta potential data). 102

Figure 5.8. Surface concentration of charged sites as a function of feed pH, calculated from the model (Equation 5.13), with pKa = 4.6 for the amines and carboxylic acids, $[RNH_2]_{tot} = 0.475 \times 10^{-7}$ mol/m^2 and $[RCOOH]_{tot} = 1.03 \times 10^{-7}$ mol/m^2, and from Equation 5.2 (i.e., using experimental zeta potential data).....103

Figure 6.1. ATR-FTIR spectra in the range 1000 – 1200 cm^{-1} for (a) the unmodified XLE membrane (1) and XLE membranes modified with 1% (w/w) MW 200 PEGDE (2), 1% (w/w) MW 1000 PEGDE (3), 15% (w/w) MW 200 PEGDE (4), and 15% (w/w) MW 1000 PEGDE (5), and (b) the unmodified NF90 membrane (1) and NF90 membranes modified with 1% (w/w) MW 1000 PEGDE (2) and 15% (w/w) MW 1000 PEGDE (3).....107

Figure 6.2. Graft density for XLE membranes modified with 1% (w/w) and 15% (w/w) MW 200 and MW 1000 PEGDE, and NF90 membranes modified with 1% (w/w) and 15% (w/w) MW 1000 PEGDE. The unmodified XLE and NF90 membranes (i.e., 0% (w/w) PEGDE concentration in water) are shown on this figure at zero graft density. Error bars associated with graft density indicate the standard deviation of the results for at least three membrane samples. 108

Figure 6.3. (a) Water flux and (b) true NaCl rejection in 2000 mg/L NaCl feed, for unmodified XLE and NF90 membranes (i.e., 0% (w/w) PEGDE concentration in water), XLE membranes modified with 1% (w/w) and 15% (w/w) MW 200 and MW 1000 PEGDE, and NF90 membranes modified with 1% (w/w) and 15% (w/w) MW 1000 PEGDE. Error bars in the figures indicate the standard deviation of the performance of at least six membrane samples. 112

Figure 6.4. Water flux in a 2000 mg/L NaCl feed versus graft density measured using the magnetic suspension balance, for XLE membranes modified with 1% (w/w) and 15% (w/w) MW 200 and MW 1000 PEGDE, and NF90 membranes modified with 1% (w/w) and 15% (w/w) MW 1000 PEGDE. The unmodified XLE and NF90 membranes (i.e., 0% (w/w) PEGDE concentration in water) are shown on this figure at zero graft density. Error bars associated with $J_{w(NaCl)i}$ are defined in Figure 6.3; error bars associated with graft density are defined in Figure 6.2. 114

Figure 6.5. Typical fouling behavior observed in all fouling tests, using SDS fouling results obtained for unmodified LE and XLE membranes and an XLE membrane modified with 1% (w/w) MW 1000 PEGDE. (a) Water flux and (b) normalized water flux, as a function of time. 115

Figure 6.6. Typical fouling behavior observed in all fouling tests, using SDS fouling results obtained for unmodified LE and XLE membranes and an XLE membrane modified with 1% (w/w) MW 1000 PEGDE. (a) Water flux and (b) normalized water flux, as a function of volumetric throughput. 116

Figure 6.7. (a) Fraction of flux retained after fouling with 150 mg/L SDS and (b) fraction of flux regained after fouling and cleaning, as a function of initial water flux. Definition of symbols: ○ LE, ◿ LE (Δp = 9.0 bar), ▷ LE (Δp = 8.6 bar), ◺ XLE, ▽ NF90, ▲ 1% (w/w) MW 200 XLE, ▼ 15% (w/w) MW 200 XLE, ● 1% (w/w) MW 1000 XLE, ■ 15% (w/w) MW 1000 XLE, ◣ 1% (w/w) MW 1000 NF90, and ◢ 15% (w/w) MW 1000 NF90. Lines have been drawn through the modified and unmodified membrane data to guide the eye. 117

Figure 6.8. Ratio of foulant layer permeance to membrane permeance as a function of initial water flux during fouling with 150 mg/L SDS. Definition of symbols: ○ LE, ◿ LE (Δp = 9.0 bar), ▷ LE (Δp = 8.6 bar), ◺ XLE, ▽ NF90, ▲ 1% (w/w) MW 200 XLE, ▼ 15% (w/w) MW 200 XLE, ● 1% (w/w) MW 1000 XLE, ■ 15% (w/w) MW 1000 XLE, ◣ 1% (w/w) MW 1000 NF90, and ◢ 15% (w/w) MW 1000 NF90. Lines have been drawn through the modified and unmodified membrane data to guide the eye.....119

Figure 6.9. (a) Fraction of flux retained after fouling with 150 mg/L DTAB and (b) fraction of flux regained after fouling and cleaning, as a function of initial water flux. Definition of symbols: ○ LE, ◿ LE (Δp = 9.0 bar), ▷ LE (Δp = 8.6 bar), ◺ XLE, ▽ NF90, ▲ 1% (w/w) MW 200 XLE, ▼ 15% (w/w) MW 200 X LE, ● 1% (w/w) MW 1000 X LE, ■ 15% (w/w) MW 1000 XLE, ◣ 1% (w/w) MW 1000 NF90, and ◢ 15% (w/w) MW 1000 NF90. Lines have been drawn through the modified and unmodified membrane data to guide the eye. 119

Figure 6.10. (a) Fraction of flux retained after fouling with a 150 mg/L 9:1 *n*-decane:SDS emulsion and (b) fraction of flux regained after fouling and cleaning, as a function of initial water flux. Definition of symbols: ○ LE, ▷ LE (Δp = 8.6 bar), ◺ XLE, ▽ NF90, ▲ 1% (w/w) MW 200 XLE, ▼ 15% (w/w) MW 200 X LE, ● 1% (w/w) MW 1000 X LE, ■ 15% (w/w) MW 1000 X LE, ◣ 1% (w/w) MW 1000 NF90, and ◢ 15% (w/w) MW 1000 NF90. Lines have been drawn through the modified and unmodified membrane data to guide the eye.....120

Figure 6.11. (a) Fraction of flux retained after fouling with a 150 mg/L 9:1 *n*-decane:DTAB emulsion and (b) fraction of flux regained after fouling and cleaning, as a function of initial water flux. Definition of symbols: ○ LE, ▷ LE (Δp = 8.6 bar), □ LE (Δp = 5.5 bar), ◺ XLE, ▽ NF90, ▲ 1% (w/w) MW 200 X LE, ▼ 15% (w/w) MW 200 X LE, ● 1% (w/w) MW 1000 XLE, ■ 15% (w/w) MW 1000 X LE, ◣ 1% (w/w) MW 1000 NF90, ◢ 15% (w/w) MW 1000 NF90, and ◆ 15% (w/w) MW 1000 XLE (Δp = 5.5 bar). Lines have been drawn through the modified and unmodified membrane data (excluding data obtained for Δp = 5.5 bar) to guide the eye. 121

Figure 7.1. Epoxidation of a vinyl group using *m*-chloroperoxybenzoic acid (MCPBA). 130

Figure 7.2. Chemical structures of potential acrylates for epoxidation and use in surface modification of polyamide membranes: poly(ethylene glycol) acrylate (PEGA), 2,2,2 – trifluoroethyl α – fluoroacrylate (TFEFA), 2,2,3,3,3 – pentafluoropropyl α – fluoroacrylate (PFPFA), 2,2,3,3 – tetrafluoropropyl α – fluoroacrylate (TFPFA), and poly(ethylene glycol) diacrylate (PEGDA). 131

Figure A1. Pure water flux (dead end, Δp = 10.3 bar) as a function of PEGDE aqueous treatment solution concentration for XLE membranes dip coated with MW 200 and 1000 PEGDE (40°C, 10 minutes). 136

Figure A2. Chemical structure of (2,2,3,3,4,4,5,5,6,6,7,7,8,8,9,9,9 – heptadecafluorononyl) oxirane. 138

Figure A3. Zeta potential of unmodified LE, XLE and NF90 membranes and PEGDE – modified XLE and NF90 membranes in 10 mM NaCl. 139

Figure A4. Zeta potential of unmodified LE, XLE and NF90 membranes and PEGDE – modified XLE and NF90 membranes in 10 mM NaCl + 150 mg/L DTAB. 140

Figure A5. Zeta potential of unmodified LE, XLE and NF90 membranes and PEGDE – modified XLE and NF90 membranes in 10 mM NaCl + 150 mg/L SDS. 141

Figure A6. (a) Fraction of flux retained after fouling in absence of intentionally added foulant and (b) fraction of flux regained after fouling and cleaning, as a function of initial water flux. Definition of symbols: ○ LE, ◺ XLE, ▽ NF90, ▲ 1% (w/w) MW 200 XLE, ▼ 15% (w/w) MW 200 XLE, ● 1% (w/w) MW 1000 XLE, ■ 15% (w/w) MW 1000 XLE, ◣ 1% (w/w) MW 1000 NF90, and ◢ 15% (w/w) MW 1000 NF90. Lines have been drawn through the modified and unmodified membrane data to guide the eye.....142

This page is intentionally left blank

1 INTRODUCTION

1.1 Water Shortage Issues Facing the World

Water is one of the most basic resources necessary for human survival, yet in 2006, the World Health Organization estimated that one billion people worldwide did not have access to clean water [1]. The situation will undoubtedly become more severe, as the world's population is increasing at a rate of 80 million people per year [1]. Although water covers approximately 70% of the earth's surface, oceans account for 97% of this water, leaving only 3% of the world's water with a potable salinity level (<1000 mg/L total dissolved solids (TDS)) [2]. However, much of this fresh water is either located far below ground or is frozen in icecaps and glaciers, leaving less than 1% of the world's water as readily accessible fresh water [2].

1.2 Desalination

Since fresh water sources are finite and limited, treatment of alternative water sources must be considered. One well-established and growing treatment method is desalination of brackish water and seawater. Brackish water typically has TDS content in the range 1,000-15,000 mg/L, while seawater has an average TDS content of 35,000 mg/L, although there is wide variability in observed TDS values [2]. In 1953, there were approximately 225 desalination plants worldwide, with a total capacity of 27 million gallons per day (mgd) [2]. By 2004, the number had grown to more than 15,000 plants worldwide, with an estimated total capacity of 8,560 mgd, about 25% of the United States' annual water consumption [1]. Thermal technologies, where salt is removed by evaporating brackish water or seawater and condensing the water vapor to yield fresh water, dominated the desalination industry until the late 1990s [2]. Membrane technologies have now surpassed thermal technologies in terms of desalination capacity, due largely to the development of reverse osmosis in the 1960s [2]. A reverse osmosis desalination plant requires as little as ten percent of the energy of a thermal distillation plant, making reverse osmosis a more cost-effective option and leading to its use in nearly all new desalination plants being constructed today [1]. The exception is the Middle East, where thermal technologies still dominate the market due to abundant cheap supplies of fossil fuels [3].

1.3 Produced Water

Another potential alternative water source gaining interest today is produced water, the main byproduct of oil and natural gas production [4]. One source of produced water is the water located in underground formations with oil and gas, which is brought to the surface when the hydrocarbons are produced. In the United States, approximately seven barrels of water are brought to the surface with every barrel of oil generated, although the

location, type, and age of the well affect the amount of water produced [4]. Worldwide, an estimated 77 billion barrels of produced water were generated in 1999 [4]. This water is typically unfit for beneficial use and must be disposed of in accordance with regulatory requirements, most often by reinjection at onshore sites and discharge at offshore sites, at a high cost to oil production companies. If this water could be purified for beneficial use instead of discarded, not only would production costs be lowered drastically and the threat to the environment lessened, but a new and much-needed water source would result, since oil is often produced in arid regions lacking sufficient fresh water resources.

Produced water composition varies by geographic location, geological formation, and product being produced, and may include dispersed oil and other organics, salts, metals, and treatment chemicals such as scale and corrosion inhibitors, coagulants to remove solids, and emulsion breakers [4]. The composition of a single produced water source can also vary widely over the course of a reservoir lifetime, making prediction of water composition even more difficult.

1.4 Types of Water Treatment Membranes

The four major pressure-driven membrane separations used in water treatment are microfiltration (MF), ultrafiltration (UF), nanofiltration (NF) and reverse osmosis (RO) [3, 5]. Each membrane type has a different operating pressure range and separation ability. As seen in Figure 1.1, microfiltration membranes can remove contaminants larger than approximately 1000 Å, including colloidal particles and bacteria [3, 5]. Ultrafiltration membranes remove smaller components, such as proteins, from solution, in addition to colloidal particles and bacteria [3, 5]. Both microfiltration and ultrafiltration membranes achieve separation by rejecting components larger than their pore sizes, but reverse osmosis membranes, on the other hand, are so dense they are considered effectively nonporous [5]. Reverse osmosis membranes, therefore, can remove molecularly dissolved salts from solution, while nanofiltration membranes, or "loose RO" membranes, typically have lower salt rejection capabilities than reverse osmosis membranes [3]. Figure 1.1 also illustrates the increasing pressure, or energy, required to achieve higher levels of separation with membranes.

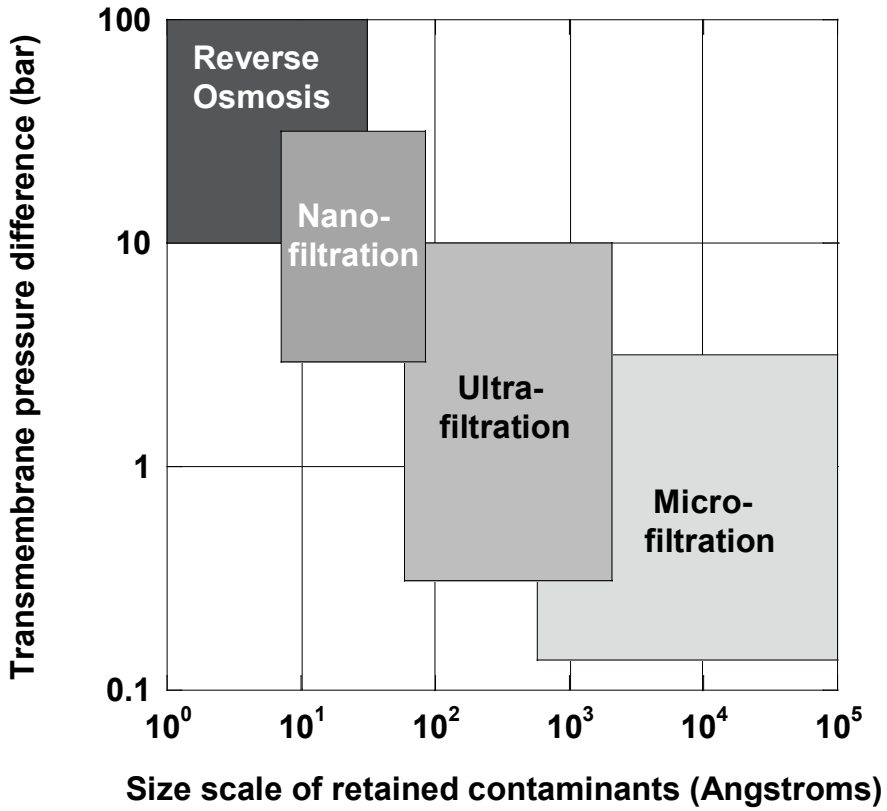

Figure 1.1. Separation characteristics of the four major pressure-driven membrane separations [3].

1.5 Membrane Fouling

Reverse osmosis membranes, which are now commonly used for desalination, cannot be used to treat produced water due to fouling, a phenomenon that decreases water throughput and reduces membrane lifetime [5]. When organic contaminants present in produced water, including emulsified oil and surfactants, deposit on the membrane surface, mass transfer resistance increases [5]. Even desalination presents fouling problems, due to suspended solids in the feed and microbial growth on the membrane surface. Thus, seawater is typically pretreated before being fed to reverse osmosis membrane modules, to protect the membranes from biological and particulate fouling [3]. Conventional pretreatment includes sedimentation and sand and cartridge filtration, but membrane-based pretreatment, including ultrafiltration and microfiltration, has also been used recently [6, 7]. Pretreatment, both conventional and membrane-based, is being considered as an option for produced water purification, to remove most of the contaminants before sending the treated feed water to a reverse osmosis membrane module for desalination [8]. However, there is also significant interest in eliminating the pretreatment step, so that produced water purification (organic and salt removal) may be

performed in a single step. Improvements in fouling resistance of reverse osmosis membranes are necessary, and surface modification, generally involving physical coating of antifouling polymers on to the surface of commercial membranes, is one of the major focal points of this area of research [9, 10]. The research reported in this dissertation is also geared towards surface modification to enhance the fouling resistance of commercial reverse osmosis membranes for produced water purification.

1.6 Goals and Organization of the Dissertation

Two major goals provided the framework for this research. First, the commercial reverse osmosis membranes chosen for use in surface modification studies were thoroughly characterized, to determine the effect of testing conditions on membrane performance. Surface modification will affect membrane performance, and it is important to understand what changes in performance can be attributed to surface modification and what changes are due to the conditions at which the membranes are tested. The second goal of this research was to modify the surface of commercial reverse osmosis membranes by chemical grafting and evaluate the modified membranes' resistance to fouling by model produced water contaminants. The fouling resistance of modified membranes was compared to that of unmodified control membranes, and surface properties of control and modified membranes were measured.

This dissertation includes seven chapters, including this introductory chapter, and one appendix. Chapter 2 describes the background and theory relevant to the research, including the development of current commercial reverse osmosis membranes, the solution-diffusion model used to explain their behavior, and previous surface modification work, including poly(ethylene glycol)-based modifications. Chapter 3 details the experimental materials and methods used in this work.

Chapter 4 presents the results of the commercial reverse osmosis membrane performance characterization studies. The influence of concentration polarization, continuous feed filtration, and feed pH on membrane performance was measured, and performance values consistent with the manufacturer benchmarks were achieved by matching their test conditions. Chapter 5 discusses the chemical structure and surface properties of the commercial reverse osmosis membranes, including their surface roughness, hydrophilicity and charge. Chapter 6 presents the results of surface modification of commercial membranes by poly(ethylene glycol) diglycidyl ether (PEGDE) using a top surface treatment method. The effects of modification on water flux, salt rejection, and fouling resistance to charged surfactants and oil-in-water emulsions of *n*-decane and charged surfactant were measured. Flux recovery of PEGDE-modified membranes after cleaning was also evaluated, and the fouling resistance and flux recovery of modified and unmodified membranes were compared. Finally, Chapter 7 gives conclusions and recommendations for future work. The appendix includes other surface modification methods studied, surface charge data in the presence of charged surfactants, and fouling data for blank foulant tests.

1.7 References

[1] R.F. Service, Desalination freshens up, Science, 313 (2006) 1088-1090.

[2] Review of the Desalination and Water Purification Technology Roadmap, The National Academies Press, Washington, D.C., 2005.

[3] C. Fritzmann, J. Löwenberg, T. Wintgens, T. Melin, State-of-the-art of reverse osmosis desalination, Desalination, 216 (2007) 1-76.

[4] J.A. Veil, M.G. Puder, D. Elcock, R.J. Redweik, A White Paper Describing Produced Water from Production of Crude Oil, Natural Gas, and Coal Bed Methane, Contract No. W-31-109-Eng-38; U.S. Department of Energy National Energy Technology Laboratory, Argonne National Laboratory, 2004.

[5] R.W. Baker, Membrane Technology and Applications, 2nd ed., John Wiley & Sons Ltd., West Sussex, 2004.

[6] D. Vial, G. Doussau, The use of microfiltration membranes for seawater pre-treatment prior to reverse osmosis membranes, Desalination, 153 (2002) 141-147.

[7] G. Pearce, S. Talo, K. Chida, A. Basha, A. Gulamhusein, Pretreatment options for large scale SWRO plants: case studies of UF trials at Kindasa, Saudi Arabia, and conventional pretreatment in Spain, Desalination, 167 (2004) 175-189.

[8] M. Çakmakci, N. Kayaalp, I. Koyuncu, Desalination of produced water from oil production fields by membrane processes, Desalination, 222 (2008) 176-186.

[9] J.S. Louie, I. Pinnau, I. Ciobanu, K.P. Ishida, A. Ng, M. Reinhard, Effects of polyether-polyamide block copolymer coating on performance and fouling of reverse osmosis membranes, Journal of Membrane Science, 280 (2006) 762-770.

[10] A.C. Sagle, E.M. Van Wagner, H. Ju, B.D. McCloskey, B.D. Freeman, M.M. Sharma, PEG-coated reverse osmosis membranes: desalination properties and fouling resistance, Journal of Membrane Science, 340 (2009) 92-108.

This page is intentionally left blank

2 BACKGROUND AND THEORY

2.1 Osmosis and Reverse Osmosis

Osmosis is a naturally occurring phenomenon in which water (solvent) flows through a semi-permeable membrane (i.e., a membrane that is permeable to water but not salt) from regions of low solute (salt) concentration to regions of high solute concentration, to achieve equilibrium between the two solutions [1, 2]. However, if a hydrostatic pressure equivalent to the so-called osmotic pressure difference between the two solutions is applied to the high solute concentration solution, net water flow through the membrane will stop, and if pressure greater than the osmotic pressure difference is applied, the direction of water flow will be reversed [1, 2]. Reverse osmosis, therefore, is the process of water transport against its concentration gradient, from the low water concentration (i.e., high solute concentration) side of the membrane to the high water concentration (i.e., low solute concentration) side of the membrane. Figure 2.1 illustrates the hydrostatic pressure difference and direction of water flow for the processes of osmosis, osmotic equilibrium and reverse osmosis.

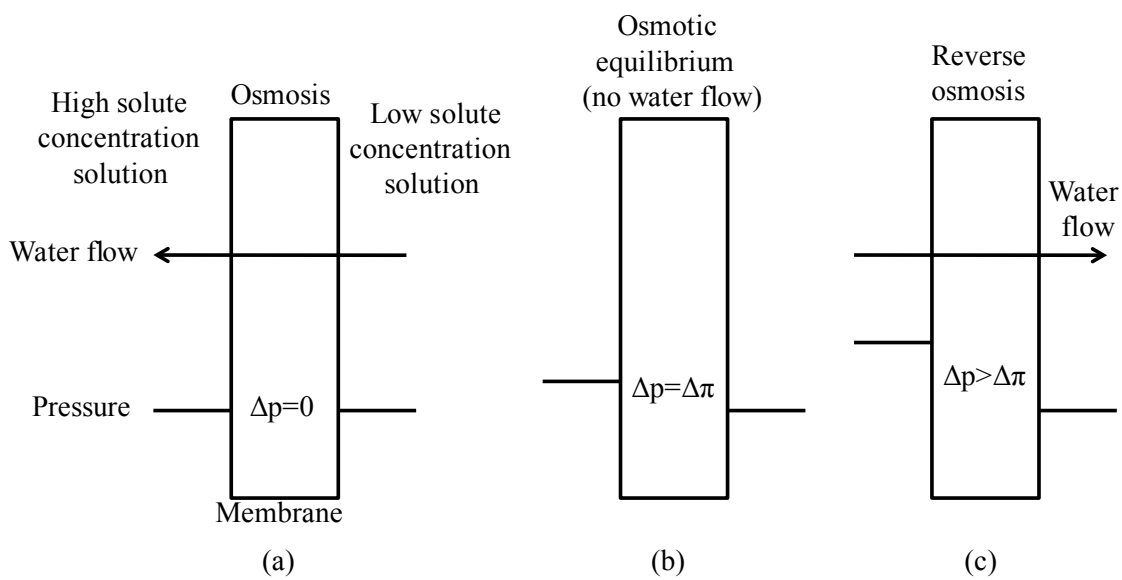

Figure 2.1. Direction of water flow and pressure difference for an osmotic membrane in (a) osmosis, (b) osmotic equilibrium and (c) reverse osmosis [1, 2]. The solute (i.e., salt) concentration is higher on the left hand side of each membrane in this figure.

2.2 Membrane Transport Model

In pressure-driven permeation through a membrane, the pressure difference across the membrane induces a chemical potential gradient [2]. Two models are used to describe transport through membranes. The solution-diffusion model, which assumes the pressure within the membrane is uniform and equal to the value on the high-pressure side of the membrane, applies to dense, nonporous membranes such as reverse osmosis membranes [3]. The pore-flow model, on the other hand, assumes the pressure decreases uniformly across the membrane thickness, and is used to describe, for example, flow through the pores of porous ultrafiltration membranes [2]. For charged membranes (e.g., polyamides), the electrochemical potential (i.e., μ_{ie}) is used instead of the chemical potential (i.e., μ_i), to account for the electrostatic potential of the membrane [4]. The solvent electrochemical potential gradient and the pressure and solvent activity profiles in a charged membrane corresponding to the solution-diffusion and pore-flow models are depicted in Figure 2.2.

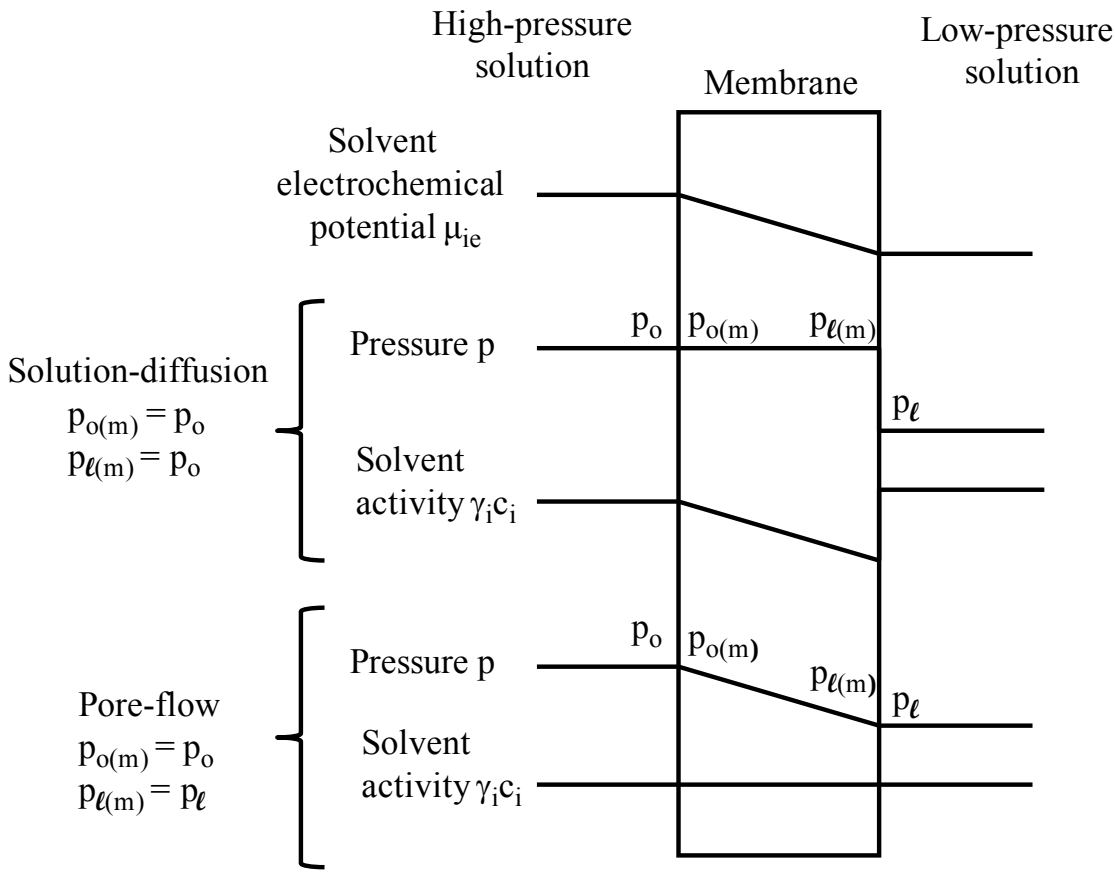

Figure 2.2. Solvent electrochemical potential gradient and corresponding pressure and solvent activity profiles in a charged membrane according to the solution-diffusion and pore-flow models [2].

The flux of a component in a feed stream is determined by the gradient in its electrochemical potential across a charged membrane, and is given by:

$$J_i = -L_i \frac{d\mu_{ie}}{dx} \tag{2.1}$$

where J_i is the flux of component i, $d\mu_{ie}/dx$ is the gradient in electrochemical potential of component i, and L_i is a coefficient of proportionality [2].

The electrochemical potential gradient is the driving force for permeation, and for charged membranes, this driving force is generated by a combination of concentration, pressure and electrostatic potential gradients, expressed as [2, 4]:

$$d\mu_{ie} = RTd\ln(\gamma_i c_i) + \upsilon_i dp + z_i e d\Psi \tag{2.2}$$

where γ_i is the activity coefficient, c_i is the molar concentration, υ_i is the molar volume and z_i is the charge number of component i, R is the gas constant, T is the temperature, p is the pressure, e is the charge on an electron, and Ψ is the electrostatic potential of the membrane. For incompressible phases, the molar volume, υ_i, is independent of pressure, so Equation 2.2 may be integrated to give:

$$\mu_{ie} = \mu_{ie}^o + RT\ln(\gamma_i c_i) + \upsilon_i (p - p_i^o) + z_i e\Psi \tag{2.3}$$

where μ_{ie}^o is the electrochemical potential of component i at a reference pressure p_i^o (typically defined as the saturation vapor pressure of i, $p_{i,sat}$).

Assuming the activity coefficient, γ_i, is constant, Equations 2.1 and 2.2 may be combined to give the following:

$$J_i = -L_i\left(RT\frac{d\ln(\gamma_i c_i)}{dx} + \upsilon_i \frac{dp}{dx} + z_i e\frac{d\Psi}{dx}\right) = -D_i\frac{dc_i}{dx} - k\frac{dp}{dx} - L_i z_i e\frac{d\Psi}{dx} \tag{2.4}$$

where the diffusion coefficient, D_i, is given by:

$$D_i = \frac{L_i RT}{c_i} \tag{2.5}$$

and the Darcy's law coefficient, k, is given by:

$$k = L_i \upsilon_i \tag{2.6}$$

Integration of Equation 2.4 across the membrane thickness gives:

$$J_i = \frac{\overline{D_i}\left(c_{io(m)} - c_{i\ell(m)}\right)}{\ell} + \frac{k\left(p_{o(m)} - p_{\ell(m)}\right)}{\ell} + \frac{L_i z_i e\left(\Psi_{o(m)} - \Psi_{\ell(m)}\right)}{\ell} \tag{2.7}$$

where $\overline{D_i}$ is the concentration averaged, effective diffusion coefficient across the membrane thickness (average value must be used because D_i may be concentration dependent), $c_{io(m)}$ is the concentration of component i in the membrane at the feed side interface, $c_{i\ell(m)}$ is the concentration of component i in the membrane at the permeate side interface, $p_{o(m)}$ is the pressure in the membrane at the feed side interface, $p_{\ell(m)}$ is the pressure in the membrane at the permeate side interface, $\Psi_{o(m)}$ is the electrostatic potential in the membrane at the feed side interface, $\Psi_{\ell(m)}$ is the electrostatic potential in the membrane at the permeate side interface, and ℓ is the membrane thickness. The charge within the membrane is assumed to be uniform (i.e., $\Psi_{o(m)} = \Psi_{\ell(m)}$).

The fluids on either side of the membrane are assumed to be in equilibrium with the membrane material at the interface, which allows interfacial concentrations in the membrane ($c_{io(m)}$ and $c_{i\ell(m)}$) to be determined by equating the electrochemical potential on either side of the interface (i.e., in the feed and in the membrane at the feed side interface, or in the permeate and in the membrane at the permeate side interface) [2, 4].

Equating electrochemical potentials (cf. Equation 2.3) at the feed side interface (noting that the feed fluid is uncharged, i.e., $\Psi_o = 0$) gives the following:

$$RT\ln\left(\gamma_{io}c_{io}\right) + \upsilon_i\left(p_o - p_{i,sat}\right) = RT\ln\left(\gamma_{io(m)}c_{io(m)}\right) + \upsilon_i\left(p_{o(m)} - p_{i,sat}\right) + z_i e\Psi_{o(m)} \tag{2.8}$$

As seen in Figure 2.2, the pressure in the feed solution (p_o) is equal to the pressure in the membrane at the feed side interface ($p_{o(m)}$) for both the solution-diffusion and pore flow models. The concentration of component i in the membrane at the feed side interface, $c_{io(m)}$, is simply:

$$c_{io(m)} = \frac{\gamma_{io}}{\gamma_{io(m)}} c_{io} \exp\left(-\frac{z_i e\Psi_{o(m)}}{RT}\right) = K_i c_{io} \tag{2.9}$$

where K_i is the sorption or partition coefficient of component i.

Equating electrochemical potentials (cf. Equation 2.3) at the permeate side interface (noting that the permeate fluid is uncharged, i.e., $\Psi_\ell = 0$) gives:

$$RT\ln\left(\gamma_{i\ell}c_{i\ell}\right) + \upsilon_i\left(p_\ell - p_{i,sat}\right) = RT\ln\left(\gamma_{i\ell(m)}c_{i\ell(m)}\right) + \upsilon_i\left(p_{\ell(m)} - p_{i,sat}\right) + z_i e\Psi_{\ell(m)} \tag{2.10}$$

which can be rearranged to give:

$$c_{i\ell(m)} = \frac{\gamma_{i\ell}}{\gamma_{i\ell(m)}} c_{i\ell} \exp\left(-\frac{\upsilon_i\left(p_{\ell(m)} - p_\ell\right)}{RT}\right)\exp\left(-\frac{z_i e\Psi_{\ell(m)}}{RT}\right) \tag{2.11}$$

where p_ℓ is the pressure in the permeate. Substituting for the sorption coefficient, K_i, gives:

$$c_{i\ell(m)} = K_i c_{i\ell} \exp\left(-\frac{\upsilon_i\left(p_{\ell(m)} - p_\ell\right)}{RT}\right) \tag{2.12}$$

The expressions for the concentrations of component i in the membrane at the feed and permeate side interfaces (Equations 2.9 and 2.12, respectively) can be substituted into Equation 2.7 to obtain:

$$J_i = \frac{\overline{D_i} K_i}{\ell}\left[c_{io} - c_{i\ell} \exp\left(-\frac{\upsilon_i\left(p_{\ell(m)} - p_\ell\right)}{RT}\right)\right] + \frac{k}{\ell}\left(p_o - p_{\ell(m)}\right) \tag{2.13}$$

Equation 2.13 gives the flux of component i across a membrane in terms of the pressure and concentration gradients across the membrane. According to the pore-flow model (cf. Figure 2.2), the pressure in the membrane at the permeate side interface, $p_{\ell(m)}$, is equal to the permeate pressure, p_ℓ, and the concentration is assumed to be uniform across the membrane ($c_{io} = c_{i\ell}$). Equation 2.13 may be simplified to give the governing equation for transport through a pore-flow membrane, Darcy's law:

$$J_i = \frac{k}{\ell}\left(p_o - p_\ell\right) \tag{2.14}$$

The solution-diffusion model assumes that the pressure in the membrane at the permeate side interface, $p_{\ell(m)}$, is equal to the feed pressure, p_o, so Equation 2.13 may be simplified to give:

$$J_i = \frac{\overline{D_i} K_i}{\ell}\left[c_{io} - c_{i\ell} \exp\left(-\frac{\upsilon_i\left(p_o - p_\ell\right)}{RT}\right)\right] \tag{2.15}$$

Equation 2.15 gives the flux of component i across a reverse osmosis membrane in terms of the pressure and concentration gradients across the membrane. Typically, water (component w, solvent) and salt (component s, solute) are the species of interest in reverse osmosis applications. At osmotic equilibrium, the applied transmembrane hydrostatic pressure exactly balances the difference in osmotic pressure of the feed and

product solutions ($\Delta p = \Delta\pi$), and water flux, J_w, is zero. Inserting this information into Equation 2.15 gives:

$$c_{w\ell} = c_{wo} \exp\left(\frac{\upsilon_w \Delta\pi}{RT}\right) \tag{2.16}$$

Substituting Equation 2.16 into Equation 2.15 yields the following expression for water flux:

$$J_w = \frac{\overline{D_w} K_w c_{wo}}{\ell}\left[1 - \exp\left(-\frac{\upsilon_w(\Delta p - \Delta\pi)}{RT}\right)\right] \tag{2.17}$$

The approximation $(1-\exp(-x)) \to x$ as $x \to 0$ applies, since $x \approx 0$ in Equation 2.17. Therefore, Equation 2.17 may be written:

$$J_w = \frac{\overline{D_w} K_w c_{wo} \upsilon_w}{\ell RT}(\Delta p - \Delta\pi) \tag{2.18}$$

Equation 2.15 can also be used to give a simplified expression for salt flux, J_s. Using the approximation $\exp(-x) \to 1$ as $x \to 0$ in Equation 2.15 (since salt flux is assumed to be dependent on concentration and independent of pressure [5]), salt flux may be written:

$$J_s = \frac{\overline{D_s} K_s}{\ell}(c_{so} - c_{s\ell}) \tag{2.19}$$

In Equations 2.18 and 2.19, J is the flux of water (J_w) or salt (J_s), $\overline{D}$ is the average diffusion coefficient of water ($\overline{D_w}$) or salt ($\overline{D_s}$), K is the sorption coefficient of water (K_w) or salt (K_s), υ_w is the molar volume of water, Δp is the transmembrane pressure difference, $\Delta\pi$ is the osmotic pressure difference (due to the ionic content of the feed and permeate), c_{wo} is the water concentration in the feed, c_{so} is the salt concentration in the feed, and $c_{s\ell}$ is the salt concentration in the permeate. Solution ideality may be assumed at low concentrations, so the osmotic pressure of a sodium chloride feed is approximated as 2cRT, and $\Delta\pi$ is given by $2(c_{so} - c_{s\ell})RT$ [6].

Equations 2.18 and 2.19 can be simplified by defining the water permeance (A) and salt permeance (B) as:

$$A = \frac{\overline{D_w} K_w c_{wo} \upsilon_w}{\ell RT} \tag{2.20}$$

and

$$B = \frac{\overline{D_s} K_s}{\ell} \tag{2.21}$$

Equations 2.18 and 2.19 are thus typically written as:

$$J_w = A(\Delta p - \Delta \pi) \tag{2.22}$$

and

$$J_s = B(c_{so} - c_{s\ell}) \tag{2.23}$$

Units typically used in Equations 2.22 and 2.23 are: J_w, L/(m^2 h), or LMH; J_s, mg/(m^2 h); A, LMH/bar; B, LMH; Δp and $\Delta\pi$ (bar); and c_{so} and $c_{s\ell}$ (mg/L). Permeate salt concentration is related to the water and salt fluxes as follows [1]:

$$c_{s\ell} = \frac{J_s}{J_w} \tag{2.24}$$

Another defining property of a reverse osmosis membrane is its apparent salt rejection (R_{app}), which is given by:

$$R_{app} = \left(1 - \frac{c_{s\ell}}{c_{so}}\right) \times 100\% \tag{2.25}$$

Equation 2.24 may be used with Equation 2.25 to give an expression for apparent salt rejection in terms of water and salt flux [1]:

$$R_{app} = \left(1 - \frac{J_s}{J_w c_{so}}\right) \times 100\% \tag{2.26}$$

Equations 2.22 and 2.23 may be combined with Equation 2.26 to give an expression for the apparent salt rejection of a solution-diffusion membrane in terms of its water and salt permeance [1]:

$$R_{app} = \frac{\frac{A}{B}(\Delta p - \Delta \pi)}{1 + \frac{A}{B}(\Delta p - \Delta \pi)} \times 100\% \tag{2.27}$$

2.3 Concentration Polarization

Commercial reverse osmosis membranes typically reject more than 98% of salt, but this high selectivity makes them prone to concentration polarization, a phenomenon illustrated in Figure 2.3 [1, 6-8]. Diffusion of rejected salt ions from the membrane surface into the bulk feed solution does not occur rapidly enough to maintain a uniformly mixed feed, leading to a buildup of salt in a boundary layer on the feed side membrane interface [7]. A mass balance on the salt within the boundary layer (where permeate salt flux is set equal to convective flux towards the membrane minus diffusive flux away from the membrane) yields the following (cf. Figure 2.3) [1]:

$$J_w c_s - D_{so} \frac{dc_s}{dx} = J_w c_{s\ell} \tag{2.28}$$

where x is the coordinate direction perpendicular to the membrane surface and D_{so} is the diffusion coefficient of salt in the feed solution. Integrating Equation 2.28 over the boundary layer thickness gives the expression for the concentration polarization modulus, M, according to the film model [1, 9]:

$$M = \frac{c_{so(m)} - c_{s\ell}}{c_{so} - c_{s\ell}} = \exp\left(\frac{J_w}{k}\right) \tag{2.29}$$

where c_{so} is the bulk feed salt concentration, $c_{so(m)}$ is the salt concentration in the feed contiguous to the membrane surface (equivalent to the salt concentration in the membrane at the feed side interface due to equilibrium at the boundary), and k is the mass transfer coefficient, given by [9]:

$$k = \frac{D_{so}}{\delta} \tag{2.30}$$

where δ is the boundary layer thickness.

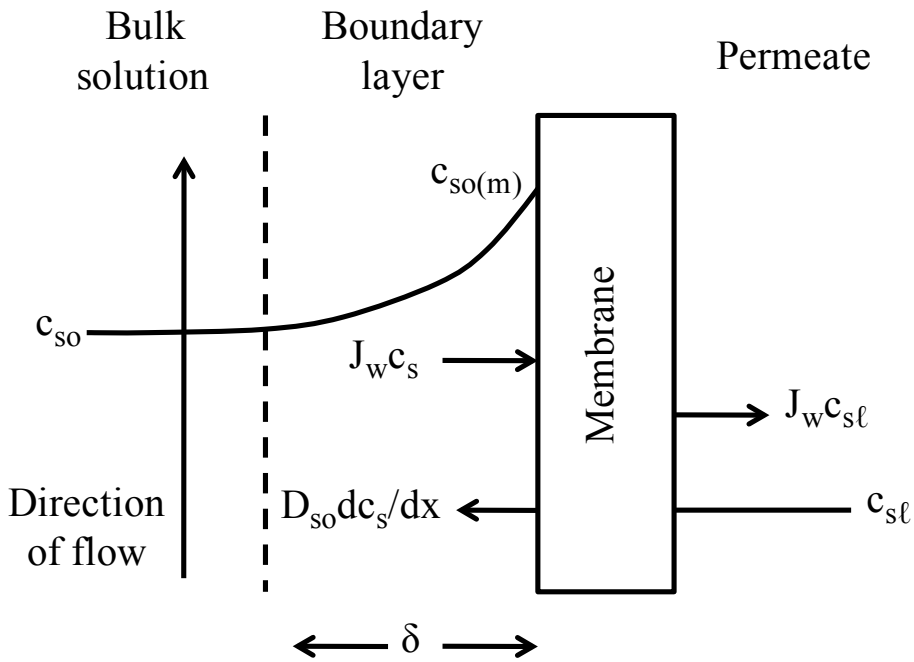

Figure 2.3. Schematic of salt boundary layer profile for reverse osmosis membranes. Feed salt concentration at the membrane interface ($c_{so(m)}$) is greater than the bulk feed concentration (c_{so}) due to accumulation of rejected salt in a boundary layer at the membrane surface [7].

Apparent salt rejection, calculated using the bulk feed salt concentration (c_{so}), is less than the true salt rejection of the membrane, which must be determined using the salt concentration in the feed contiguous to the membrane surface ($c_{so(m)}$). The film model may be used to find $c_{so(m)}$, but estimation of the mass transfer coefficient is difficult. Thus, a model correlating salt concentration at the membrane surface to easily measured experimental quantities is needed to determine the true salt rejection of a reverse osmosis membrane, R_{true}.

One simple model that has proven useful relies on the fact that the water permeance of a membrane, A, is a material property and should be, to a first approximation, independent of feed composition, at least over narrow ranges of feed composition [10]. For a pure water feed solution (i.e., $\Delta\pi = 0$), Equation 2.22 can be simplified to give the pure water flux, $J_{w(pw)}$:

$$J_{w(pw)} = A \times \Delta p \tag{2.31}$$

Water flux in a feed containing NaCl, $J_{w(NaCl)}$, is given by:

$$J_{w(NaCl)} = A\left(\Delta p - \left(\pi_{so(m)} - \pi_{s\ell}\right)\right) \tag{2.32}$$

where $\pi_{so(m)}$ and $\pi_{s\ell}$ are the osmotic pressure ($\pi = 2cRT$ [6]) at the membrane surface and in the permeate, respectively. Since A is assumed to be constant, Equations 2.31 and 2.32 may be combined to give [10]:

$$\pi_{so(m)} = \pi_{s\ell} + \Delta p \times \left(1 - \frac{J_{w(NaCl)}}{J_{w(pw)}}\right) \tag{2.33}$$

Equation 2.33 may be used to find the feed osmotic pressure at the membrane surface from experimentally measured quantities (i.e., water flux in pure water and salt water feeds, permeate concentration, and applied pressure), and true rejection can then be calculated [10]:

$$R_{true} = \left(1 - \frac{\pi_{s\ell}}{\pi_{so(m)}}\right) \times 100\% \tag{2.34}$$

Using the previously determined expression for $\pi_{so(m)}$ (cf. Equation 2.33), the concentration polarization modulus can also be found from experimentally measured quantities, using the following expression:

$$M = \frac{\pi_{so(m)} - \pi_{s\ell}}{\pi_{so} - \pi_{s\ell}} = \frac{\Delta p}{\pi_{so} - \pi_{s\ell}} \times \left(1 - \frac{J_{w(NaCl)}}{J_{w(pw)}}\right) \tag{2.35}$$

where π_{so} is the osmotic pressure of the bulk feed solution.

2.4 Evolution of Reverse Osmosis Membranes

The evolution of reverse osmosis membranes can be traced to 1959, when Reid and Breton first reported the utility of dense cellulose acetate membranes for desalination [11]. A few years later, Loeb and Sourirajan described the use of asymmetric cellulose acetate membranes, consisting of a thick porous sublayer with only a thin dense skin layer [12]. Francis, working at North Star Research and Development Institute, hypothesized that forming the two layers separately and laminating the dense barrier layer to the porous support would give better performance (i.e., higher flux membranes) and produced the first thin-film composite reverse osmosis membrane in 1964 [13]. Problems with compaction of the microporous cellulose acetate support fueled the search for alternative support materials, and in 1966, Cadotte developed a method of casting microporous, compaction-resistant polysulfone support membranes [13]. Polysulfone remains the standard support membrane in the reverse osmosis industry today.

Cadotte was also responsible for significant advances in membrane separation layer performance. In 1970, he developed a completely noncellulosic thin-film composite

membrane, NS-100, containing an aryl-alkyl polyurea barrier layer formed *in situ* on a microporous polysulfone support [13]. Properties of this membrane, including flux, rejection, and resistance to biodegradation and compaction, were superior to those of cellulosic membranes, and from that point forward, most improvements in barrier layer materials have centered on synthetic polymers. Additionally, the *in situ* formation method opened the door for a wide variety of materials to be considered for the barrier layer [14]. Approximately ten years later, Cadotte and colleagues announced the FT-30 polyamide membrane, based on interfacial polymerization of trimesoyl chloride and *m*-phenylene diamine [14, 15]. The chemical structure of the monomers and polymer are given in Figure 2.4, and the composite membrane structure is illustrated in Figure 2.5. Many current reverse osmosis membranes are based on chemistry similar to that developed by Cadotte for the FT-30.

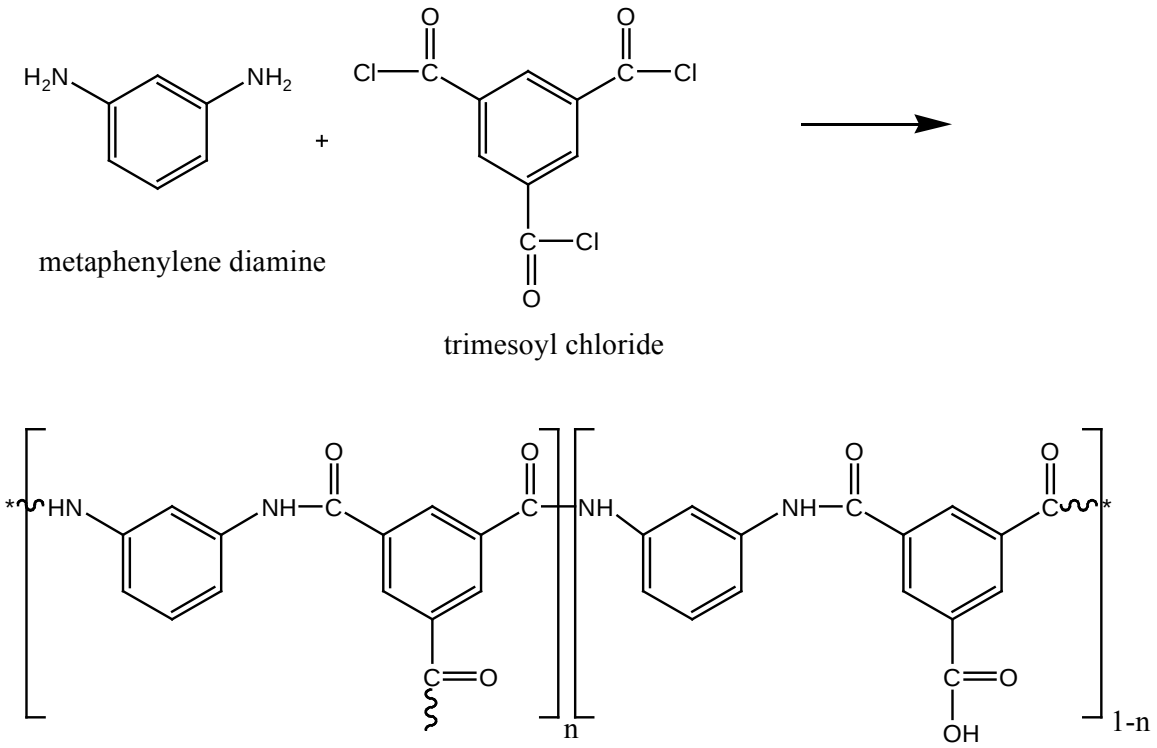

Figure 2.4. Chemical structures of metaphenylene diamine, trimesoyl chloride, and resulting interfacially polymerized polyamide membrane, where n characterizes the degree of crosslinking [16].

Figure 2.5. Composite reverse osmosis membrane structure. The reinforcing fabric base (~120 μm) is coated with a thin layer of microporous polysulfone (~40 μm) and the interfacially polymerized selective polyamide layer (~0.1 μm) [16].

2.5 Membrane Performance as a Function of Test Conditions

Early work on the FT-30 membrane highlighted the effects of operational variables, including feed pressure, salt concentration, temperature, and pH, on membrane performance in seawater desalination [14, 17]. Figure 2.6 illustrates observed trends in water flux and salt rejection of an FT-30 membrane. For a synthetic seawater feed (3.5% salt), water flux increased linearly with pressure above the feed osmotic pressure (~400 psi), and salt rejection increased quickly as pressure increased, before beginning to level off at applied pressures greater than 700 psig (cf. Figure 2.6 (a)). According to the solution-diffusion model equations for water and salt flux (Equations 2.22 and 2.23, respectively), water flux is directly proportional to feed pressure, while salt flux is independent of applied pressure. Thus, as feed pressure is increased, more water flows through the membrane but salt flux remains constant, so salt rejection increases. Water flux and salt rejection decreased with increasing feed salt concentration (cf. Figure 2.6(b)). Equation 2.22 predicts decreasing water flux with increasing osmotic pressure, π (or, equivalently, increasing feed concentration). According to Equation 2.23, salt flux increases linearly with increasing salt concentration, and higher salt flux combined with lower water flux results in lower salt rejection. Linear increases in water flux with increasing temperature (20-60°C) were observed, while salt rejection decreased from 99.5% to 99% over the same temperature range (cf. Figure 2.6 (c)). Water flux was independent of feed pH, but salt rejection decreased at extreme pH values (i.e., below pH 5 and above pH 11) (cf. Figure 2.6(d)). Over the pH range 3-11, the pH effects were reversible, indicating no permanent change in membrane structure [14].

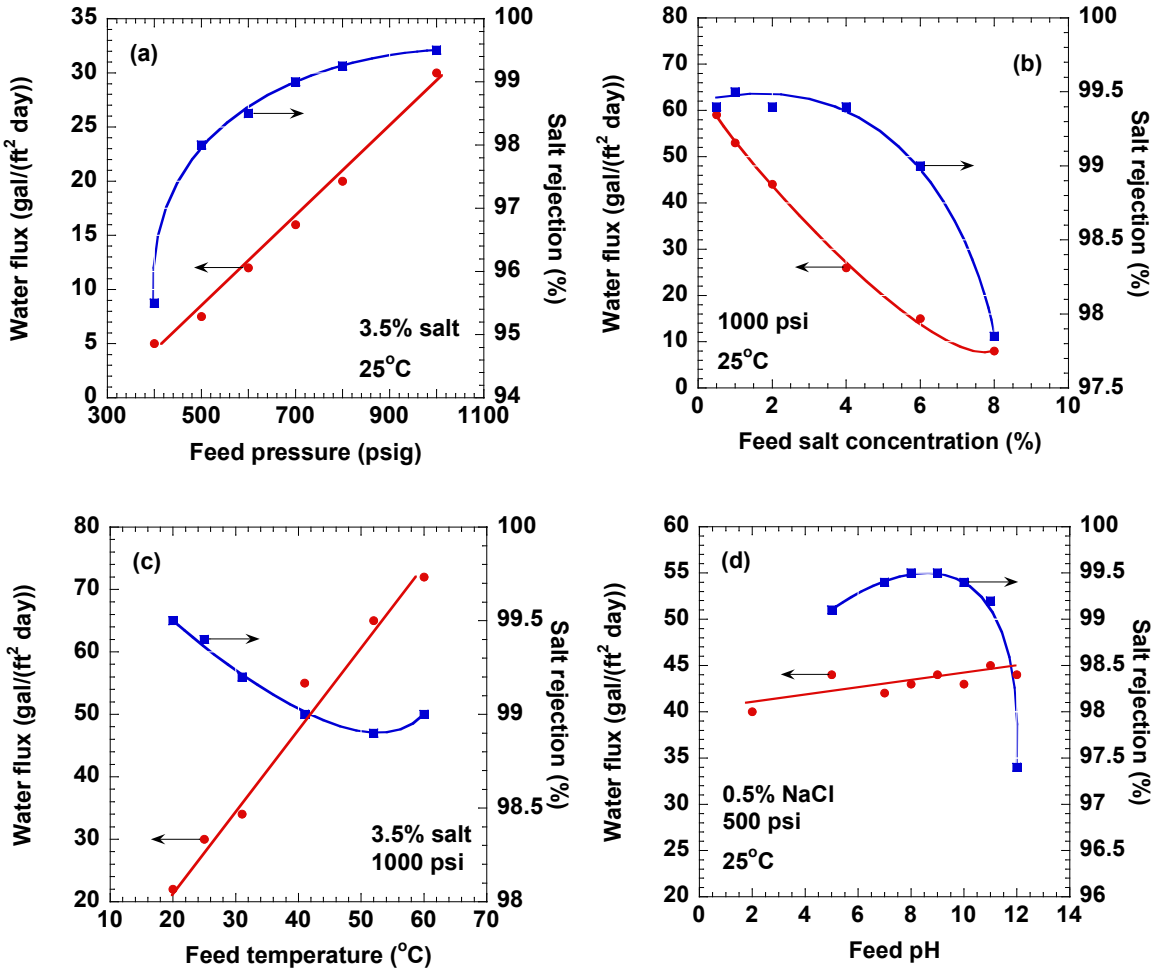

Figure 2.6. Influence of (a) feed pressure, (b) feed salt concentration, (c) feed temperature, and (d) feed pH on water flux and NaCl rejection of an FT-30 membrane [14].

2.6 Salt Rejection Mechanism

In membranes with fixed charged groups, charge interactions also contribute, at least in part, to observed salt rejection behavior. Electrostatic repulsion between fixed charged groups on the membrane and similarly charged ions in solution (co-ions) leads to a reduction of salt flux relative to water flux [18, 19]. The so-called Donnan effect has more influence on salt rejection at lower electrolyte concentrations, because the counterion concentration in the external electrolyte solution must be lower than that in the membrane to drive counterions from the membrane and establish the charge gradient that serves to repel the co-ions of the electrolyte [18, 20]. Thus, co-ion exclusion improves salt rejection when the electrolyte concentration is lower than the fixed charge concentration in the membrane [18]. For solution-diffusion membranes, charge

interaction effects are included in the salt solubility term, since co-ion exclusion results in decreased partitioning of co-ions into the membrane [19].

Parameters important in determining salt rejection, including polymer crosslink density and water and salt solubility and diffusivity, are difficult to measure in polyamide thin film composite membranes. Molecular dynamics simulations of the FT-30 membrane found lower water diffusion coefficients in crosslinked polyamides than in linear polyamides [21]. The simulations also indicated significantly lower ion mobility than water mobility, suggesting that the difference in salt and water diffusivities is responsible for the salt rejection ability of the FT-30 membrane [21]. In addition, chloride ion mobility was significantly lower than sodium ion mobility, thus chloride ions limit the rate of salt diffusion through the membrane [21].

2.7 Surface Properties and Membrane Fouling

Fouling is a major roadblock to wider use of membranes for water purification applications. Membranes can experience both internal (pore plugging) and external (surface buildup) fouling by impurities present in water [1]. Fouling reduces water flux, increases operating costs (including membrane cleaning costs and increased energy costs), and eventually requires membrane replacement [1]. The dense, nonporous nature of polyamide reverse osmosis membranes makes them susceptible to surface fouling. Three main surface properties are thought to influence surface fouling of reverse osmosis membranes: roughness, hydrophilicity, and electrostatic charge [22]. Polyamide reverse osmosis membranes have rough, peaks-and-valleys surfaces, with an average surface roughness on the order of 100 nm, and a maximum peak to valley distance of nearly 500 nm [23, 24]. The valleys of this rough membrane surface can catch small particles, blocking surface area and thereby reducing water flux [25]. Hydrophilicity and electrostatic charge effects are dependent on the nature of the foulant. Hydrophobic interactions between a hydrophobic foulant (e.g., oil) and a hydrophobic surface promote fouling, so increasing surface hydrophilicity can reduce fouling by lessening the attraction between hydrophobic foulants and the membrane surface, while simultaneously increasing the affinity of water for the surface [26]. Electrostatic attraction between the membrane surface and an oppositely charged foulant is also known to cause fouling [22].

Surface roughness is typically measured using an atomic force microscope (AFM), an instrument that maps surface contours using a small tip that scans across the surface of a sample. In contact mode, the tip is dragged along the surface and the displacement of the tip is used to measure the surface height at a particular position. In the tapping mode, short, rapid tapping of the tip on the membrane surface is used to map the surface. The tapping mode is preferred for soft samples that may be easily deformed by the tip (e.g., polyamide membranes) [23].

Surface hydrophilicity is commonly determined by the contact angle formed between a membrane surface, a deposited droplet, and the surrounding medium. Contact angle is

commonly measured using either the sessile drop or captive bubble method [27, 28]. The sessile drop method involves simply depositing a droplet (e.g., water) on the membrane surface in air, as shown in Figure 2.7(a). In the captive bubble method, a droplet (e.g., oil) is released under the surface of a membrane in a surrounding fluid with higher density than the droplet fluid (e.g., water), so that the droplet rises and attaches to the membrane surface. Figure 2.7(b) illustrates a captive bubble measurement of oil-in-water contact angle. The captive bubble measurement, although more difficult to perform, is preferred for desalination membranes because their performance is measured in water. For both the sessile drop and captive bubble methods, the angle measured through the water phase can be used to designate the relative hydrophilicity of a membrane (i.e., a smaller angle indicates a more hydrophilic membrane, and a larger angle indicates a more hydrophobic membrane, cf. Figure 2.7).

Polyamide membranes contain ionizable surface functional groups, including carboxylic acids from hydrolysis of unreacted acyl chloride groups and carboxylic acids and amines on chain ends (cf. Figure 2.4). At low pH values, the carboxylic acid and amine groups are protonated (-COOH and $-NH_3^+$), giving rise to an overall positive surface charge,

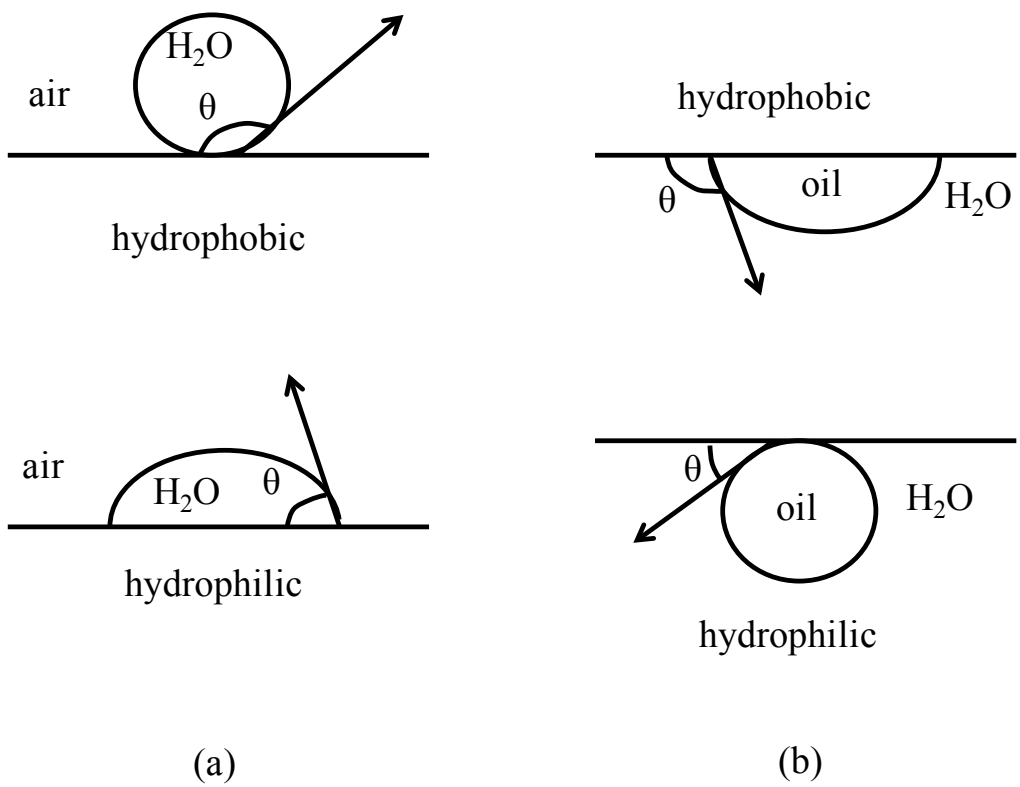

Figure 2.7. Contact angle, θ, measured using (a) the sessile drop method with a water droplet in air and (b) the captive bubble method with an oil droplet in water. A smaller contact angle indicates a more hydrophilic surface.

while at higher pH, both groups are deprotonated (-COO^- and –NH_2) and the membrane surface is negatively charged [28, 29]. The pH at which there is no net surface charge is termed the isoelectric point [6]. For polyamide membranes, the isoelectric point is reported to be in the pH range from 3 to 5 [29-31]. Thus, at normal solution pH (6-8), polyamide membranes have a negative surface charge.

The negative surface charge is balanced by an excess of counterions distributed in an electric double layer adjacent to the membrane surface. The term double layer refers to the counterions contiguous to the membrane surface in the Stern layer and the ions distributed farther from the surface in the diffuse layer [28, 32]. The Stern layer thickness is approximated by the hydrated counterion radius, r_{hi} (0.22 nm for Na^+), while the diffuse layer thickness is given by the Debye length, λ_D (approximately 3 nm for a 10 mM NaCl solution) [6]. The Stern potential, φ_s, located at the boundary between the Stern and diffuse layers, cannot be measured, and the zeta potential, ζ, is used instead [29]. Zeta potential is measured at the shear surface between the membrane surface and the surrounding electrolyte solution (i.e., where the mobile portion of the diffuse layer can flow past the charged membrane surface), and is close to the Stern potential [6, 28]. Figure 2.8 illustrates the structure of the electric double layer as well as the potential decay with increasing distance from the membrane surface.

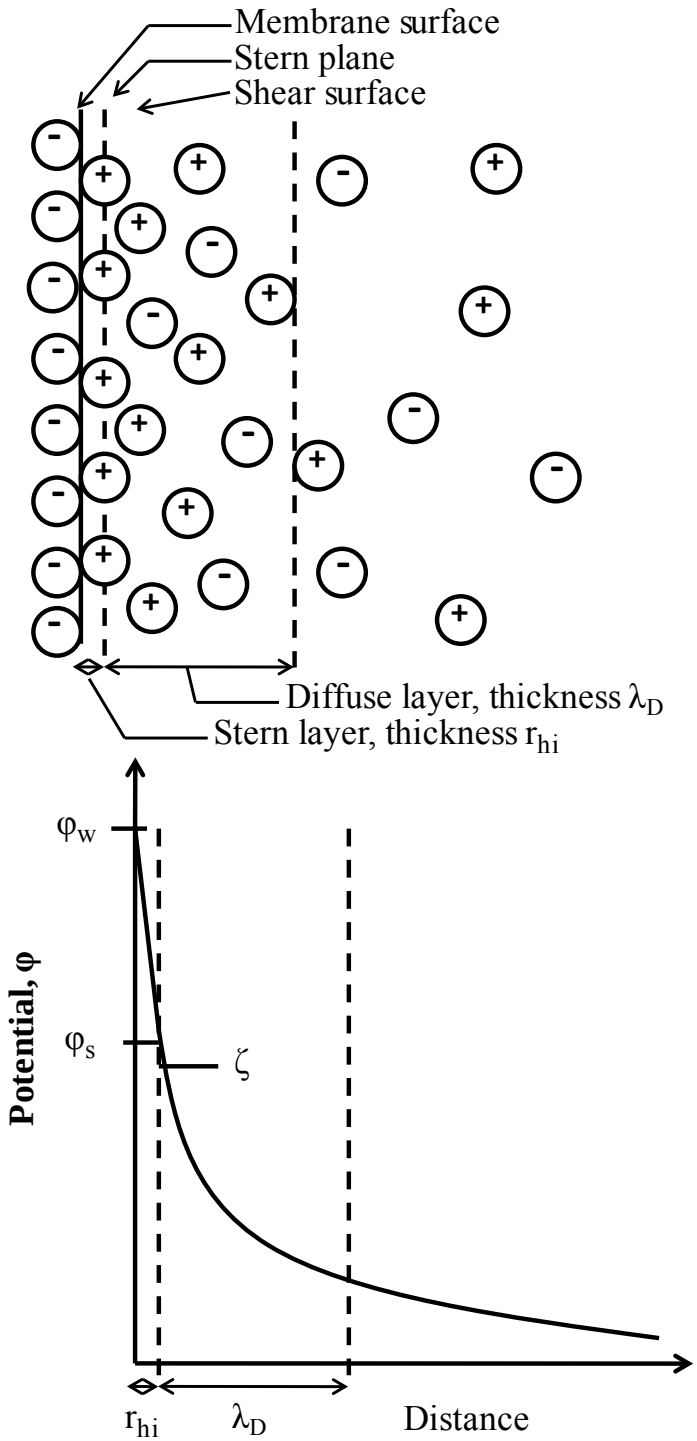

Figure 2.8. Structure of electric double layer, including Stern layer and diffuse layer, and potential as a function of distance from the membrane surface [6].

For flat surfaces, measurement of streaming potential is most often used to determine zeta potential [29, 30]. When an electrolyte solution flows through a channel formed by two membranes, a streaming current (I_s) is generated, which leads to a buildup of charge downstream and a potential gradient, E [29]. The potential gradient opposes the transfer of charge and leads to a leak current, I_L, in the opposite direction. At equilibrium, the streaming current exactly balances the leak current, and the measured potential difference is the streaming potential [29]. Figure 2.9 shows the development of the streaming potential at one of the membrane-solution interfaces.

Streaming potential is related to zeta potential by the Helmholtz-Smoluchowski equation [29, 30]:

$$\zeta = \frac{\Delta U_s}{\Delta P}\frac{\eta}{\varepsilon\varepsilon_o}\frac{L}{A}\frac{1}{R} \tag{2.36}$$

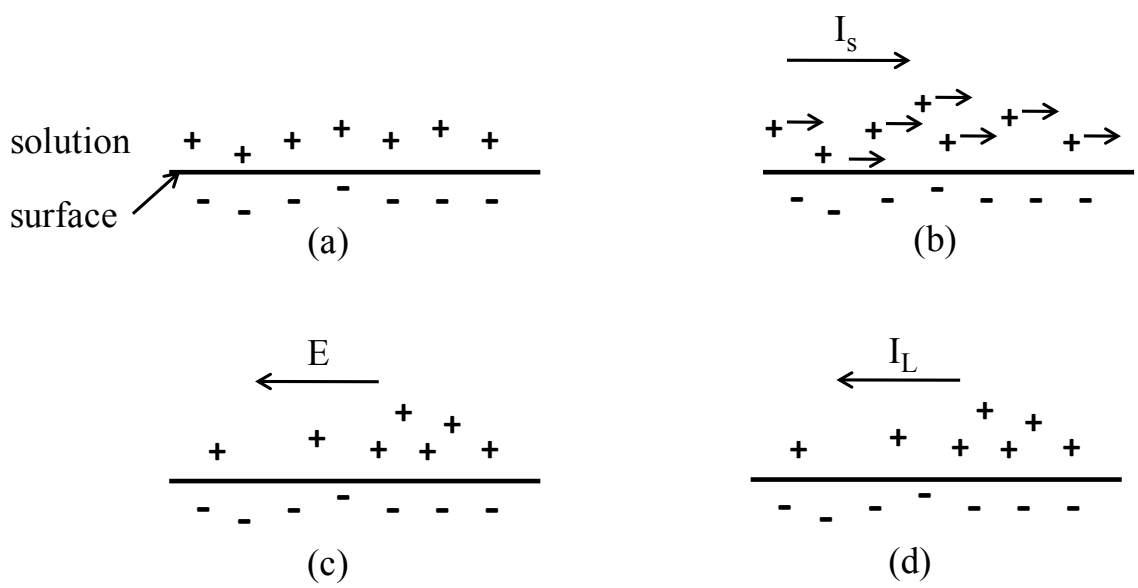

Figure 2.9. Development of the streaming potential at the membrane-solution interface. (a) The electric double layer is at rest until (b) an applied pressure causes liquid flow, ion movement, and the development of a streaming current, I_s. (c) The accumulation of counterions leads to formation of a potential difference, E, and (d) a leak current, I_L. At equilibrium, I_s=I_L and the measured potential difference is the streaming potential [29].

where ζ is the zeta potential, U_s is the streaming potential, P is the applied hydraulic pressure, $\Delta U_s/\Delta P$ is the slope of streaming potential versus pressure, η is the viscosity of the test solution, ε is the permittivity of the test solution, ε_o is the permittivity of free space (8.854×10^{-12} $C^2/(J\ m)$), L is the channel length, A is the cross-sectional area of the channel, and R is the electrical resistance of the channel.

The ratio L/A may be calculated using the dimensions of the test channel. Alternatively, at solution concentrations greater than 10^{-3} M, the Fairbrother and Mastin approach may be used [29, 30]:

$$\frac{L}{A} = \kappa R \tag{2.37}$$

where κ is the solution conductivity. Equation 2.36 is then reduced to the following [29, 30]:

$$\zeta = \frac{\Delta U_s}{\Delta P}\frac{\eta\kappa}{\varepsilon\varepsilon_o} \tag{2.38}$$

The surface charge density, σ_s (C/m^2), is related to the surface potential, φ_w (mV) (cf. Figure 2.8), by [28]:

$$\sigma_s = \left(8RT\varepsilon\varepsilon_o c \times 10^3\right)^{1/2} \sinh\left(\frac{zF\varphi_w}{2\times 10^3 RT}\right) \tag{2.39}$$

where c is the electrolyte concentration (M), z is the ionic charge, and F is the Faraday constant (96485 C/mol).

2.8 Fouling Resistance of Poly(ethylene glycol)

Poly(ethylene glycol) (PEG), whose structure is shown in Figure 2.10, was originally recognized for its ability to prevent protein and bacterial adhesion to surfaces [33-36]. Applications include preventing bacterial infections of biomedical devices [33], improving the blood compatibility of implants [34, 37], and limiting protein adsorption on contact lenses [35, 36]. The hydrophilicity of PEG is thought to be one underlying factor in the observed fouling resistance of PEG-grafted surfaces, since surface hydrophobicity has been positively correlated with protein adsorption [34, 35, 38]. PEG is also electrically neutral, another characteristic that lends itself to resisting protein adsorption [35]. Steric hindrance imparted by the grafted PEG molecules is hypothesized to be the other major contribution to decreased adhesion [33, 37, 38]. The large excluded volume of PEG renders proteins, bacteria, and other components of a fluid unable to approach a PEG-grafted surface as closely as a bare surface, diminishing the attractive

van der Waals interaction forces [33, 38]. In addition, the surface crowding-induced potential barrier and the increased solution viscosity near PEG-grafted surfaces result in a decreased adsorption rate [38].

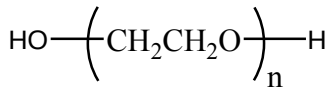

Figure 2.10. Chemical structure of poly(ethylene glycol) (PEG), where n is the number of repeat ethylene oxide units.

The configuration of PEG on a surface is also of interest. If the density of attachment sites on the surface is sufficiently low, the grafted PEG chains adopt the equilibrium configuration of free PEG chains in solution, a so-called mushroom configuration [38]. The grafted PEG chains become increasingly crowded at higher attachment site densities, forcing them to stretch out into a brush structure when the distance between sites is less than the radius of gyration for PEG [33, 38, 39]. The transition from the mushroom to the brush regime with increasing attachment site density is depicted in Figure 2.11. The figure also illustrates the increase in PEG layer thickness associated with the elongation of the chains from the mushroom to brush structure.

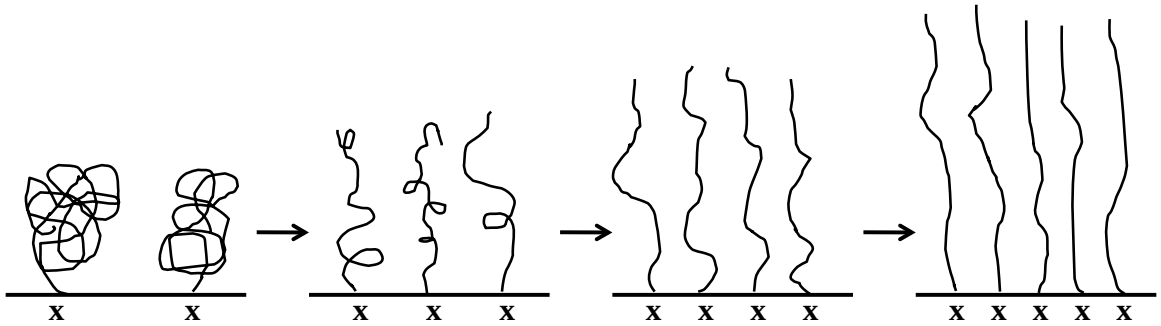

Figure 2.11. The configuration of PEG molecules grafted to a surface transitions from a mushroom to a brush structure as the attachment site density increases [33]. An attachment site is indicated by "x."

PEG grafting density (number of chains in a unit area of surface), and thus layer thickness, has been shown to increase with increasing grafting time and temperature, and is only limited in extent by the number of attachment sites available and molecular weight of the PEG chains being grafted [39, 40]. Protein adsorption resistance increases with increasing PEG graft density [35]. For surfaces with low attachment site density, higher molecular weight PEGs (i.e., longer chains) can effectively fill in unprotected

surface area and prevent protein adsorption [36]. However, above the critical entanglement molecular weight (~4400 g/mol, or 100 repeat ethylene oxide units), PEG chains are slow to align their reactive ends with the surface, and grafting efficiency decreases [40]. Thus, the combination of PEG chain length and graft density determines the resulting adsorption resistance of a PEG-grafted surface.

The demonstrated ability of PEG to resist protein adsorption has naturally led to its consideration for improving the fouling resistance of membranes in water purification applications [22, 26, 41-43]. Biofouling is a major issue in desalination plants [5, 44-46], and consideration of alternative water sources such as produced water raises even more serious fouling problems [47, 48]. Qualities of PEG that contribute to protein resistance, such as hydrophilicity and neutrality, are expected to yield resistance to other types of organic contaminants as well. Other properties of PEG, including its solubility in water and nontoxic nature, also make it an attractive candidate for membrane modification, since modification can be performed without harsh solvents that damage the membrane and without introducing harmful chemicals to the water supply. In addition, PEG is available or can be synthesized with a wide variety of endgroups, facilitating adsorption or grafting of PEG to a membrane surface.

2.9 Surface Modification in the Literature

The high level of interest in fouling resistance research is clearly indicated by the extent of surface modification studies in the literature. One long-running study by the Belfer group in Israel focused on redox-initiated radical grafting of vinyl monomers including acrylic acid, methacrylic acid, poly(ethylene glycol) methacrylate, and sulfopropyl methacrylate to commercial polyamide membrane surfaces [26, 46, 49-52]. A redox system consisting of potassium persulfate and potassium metabisulfite was used to generate monomer radicals to attack the polymer backbone, initiating grafting to the membrane surface [52]. Polymerization then occurred via propagation [52]. Surface characterization techniques including attenuated total reflectance Fourier transform infrared spectroscopy (ATR-FTIR) and x-ray photoelectron spectroscopy (XPS) demonstrated expected changes in surface chemical composition for modified membranes [49-52]. Other surface characterization techniques, including contact angle analysis, atomic force microscopy (AFM), and streaming potential analysis were used to determine changes in surface properties thought to influence fouling (i.e., hydrophilicity, roughness, and charge) [26, 49, 52]. Membranes grafted with methacrylic acid were more negatively charged than their unmodified counterparts [49]. Some membranes modified with poly(ethylene glycol) methacrylate and sulfopropyl methacrylate had lower contact angles, and therefore were more hydrophilic than unmodified membranes [26]. Modification with these two monomers decreased the surface roughness of one polyamide reverse osmosis membrane from 90 nm to 30 nm [52]. In a field test at a seawater desalination plant, a reverse osmosis membrane modified with sulfopropyl methacrylate retained 77% of its flux, as compared to 69% for the unmodified membrane

[46]. The increased hydrophilicity and decreased roughness of the modified membrane could explain the improvement in fouling resistance.

Chapman Wilbert et al. used poly(ethylene oxide)-containing surfactants to modify the surface of commercial cellulose acetate and polyamide membranes [43]. Hydrophobic interactions between the membrane and the hydrophobic portion of the surfactant were used to promote adsorption, in contrast to other modification methods involving covalent attachment to the surface. AFM indicated surfactant adsorption caused an increase in roughness of the relatively smooth cellulose acetate membrane surface and a decrease in roughness of the rough polyamide membrane surface. The water flux and salt rejection of unmodified and surfactant-modified membranes were measured before and after soaking the membranes in a vegetable broth fouling solution. While the cellulose acetate results were highly variable and inconclusive, some of the surfactant-modified polyamide membranes retained a higher percentage of their flux after foulant adsorption, as compared to the unmodified membranes. However, surfactant modification caused a larger decrease in water flux of the unmodified membrane than did exposure of the unmodified membrane to the foulant solution.

Louie et al. performed another physical coating study of commercial polyamide reverse osmosis membranes, using PEBAX® 1657, a hydrophilic block copolymer of nylon-6 and poly(ethylene glycol) [22]. The PEBAX® coating reduced pure water flux by 29-81%, decreased surface roughness by 35-63%, and caused no measurable change in contact angle. Coated and unmodified control membranes were tested for 106 days in an oil/surfactant emulsion containing 10,000 mg/L of motor oil and 1,000 mg/L of a silicone glycol copolymer. Although the PEBAX®-coated membranes had lower initial water fluxes, they also had slower rates of flux decline, which allowed their water fluxes to surpass the water fluxes of the control membranes after several weeks of operation. Cleaning the membranes at the end of the fouling experiment did not result in any recovery of water flux.

Kang et al. described efforts to modify the surface of a polyamide membrane by grafting aminopoly(ethylene glycol) monomethylether (MPEG-NH_2), using the unreacted acyl chloride groups of the polyamide and the amine functionality of the grafting molecule [41]. MPEG-NH_2 was synthesized from poly(ethylene glycol) monomethylether (MPEG), then the membrane surface was covered with a 5% (w/w) aqueous solution of MPEG-NH_2 for five minutes to effect grafting. ATR-FTIR and XPS were used to confirm grafting of MPEG-NH_2 to the membrane surface. Increased peak intensities were observed in regions attributable to PEG, and the grafted membrane also had higher oxygen and lower nitrogen content than the unmodified membrane, consistent with a PEG-grafted surface. The surface roughness of the membrane increased upon PEG grafting, from 60 nm to 90 nm. In short (2 hour) fouling tests using 100 mg/L of tannic acid or dodecyltrimethylammonium bromide (DTAB), the modified membrane retained more of its initial flux (10% and 15%, respectively) and regained more of its initial flux

after being cleaned with pure water (15% and 20%, respectively) than the unmodified control membrane.

These reports of surface modification of polyamide membranes using PEG-based materials serve as the motivation for the research described in this dissertation.

2.10 References

[1] R.W. Baker, Membrane Technology and Applications, 2nd ed., John Wiley & Sons Ltd., West Sussex, 2004.

[2] J.G. Wijmans, R.W. Baker, The solution-diffusion model: a review, Journal of Membrane Science, 107 (1995) 1-21.

[3] D.R. Paul, Reformulation of the solution-diffusion theory of reverse osmosis, Journal of Membrane Science, 241 (2004) 371-386.

[4] I.N. Levine, Physical Chemistry, 4th ed., McGraw-Hill, Inc., New York, 1995.

[5] C. Fritzmann, J. Löwenberg, T. Wintgens, T. Melin, State-of-the-art of reverse osmosis desalination, Desalination, 216 (2007) 1-76.

[6] R.F. Probstein, Physicochemical Hydrodynamics: An Introduction, 2nd ed., John Wiley & Sons, Inc., New York, 1994.

[7] T.K. Sherwood, P.L.T. Brian, R.E. Fisher, L. Dresner, Salt concentration at phase boundaries in desalination by reverse osmosis, I & EC Fundamentals, 4 (1965) 113-118.

[8] U. Merten, H.K. Lonsdale, R.L. Riley, Boundary-layer effects in reverse osmosis, I & EC Fundamentals, 3 (1964) 210-213.

[9] R. Rautenbach, R. Albrecht, Membrane Processes, John Wiley & Sons Ltd., West Sussex, 1989.

[10] I. Sutzkover, D. Hasson, R. Semiat, Simple technique for measuring the concentration polarization level in a reverse osmosis system, Desalination, 131 (2000) 117-127.

[11] C.E. Reid, E.J. Breton, Water and ion flow across cellulosic membranes, Journal of Applied Polymer Science, 1 (1959) 133-143.

[12] S. Loeb, S. Sourirajan, Sea water demineralization by means of an osmotic membrane, in Advances in Chemistry Series, 38th ed., American Chemical Society, 1963, pp. 117-132.

[13] J.E. Cadotte, R.J. Petersen, Thin-film composite reverse-osmosis membranes: origin, development, and recent advances, in Synthetic Membranes: Desalination, A.F. Turbak (Ed.), ACS Symposium Series, 153rd ed., Vol. 1, American Chemical Society, 1981, pp. 305-326.

[14] J.E. Cadotte, R.J. Petersen, R.E. Larson, E.E. Erickson, A new thin-film composite seawater reverse osmosis membrane, Desalination, 32 (1980) 25-31.

[15] J.E. Cadotte, Interfacially Synthesized Reverse Osmosis Membrane, U.S. Patent 4,277,344, 1981.

[16] R.J. Petersen, Composite reverse osmosis and nanofiltration membranes, Journal of Membrane Science, 83 (1993) 81-150.

[17] R.E. Larson, J.E. Cadotte, R.J. Petersen, Development of the FT-30 thin-film composite membrane for seawater desalting applications, NWSIA Journal, 8 (1981) 15-25.

[18] W.J. Koros, G.K. Fleming, S.M. Jordan, T.H. Kim, H.H. Hoehn, Polymeric membrane materials for solution-diffusion based permeation separations, Progress in Polymer Science, 13 (1988) 339-401.

[19] H. Yasuda, C.E. Lamaze, A. Schindler, Salt rejection by polymer membranes in reverse osmosis. II. ionic polymers, Journal of Polymer Science: Part A-2, 9 (1971) 1579-1590.

[20] G.E. Zaikov, A.L. Iordanskii, V.S. Markin, Diffusion of Electrolytes in Polymers, VSP BV, Utrecht, 1988.

[21] M.J. Kotelyanskii, N.J. Wagner, M.E. Paulaitis, Atomistic simulation of water and salt transport in the reverse osmosis membrane FT-30, Journal of Membrane Science, 139 (1998) 1-16.

[22] J.S. Louie, I. Pinnau, I. Ciobanu, K.P. Ishida, A. Ng, M. Reinhard, Effects of polyether-polyamide block copolymer coating on performance and fouling of reverse osmosis membranes, Journal of Membrane Science, 280 (2006) 762-770.

[23] S.-Y. Kwak, S.G. Jung, Y.S. Yoon, D.W. Ihm, Details of surface features in aromatic polyamide reverse osmosis membranes characterized by scanning electron and atomic force microscopy, Journal of Polymer Science: Part B: Polymer Physics, 37 (1999) 1429-1440.

[24] M. Elimelech, X. Zhu, A.E. Childress, S. Hong, Role of membrane surface morphology in colloidal fouling of cellulose acetate and composite aromatic

polyamide reverse osmosis membranes, Journal of Membrane Science, 127 (1997) 101-109.

[25] E.M. Vrijenhoek, S. Hong, M. Elimelech, Influence of membrane surface properties on initial rate of colloidal fouling of reverse osmosis and nanofiltration membranes, Journal of Membrane Science, 188 (2001) 115-128.

[26] J. Gilron, S. Belfer, P. Vaisanen, M. Nystrom, Effects of surface modification on antifouling and performance properties of reverse osmosis membranes, Desalination, 140 (2001) 167-179.

[27] A.W. Adamson, A.P. Gast, Physical Chemistry of Surfaces, 6th ed., John Wiley & Sons, Inc., New York, 1997.

[28] W. Stumm, Chemistry of the Solid-Water Interface: Processes at the Mineral-Water and Particle-Water Interface in Natural Systems, John Wiley & Sons, Inc., New York, 1992.

[29] M. Elimelech, W.H. Chen, J.J. Waypa, Measuring the zeta (electrokinetic) potential of reverse osmosis membranes by a streaming potential analyzer, Desalination, 95 (1994) 269-286.

[30] A.E. Childress, M. Elimelech, Effect of solution chemistry on the surface charge of polymeric reverse osmosis and nanofiltration membranes, Journal of Membrane Science, 119 (1996) 253-268.

[31] G. Hurwitz, G.R. Guillen, E.M.V. Hoek, Probing polyamide membrane surface charge, zeta potential, wettability, and hydrophilicity with contact angle measurements, Journal of Membrane Science, 349 (2010) 349-357.

[32] J.N. Israelachvili, Intermolecular and Surface Forces, 2nd ed., Academic Press, New York, 1991.

[33] H.J. Kaper, H.J. Busscher, W. Norde, Characterization of poly(ethylene oxide) brushes on glass surfaces and adhesion of Staphylococcus epidermidis, Journal of Biomaterials Science Polymer Edition, 14 (2003) 313-324.

[34] D.K. Han, K.D. Park, K.-D. Ahn, S.Y. Jeong, Y.H. Kim, Preparation and surface characterization of PEO-grafted and heparin-immobilized polyeurethanes, Journal of Biomedical Materials Research: Applied Biomaterials, 23 (1989) 87-104.

[35] E. Ostuni, R.G. Chapman, R.E. Holmlin, S. Takayama, G.M. Whitesides, A survey of structure-property relationships of surfaces that resist the adsorption of protein, Langmuir, 17 (2001) 5605-5620.

[36] P. Kingshott, H. Thissen, H.J. Griesser, Effects of cloud-point grafting, chain length, and density of PEG layers on competitive adsorption of ocular proteins, Biomaterials, 23 (2002) 2043-2056.

[37] J.H. Lee, H.B. Lee, J.D. Andrade, Blood compatibility of polyethylene oxide surfaces, Progress in Polymer Science, 20 (1995) 1043-1079.

[38] D. Leckband, S. Sheth, A. Halperin, Grafted poly(ethylene oxide) brushes as nonfouling surface coatings, Journal of Biomaterials Science Polymer Edition, 10 (1999) 1125-1147.

[39] B. Zdyrko, V. Klep, I. Luzinov, Synthesis and surface morphology of high-density poly(ethylene glycol) grafted layers, Langmuir, 19 (2003) 10179-10187.

[40] B. Zdyrko, S.K. Varshney, I. Luzinov, Effect of molecular weight on synthesis and surface morphology of high-density poly(ethylene glycol) grafted layers, Langmuir, 20 (2004) 6727-6735.

[41] G. Kang, M. Liu, B. Lin, Y. Cao, Q. Yuan, A novel method of surface modification on thin-film composite reverse osmosis membrane by grafting poly(ethylene glycol), Polymer, 48 (2007) 1165-1170.

[42] W.E. Mickols, Composite Membrane with Polyalkylene Oxide Modified Polyamide Surface, U.S. Patent 6,280,853 B1, 2001.

[43] M.C. Wilbert, J. Pellegrino, A. Zydney, Bench-scale testing of surfactant-modified reverse osmosis/nanofiltration membranes, Desalination, 115 (1998) 15-32.

[44] G. Pearce, S. Talo, K. Chida, A. Basha, A. Gulamhusein, Pretreatment options for large scale SWRO plants: case studies of UF trials at Kindasa, Saudi Arabia, and conventional pretreatment in Spain, Desalination, 167 (2004) 175-189.

[45] D. Vial, G. Doussau, The use of microfiltration membranes for seawater pre-treatment prior to reverse osmosis membranes, Desalination, 153 (2002) 141-147.

[46] S. Belfer, J. Gilron, Y. Purinson, R. Fainshtain, N. Daltrophe, M. Priel, B. Tenzer, A. Toma, Effect of surface modification in preventing fouling of commercial SWRO membranes at the Eilat seawater desalination pilot plant, Desalination, 139 (2001) 169-176.

[47] M. Çakmakci, N. Kayaalp, I. Koyuncu, Desalination of produced water from oil production fields by membrane processes, Desalination, 222 (2008) 176-186.

[48] A.C. Sagle, E.M. Van Wagner, H. Ju, B.D. McCloskey, B.D. Freeman, M.M. Sharma, PEG-coated reverse osmosis membranes: desalination properties and fouling resistance, Journal of Membrane Science, 340 (2009) 92-108.

[49] S. Belfer, Y. Purinson, R. Fainshtein, Y. Radchenko, O. Kedem, Surface modification of commercial composite polyamide reverse osmosis membranes, Journal of Membrane Science, 139 (1998) 175-181.

[50] S. Belfer, Y. Purinson, O. Kedem, Surface modification of commercial polyamide reverse osmosis membranes by radical grafting: an ATR-FTIR study, Acta Polymerica, 49 (1998) 574-582.

[51] S. Belfer, J. Gilron, O. Kedem, Characterization of commercial RO and UF modified and fouled membranes by means of ATR/FTIR, Desalination, 124 (1999) 175-180.

[52] V. Freger, J. Gilron, S. Belfer, TFC polyamide membranes modified by grafting of hydrophilic polymers: an FT-IR/AFM/TEM study, Journal of Membrane Science, 209 (2002) 283-292.

This page is intentionally left blank

3 EXPERIMENTAL MATERIALS AND METHODS

This chapter describes the materials, equipment and procedures used in the membrane characterization and modification studies described in this dissertation.

3.1 Materials

3.1.1 Commercial Membranes

Three types of polyamide thin film composite membranes manufactured by Dow Water & Process Solutions (Edina, MN) were used in this work. Membranes were supplied as glycerin-dried flat sheets for laboratory studies; however, in practice they are used in a spiral wound module form. The LE, or low energy, and XLE, or extra low energy, membranes are brackish water reverse osmosis (RO) membranes, while the NF90 is a nanofiltration, or loose RO, membrane. All three have the same general chemical structure (cf. Figure 2.4), with proprietary additives and slight changes in polymerization conditions giving rise to differences in water and salt permeance. Glycerin was applied to the membranes by the manufacturer to prevent collapse of the polysulfone membrane support structure during shipment and storage (i.e., before the membranes are contacted with water for use), and must be removed before membrane testing. Membranes were soaked in 25% (v/v) aqueous isopropanol (Sigma-Aldrich, St. Louis, MO) solutions for twenty minutes, then placed in pure water to remove glycerin.

In a 2000 mg/L NaCl feed at 150 psig (10.3 bar) feed pressure (permeate pressure is atmospheric) and pH 8 and 25°C, the LE membrane achieves a water flux of 50 L/(m^2 h) (LMH) [1]. The performance of the XLE membrane is specified at a lower feed concentration and pressure (500 mg/L NaCl feed, 100 psig (6.9 bar) feed pressure), giving a water flux of 49 LMH [2]. The NF90 membrane performance is specified at 70 psig (4.8 bar) feed pressure for a 2000 mg/L NaCl feed, giving a water flux of 40 LMH [3]. However, to better compare the behavior of all three unmodified membranes, test conditions for the XLE and NF90 membranes were matched to those of the LE membrane (2000 mg/L NaCl feed at 150 psig (10.3 bar) feed pressure at pH 8 and 25°C). Using the water permeance (A) values of the XLE and NF90 membranes, the corresponding water fluxes at these conditions are 65 and 107 LMH, respectively. Water flux can vary by as much as +25/-15%, thus a range of water permeance, salt permeance, and water flux is expected in practice [1-3]. However, salt rejection specifications are narrower. Minimum salt rejection is the lowest acceptable rejection for the membrane, while stabilized salt rejection is the expected steady-state rejection during extended use. The salt rejection values reported by the manufacturer account for the effects of concentration polarization, and are, therefore, true salt rejection values. The performance specifications of all three membranes are given in Table 3.1.

Table 3.1. Water permeance, salt permeance, and NaCl rejection values specified by Dow Water & Process Solutions for the LE, XLE, and NF90 membranes.

	LE	**XLE**	**NF90**
Type	**RO**	**RO**	**NF**
Water permeance (A) ($L/(m^2\ h\ bar)$)	5.9 (5.0 – 7.4)	7.7 (6.5 – 9.6)	12.3 (10.5 – 15.4)
Water flux at 150 psig (10.3 bar) ($L/(m^2\ h)$)	50 (42 - 62)	65 (55 – 81)	107 (91 – 134)
Salt permeance (B) ($L/(m^2\ h)$)	0.51 (0.43 – 0.63)	1.3 (1.1 – 1.7)	18.9 (16.0 – 23.6)
True NaCl rejection (minimum and stabilized) (%)	99.0 – 99.3	98.0 – 99.0	85-95

Commercial membranes of different water permeance values were chosen so that modified and unmodified membranes having similar water flux could be compared. Modification decreases water permeance, so membranes with higher water permeance (i.e., XLE and NF90) were used for modification and their performance was compared to that of unmodified membranes having a lower water permeance (i.e., LE). The motivation for this approach is based on previous observations that fouling rate increases with increasing water flux for reverse osmosis membranes [4]. Therefore, attempting to compare modified and unmodified membranes of the same (or similar) water flux is useful to minimize the effect of water flux on fouling rate.

3.1.2 Poly(ethylene glycol) Diglycidyl Ether

Grafting poly(ethylene glycol) (PEG) to the surface of a polyamide membrane requires a reactive endgroup on the PEG molecule compatible with a reactive group present on the membrane surface. Polyamide membranes have free carboxylic acid and primary amine groups (cf. Figure 2.4, free carboxylic acids on chain ends and on unc rosslinked trimesoyl chloride molecules that hydrolyze following polymerization, and free primary amines on chain ends [5]) available for chemical reaction with a grafting molecule. Epoxides are known to react with amines and carboxylic acids [6], so a PEG molecule with epoxy endgroups, poly(ethylene glycol) diglycidyl ether (PEGDE), was chosen for grafting to the polyamide membrane surface. Mickols first recognized the potential use of PEGDE for chemical grafting to improve polyamide membrane fouling resistance [7]. PEGDE was purchased from Polysciences, Inc. (Warrington, PA) and used as received.

The chemical structure of PEGDE is given in Figure 3.1. The difunctional epoxide was chosen over a monofunctional epoxide because it is commercially available with several different PEG molecular weights (MW 200, 400, 600 and 1000, or $\bar{n}$ 4, 9, 13 and 22, respectively), whereas the monofunctional analog is not readily available and would have

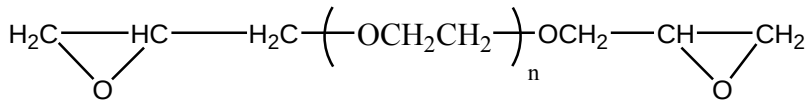

Figure 3.1. Chemical structure of poly(ethylene glycol) diglycidyl ether (PEGDE), where n is the number of repeat ethylene oxide units (n ≈ 4, 9, 13 and 22).

to be synthesized and purified before use. The highest and lowest molecular weights available (i.e., MW 200 and 1000) were chosen for this work. The molecular weights of the complete molecules, including the PEG and diglycidyl ether groups, are 330 and 1130 g/mol, respectively. While MW 200 PEGDE is a liquid, MW 1000 PEGDE is a waxy solid that must be melted prior to mixing with water (PEGDE modification was performed using aqueous treatment solutions).

Although both amine and carboxylic acid groups will react with epoxides, amines are more basic and therefore more nucleophilic than carboxylic groups, so amines react more readily with electrophilic reagents such as epoxides [8]. Figure 3.2 shows the expected reaction between an epoxide and an amine chain end of the polyamide membrane. The position of amine attack is determined by steric hindrance and the electron-withdrawing tendency of the epoxide substituents, so attack on the CH_2 carbon is expected, as depicted in Figure 3.2 [9]. PEGDE could potentially react with two amine sites on the membrane surface, generating a loop on the surface instead of the brush which would result from a single epoxide endgroup attaching to the surface.

3.1.3 Water

Ultrapure water from a Millipore MilliQ system (18.2 MΩ-cm, 1.2 μg/L TOC) (Billerica, MA) was used in all experiments (i.e., soaking, modification and testing). Feed pH was adjusted using sodium bicarbonate (Sigma-Aldrich, St. Louis, MO), hydrochloric acid (Ricca Chemical, Fisher Scientific, Pittsburgh, PA) and sodium hydroxide (Fisher Scientific, Pittsburgh, PA). Sodium chloride was purchased from Fisher Scientific (Pittsburgh, PA).

3.1.4 Foulants

The oil chosen for use in emulsion fouling testing was *n*-decane, purchased from Alfa Aesar and used as received (Ward Hill, MA). Although produced water can contain many different oil components, *n*-decane was chosen as a simple representative hydrocarbon. The chemical structures of the surfactants chosen for study, cationic dodecyltrimethylammonium bromide (DTAB) and anionic sodium dodecyl sulfate (SDS) (Sigma-Aldrich, St. Louis, MO), are given in Figure 3.3. Charged surfactants were chosen to investigate the effect of electrostatic interactions on membrane fouling behavior. The surfactants chosen for study are simple and well-studied cationic and anionic surfactant analogs for more complex surface active molecules that are typically present in produced water [10].

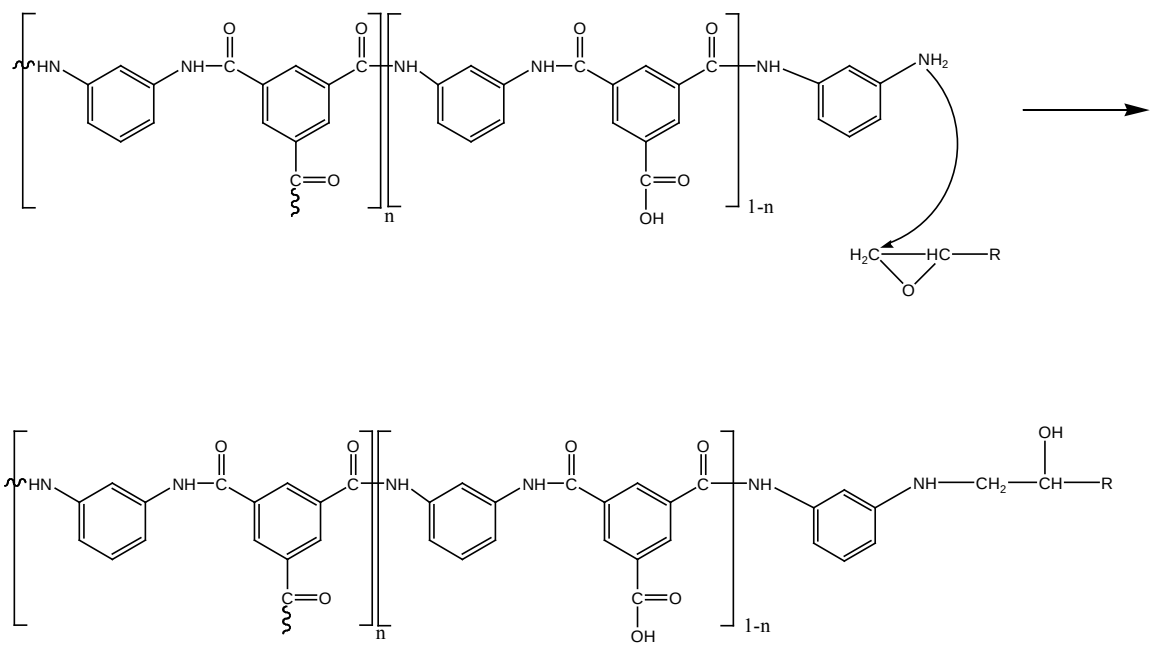

Figure 3.2. *Predicted reaction between a primary amine chain end of the polyamide membrane with an epoxide molecule. Note that since the epoxide chosen for study is difunctional, reaction may occur at both epoxide endgroups, forming loops instead of the brush structure depicted in this figure.*

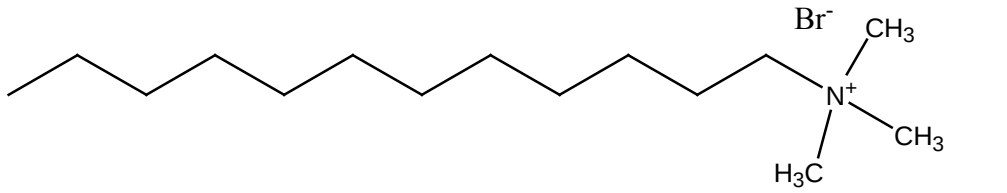

(a)

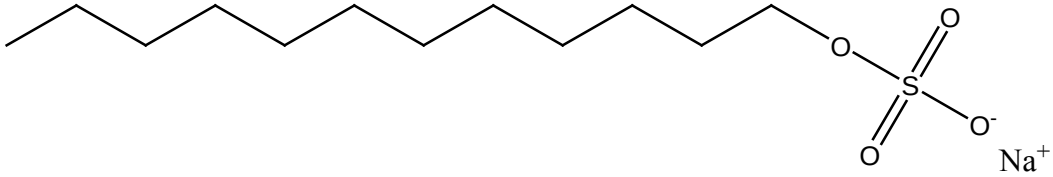

(b)

Figure 3.3. *Chemical structure of (a) dodecyltrimethylammonium bromide (DTAB) and (b) sodium dodecyl sulfate (SDS).*

3.2 Methods

3.2.1 Membrane Storage, Handling, and Pretreatment

Polyamide membrane rolls were stored vertically (to avoid applying weight to the delicate polyamide layer) in a cool, dark place. The membranes are known to age chemically in air due, presumably, to oxidation of residual functional groups on the surface of the membrane. Oxidation can contribute to variability in membrane properties. Therefore, before membrane samples were cut for each test, several (4-5) rotations of membrane were unrolled and discarded. Samples were cut larger than the active area of the membrane test cells, so that the area tested was not touched during handling or loading into the crossflow test cells.

Pretreatment procedures from the manufacturer were followed for the three membranes used in this study. LE, XLE, and NF90 flat-sheet membrane coupons were soaked in 25% (v/v) aqueous isopropanol solutions for twenty minutes, then placed in pure water to remove glycerin. The soaking water was changed three times, and membranes were left to soak overnight (~ 16 – 24 hours, covered to prevent exposure to light, which can speed chemical degradation of the polyamide layer) before modification and/or testing.

3.2.2 Modification Methods

3.2.2.1 Dip Coating

Submersion in aqueous PEGDE solutions was the first method explored for grafting PEGDE to the polyamide membrane surface. The appropriate amount of ultrapure water was heated to a given temperature (typically 40°C), a specific amount of PEGDE was added to the heated water (shaking and stirring to completely dissolve all PEGDE) and the membrane (50 mm diameter circle) was then immediately submerged in the solution. A total of 200 grams of solution was used for dip coating. The reaction was allowed to proceed for a set length of time (typically ten minutes), then the membrane was rinsed with copious amounts of pure water to remove residual PEGDE that may have adsorbed to the membrane surface. Modified membranes were stored in pure water until use. Unmodified membranes were treated in the same manner, using 200 grams of ultrapure water (i.e., no PEGDE).

3.2.2.2 Spin Coating

Dip coating, although straightforward, has potential drawbacks including contact between the membrane backing and the PEGDE solution. PEGDE that adsorbs to the backing could lower the water flux of the modified membrane but would not afford any improvement in fouling resistance, since the fouling solution does not come into direct contact with the backing. Spin coating, using a single wafer spin processor (Model WS-400E-6NPP-LITE, Laurell Technologies Corporation, North Wales, PA), was explored as one possible alternative to dip coating. Preparation of the aqueous PEGDE solution was

similar to the dip coating procedure: water was heated to 40 °C before the PEGDE was added and completely dissolved in the water. The membrane was taped to a silicon wafer and spun at 1000 rpm for a set time (20-60 seconds). A specific volume of the aqueous PEGDE solution (5-50 ml) was slowly poured over the membrane surface during spinning. At the end of the spin time, the membrane was detached from the silicon wafer, rinsed with pure water and stored in pure water until use. Unmodified membranes were treated in a similar manner, but were spun with water only (i.e., no PEGDE).

3.2.2.3 Top Surface Treatment

Spin coating was found to be poorly reproducible, possibly due to the low viscosity of the aqueous PEGDE solutions. Additionally, spin coating would be impractical for scale up to industrial membrane modification, since membranes are typically manufactured as sheets that are several hundred meters in length. Isolation of the active polyamide surface for contact and reaction with the PEGDE solution was one desirable feature of the spin coating method incorporated into a static top surface treatment method, depicted in Figure 3.4. This method, like spin coating, is expected to prevent adsorption of PEGDE to the reinforcing fabric backing or the porous polysulfone support upon which the polyamide layer is formed. Preparation of the aqueous PEGDE solution was similar to the previous procedures (the appropriate amount of ultrapure water was heated to 40 °C, immediately combined with the corresponding amount of PEGDE and shaken until the PEGDE was completely dissolved), with a total of ten grams of solution used for treatment. The membrane (11 × 11 cm^2) was placed in a petri dish with a glass casting ring (10 cm diameter) on the polyamide surface, creating a well for the aqueous PEGDE solution. Pressure was applied to the casting ring as the heated aqueous PEGDE solution was poured onto the membrane surface, creating a seal preventing the solution from leaking around the edges of the membrane. After ten minutes, the membrane was removed, rinsed several times with pure water, soaked in a 25 % (v/v) aqueous isopropanol solution for ten minutes to remove any residual unreacted PEGDE, rinsed again several times with pure water and, finally, stored in pure water until use. Unmodified membranes were treated in the same manner, using ten grams of ultrapure water rather than an aqueous solution containing PEGDE.

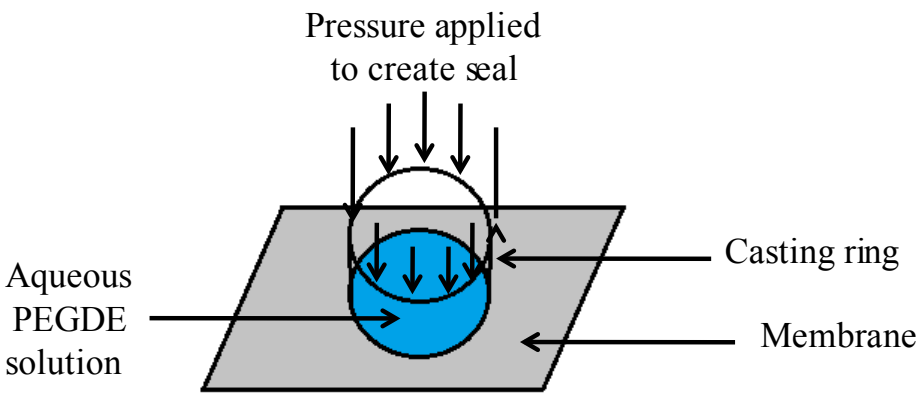

Figure 3.4. Top surface treatment method for membrane modification.

3.2.3 Dead End Testing

Although dead end testing is not recommended for determining rejection or fouling resistance due to polarization, it can be used as a fast, simple method of measuring pure water flux. Figure 3.5 illustrates a dead end cell (HP4750 stirred cell, Sterlitech Corporation, Kent, WA), where the feed (water) is pressurized using air, and the product permeating through the membrane is collected in a graduated cylinder.

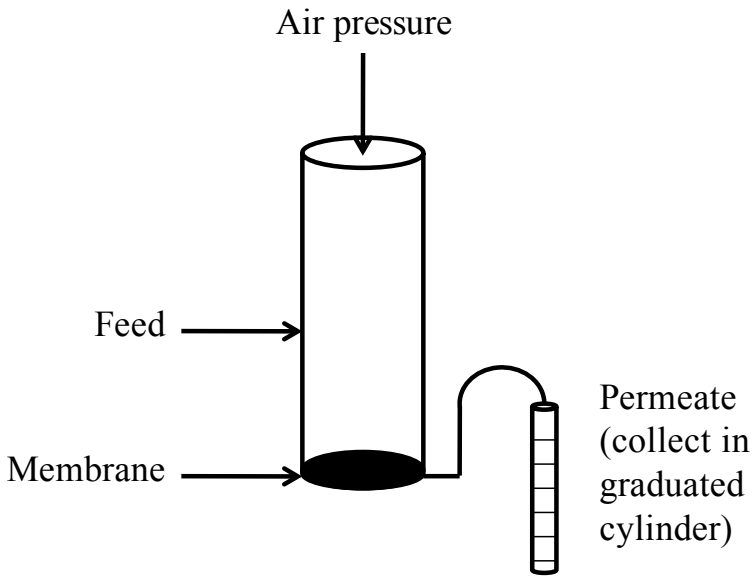

Figure 3.5. Schematic of dead end test cell.

3.2.4 Crossflow Testing

3.2.4.1 Crossflow Apparatus

All experiments (with the exception of some tests used to screen modified membranes for pure water flux) were conducted using a crossflow filtration system supplied by Separation Systems Technology (San Diego, CA) and shown schematically in Figure 3.6. The crossflow system consists of three stainless steel test cells connected in series to a 30 L feed tank, a positive displacement pump and pulsation dampener (Hydra-Cell, Wanner Engineering Inc., Minneapolis, MN), a back pressure regulator and bypass valve (Swagelok, Solon, OH) to independently control pressure (3.5-34.5 bar) and flowrate (0.8-7.6 L/min), and a pressure gauge (WIKA Instrument Corporation, Lawrenceville, GA) and flow meter (King Instrument Company, Garden Grove, CA). A system of valves connected with chemical resistant tubing (Tygon 2075, USP Plastic Corp., Lima, OH) allows feed solutions to be continuously passed through a filter (KX CTO/2 carbon block carbon/5 μm particle filter, Big Brand Water Filter, Chatsworth, CA) to prevent bacterial growth and particulate fouling, or the filter can be bypassed to determine of the effect of an unfiltered feed on membrane performance. All wetted parts of the system are stainless steel, with the exception of the chemical resistant tubing leading to and from the filter and the filter housing and feed tank, which are made of polyethylene. The feed temperature was maintained at 24-25°C by circulating chilled water from a refrigerated bath (Thermo Neslab RTE-10 Digital One Refrigerated Bath, Thermo Fisher Scientific, Inc., Waltham, MA) through a stainless steel coil in the feed tank. Feed pH was monitored using a pH meter (Accumet Research AR25 Dual Channel pH/Ion Meter, Fisher Scientific, Pittsburgh, PA). The test cell dimensions are 82 mm × 32 mm × 3 mm (l × w × h), with an active membrane surface area of 1.82×10^{-3} m^2. The feed encounters a 90° bend as it enters the test channel. Turbulence spacers are not employed in the test cells. Six equally spaced bolts around the periphery of the cell secure the cell lid to the base. The permeate stream from each membrane was collected in a beaker on a balance connected to a LabVIEW data acquisition program (National Instruments, Austin, TX) for continuous monitoring of water flux.

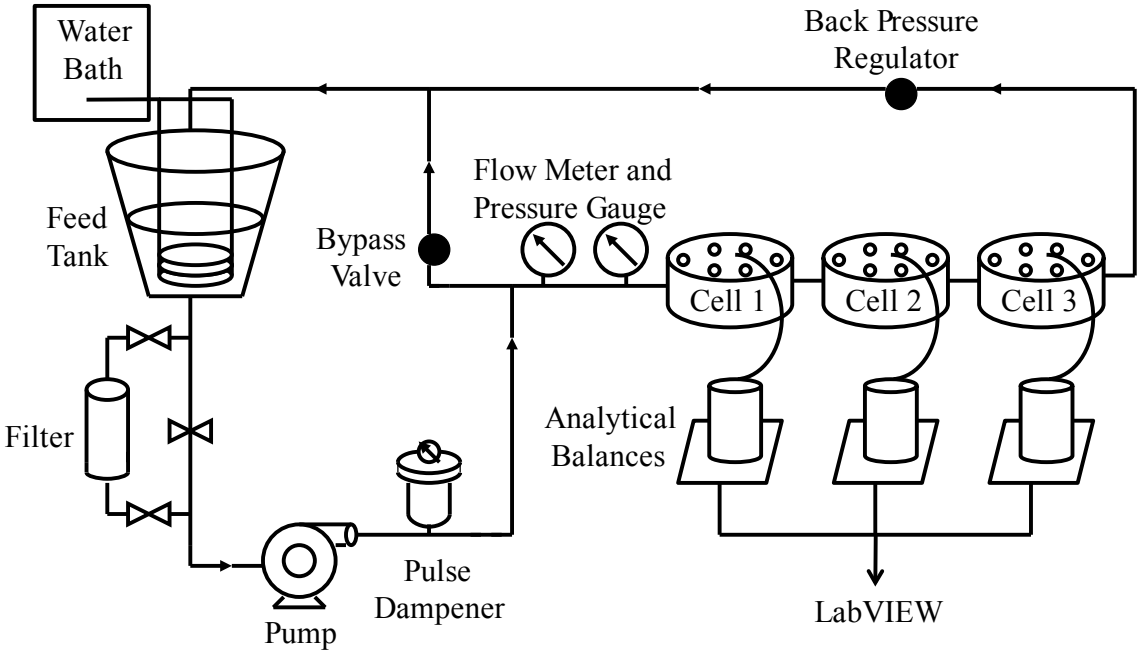

Figure 3.6. Schematic of crossflow filtration system.

3.2.4.2 Cleaning Protocol

The crossflow system was cleaned before each experiment. A 200 mg/L bleach solution (3.4 g Clorox®/L) was first circulated for one hour (feed pH ~ 9.5) to disinfect the system. If the previous experiment used a feed containing only sodium chloride (i.e., no oil or surfactant), disinfection was followed by rinsing four times with pure water to remove the bleach from the system (polyamide RO membranes are sensitive to chlorine [11]). For each rinse cycle, the system was filled with pure water, circulated for at least 10 minutes and then drained. After four rinse cycles, the feed pH was ~ 6 (i.e., the pH of water equilibrated with atmospheric CO_2 [12]) and the feed conductivity was less than 15 μS/cm, indicating essentially all residual salt (from previous experiments) had been removed from the system. The cleaning procedure following fouling experiments was slightly different. After bleach disinfection, the system was rinsed once with water, followed by circulation of a 0.25% (v/v) aqueous solution of Nalgene L900 liquid detergent (Fisher Scientific, Pittsburgh, PA) for one hour to remove residual organic components (i.e., surfactant and/or oil). The system was then rinsed four times with pure water, similar to the procedure used following sodium chloride feed water tests.

3.2.4.3 Fouling Test Procedure

Fouling experiments, using either a charged surfactant (DTAB or SDS, cf. Figure 3.3(a) or 3.3(b), respectively) or an oil-in-water emulsion containing a 9:1 ratio of *n*-decane and a charged surfactant, were performed in the crossflow system according to the protocol outlined in Figure 3.7. Figure 3.7(a) outlines the procedure followed for all fouling tests,

while Figure 3.7(b) illustrates the typical trend in water flux with time observed during a fouling experiment. A total concentration of 150 mg/L was used regardless of whether the foulant was a surfactant alone or an oil-in-water emulsion. In each experiment, three different membranes were tested simultaneously, typically one unmodified membrane and two modified membranes. The applied transmembrane pressure difference (Δp) was 10.3 bar in all experiments, unless stated otherwise, and the feed flowrate in all experiments was 4 L/min, which corresponds to a Reynolds number of 2200 in these crossflow cells. First, water flux was monitored for thirty minutes in a pure water feed ($J_{w(pw)}$) (pH was adjusted to ~ 8 with sodium bicarbonate, $NaHCO_3$). Next, 2000 mg/L NaCl was added to the feed, and water flux ($J_{w(NaCl)i}$) and NaCl rejection ($R_{NaCl,i}$) were measured. At one hour, the foulant (i.e., dissolved surfactant or oil-in-water emulsion) was introduced to the system. For surfactant tests, the surfactant was dissolved in 1 L of feed water before being added to the system. For emulsion tests, the oil and surfactant were blended with 1 L of feed water in a Waring three speed commercial blender (Waring Products, Torrington, CT) on its highest speed setting for three minutes before being added to the system. Water flux was monitored for the next twenty-three hours (the final water flux at the end of this time is $J_{w(foul)}$), and NaCl rejection ($R_{foulant}$) and organic rejection were measured at the end of the fouling portion of the test. The fouling feed was then drained from the feed tank and pure water was used to flush any residual fouling feed from the system before refilling the feed tank with pure water. Next, the membranes were subjected to a representative, two hour industrial cleaning protocol to remove foulants from the membrane surface [13, 14]. Foulants that can be removed by cleaning contribute to reversible fouling, while irreversible fouling causes permanent flux loss (i.e., fouling cannot be reversed by cleaning) [15, 16]. During the first hour of cleaning, the feed pH was increased to approximately 12 using NaOH (to remove adsorbed organic and biofoulants), then the feed pH was lowered to below 3 using HCl. Unlike some other chemical cleaning agents, using NaOH and HCl for cleaning does not introduce any new chemical constituents to the system. After the second hour of cleaning, the feed was again drained from the feed tank and replaced with an aqueous solution containing 2000 mg/L NaCl; using this solution as the feed, the flux recovery ($J_{w(NaCl)f}$) and NaCl rejection ($R_{foulant,f}$) after cleaning were determined. The feed was circulated through the system with no feed filtration at all times during these experiments, with the exception of the two hour cleaning portion, when the feed was continuously filtered through the carbon and particle filter to remove any residual foulants. The temperature in the feed tank was maintained at 24-25°C at all times, except during the first hour of the cleaning procedure (high pH), when the refrigerated bath was turned off.

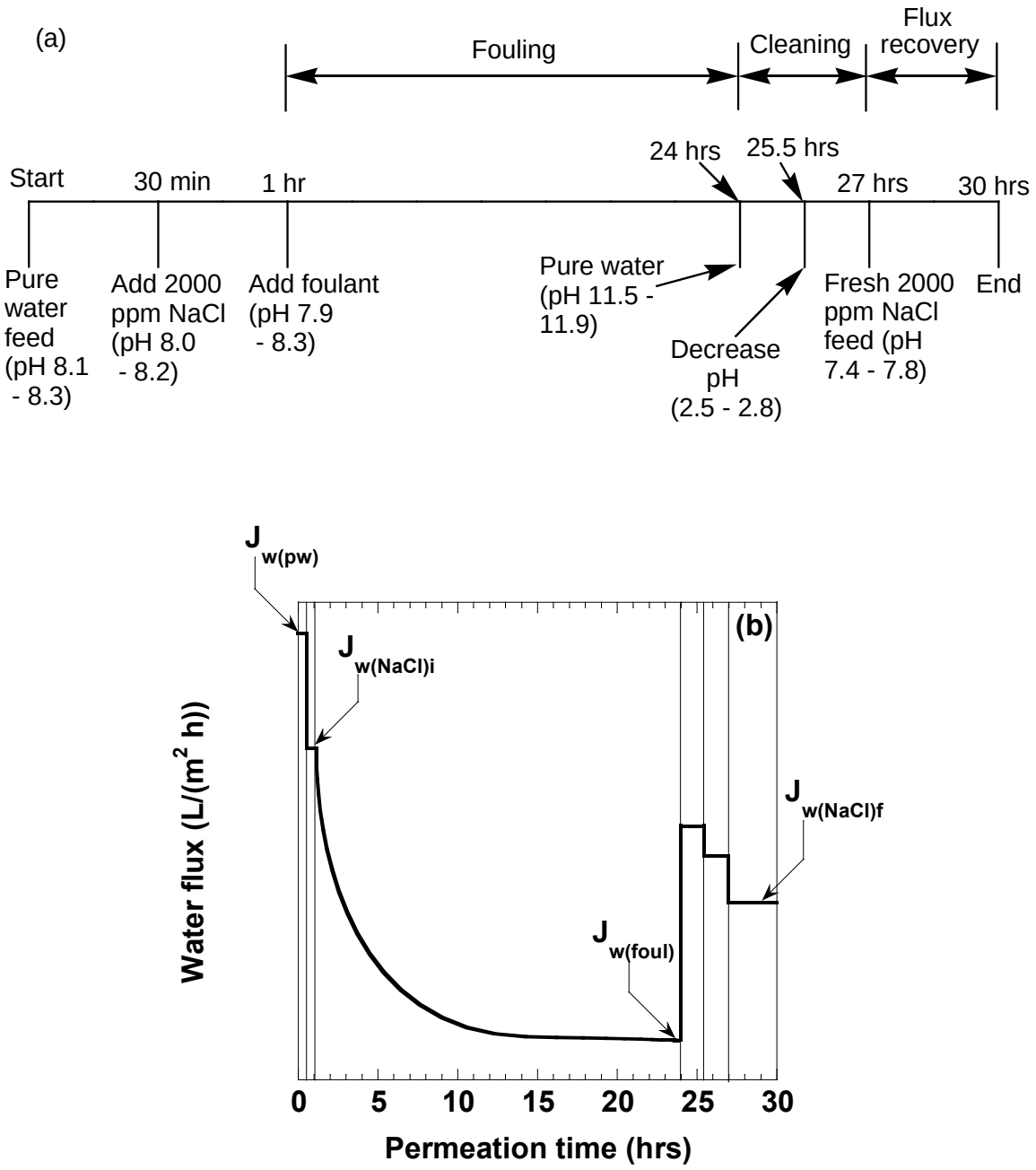

Figure 3.7. (a) Timeline and (b) typical observed water flux during a crossflow fouling experiment.

3.2.4.4 Rejection Measurements

In all experiments (i.e., fouling and sodium chloride feeds), sodium chloride content was determined by measuring ion concentration using a conductivity meter (Oakton CON 110 Advanced M eter, Fisher S cientific, P ittsburgh, P A). A c alibration c urve a llowed

determination of NaCl concentration from measured solution conductivity. Apparent and true NaCl rejections were calculated using Equations 2.25 and 2.34, respectively.

In fouling tests, organic carbon concentration was determined using a Shimadzu 5050A Total Organic Carbon Analyzer (Columbia, MD). Samples were analyzed immediately after collection, and organic rejection was calculated using the measured feed and permeate concentrations ($c_{org,feed}$ and $c_{org,perm}$, respectively, in mg/L), according to the following equation:

$$R_{organic} = \left(1 - \frac{c_{org,perm}}{c_{org,feed}}\right) \times 100\% \tag{3.1}$$

3.2.5 Surface Characterization

3.2.5.1 ATR-FTIR

Attenuated total reflectance Fourier transform infrared spectroscopy (ATR-FTIR) was used to characterize the structure of modified and control membranes. These experiments were performed using a Thermo Nicolet Nexus 470 FTIR with an Avatar Smart MIRacle ATR accessory and a ZnSe crystal (Madison, WI). Spectra were collected in air, in the mid-infrared region (400-4000 cm^{-1}), using 128 scans at resolution 4 (1.928 cm^{-1} spacing). Data analysis was performed using the Omnic software provided with the instrument. The sampling depth of ATR-FTIR is approximately 1 μm [17], thus spectra of composite membranes include the polyamide active layer (~0.1 μm thickness), as well as the polysulfone support layer.

3.2.5.2 XPS

X-ray photoelectron spectroscopy (XPS) was used to characterize the surface elemental content of modified and unmodified membranes. XPS probes a maximum depth of ~10 nm (at 0° takeoff angle, i.e., perpendicular to the membrane surface), making it a better choice than ATR-FTIR for detection of the polyamide layer (~0.1 μm) and any surface changes effected by PEGDE grafting. Surface scans were performed using an AXIS Ultra DLD XPS (Kratos Analytical Company, Chestnut Ridge, NY) equipped with a monochromatic Al $K\alpha_{1,2}$ x-ray source (2×10^{-9} Torr chamber pressure, 15 kV, 150 W). Carbon (1s), nitrogen (1s), oxygen (1s), and sulfur (2p) were detected using either a 0° or 45° takeoff angle (to probe an even thinner surface layer). A 300 μm × 700 μm area was analyzed, and a charge neutralizer was used to minimize sample charging. Sample analysis was performed by Dr. Hugo Celio at the Texas Materials Institute at the University of Texas at Austin.

3.2.5.3 Graft Density

The grafting density of PEGDE on the membrane surface (μg/cm^2) was measured using a Rubotherm Magnetic Suspension Balance with 1 μg resolution (Rubotherm GmbH,

Bochum, Germany). A diagram of the apparatus appears in Figure 3.8. An electronic control unit allows the sample pail to be raised to the measuring point and lowered to the zero point positions. Membrane samples were placed in the sample pail while in the zero point position and then raised to the measuring point position. The average difference between the measuring point and zero point balance readings (five measurements) was taken to be the mass of the pail and samples.

Twelve 1 in^2 pieces of membrane were used for grafting density experiments, in order to fit the samples into the sample pail. Membranes were pretreated following the manufacturer's recommendations, dried under vacuum for one hour and then allowed to equilibrate in air for ninety minutes before measurement. Following the mass measurement, membranes were treated with PEGDE, dried under vacuum for one hour and allowed to equilibrate in air for ninety minutes before measuring the mass of the

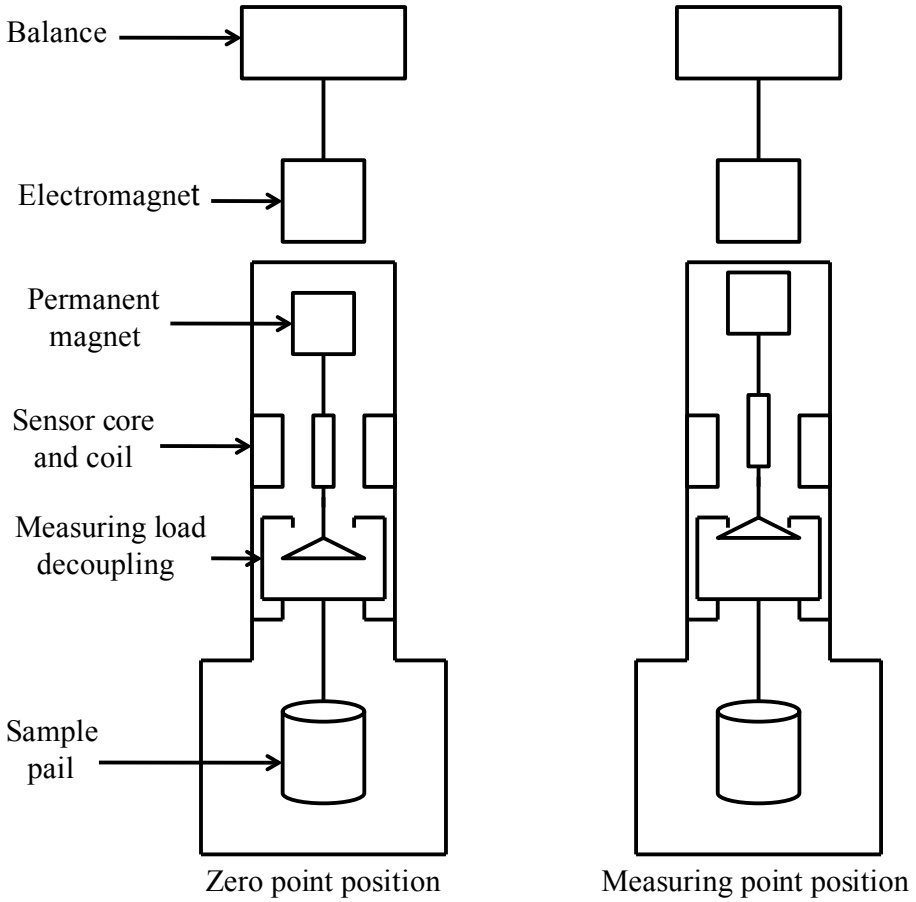

Figure 3.8. Schematic of the magnetic suspension balance, including zero point and measuring point positions. modified membranes and sample pail. Subtraction of the mass measured before modification from the mass measured after PEGDE modification gave the mass of PEGDE on the modified membrane surface.

3.2.5.4 Zeta Potential

Zeta potential was measured using an Anton Paar SurPASS Electrokinetic Analyzer and associated software (Anton Paar USA, Ashland, VA). Two membrane samples separated by a spacer were loaded into the clamping cell, creating a channel for electrolyte flow. A 10 mM NaCl solution was used as the background electrolyte for all experiments. Streaming potential was measured as a function of feed pH, and the Fairbrother-Mastin approximation was used in the calculation of zeta potential from streaming potential (cf. Equations 2.36 - 2.38). Before the start of each experiment, the feed pH was manually adjusted to pH 9 using 0.1 M NaOH. A 0.1 M HCl solution was then added automatically during each run, to decrease pH from 9 to 3. Four measurements, two in each flow direction (left to right and right to left), were made at each pH, and the average and standard deviation of those four values is reported. For experiments investigating the effect of charged surfactant on zeta potential, 150 mg/L of either DTAB or SDS was added to the electrolyte solution.

3.2.5.5 AFM

Surface roughness was analyzed by atomic force microscopy (AFM) using a Digital Instruments Dimension 3100 atomic force microscope with a Nanoscope IV controller (Woodbury, NY). Samples were dried under vacuum prior to analysis. AFM images were acquired under ambient conditions in intermittent contact mode at a 1 Hz scan rate and 256 × 256 pixel resolution with silicon cantilevers (spring constant ~ 50 N/m). The tapping mode (i.e., intermittent contact mode) was used to prevent damage to the membrane surface. Two different positions were analyzed for each membrane, each over a 5 μm × 5 μm area. Surface roughness was calculated using the data analysis software provided by the manufacturer. Sample analysis was performed by Dr. Young-Hye Na at the IBM Almaden Research Center in San Jose, CA.

3.2.5.6 Contact Angles

Contact angle analysis was performed using a Ramé-Hart Model 500 Advanced Goniometer/Tensiometer with DROPimage Advanced software version 2.4 (Ramé-Hart Instrument Co., Netcong, NJ). Figure 3.9 illustrates the experimental apparatus used for measuring oil-in-water contact angles. A strip of membrane was mounted in a sample holder with the interfacially polymerized polyamide layer facing down. A Gilmont Instruments 0.2 ml micrometer syringe (Cole-Parmer, Vernon Hills, IL) with a hooked needle was used to dispense *n*-decane droplets onto the polyamide surface of the membrane. Ultrapure water was used as the surrounding fluid. The reported contact angle is the average value of the left and right side contact angles (measured through the water phase) obtained for at least three oil droplets placed and advanced (or grown) at different positions along the length of the membrane. The advancing contact angle so measured is more reliable and reproducible than the receding contact angle. A smaller angle indicates a more hydrophilic surface.

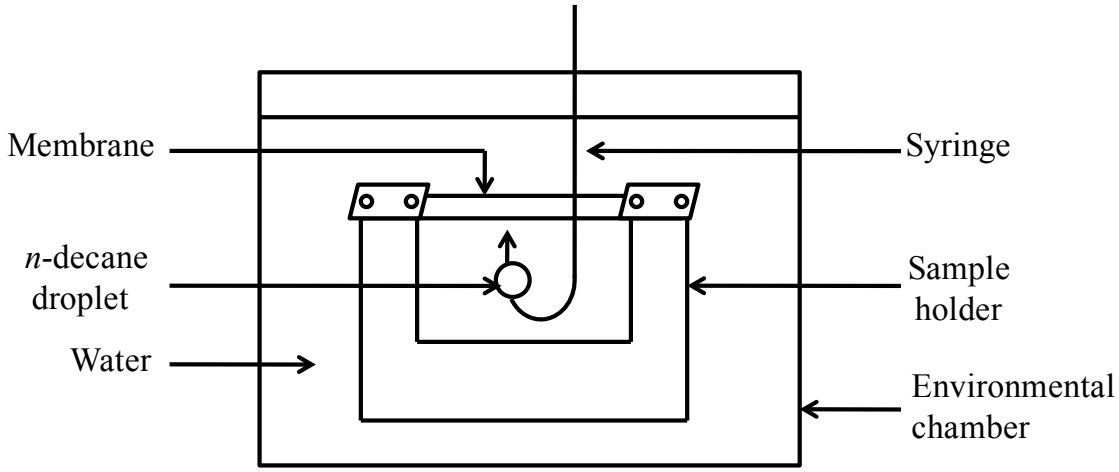

Figure 3.9 Apparatus used for captive bubble measurements of oil-in-water contact angles. The oil droplet is released under water, below the active surface of the membrane (sample is loaded with active side facing down), and floats up to the membrane surface.

3.3 References

[1] Dow Water & Process Solutions LE-400 Product Specification, http://www.dow.com/liquidseps/prod/le_400.htm.

[2] Dow Water & Process Solutions XLE-440 Product Specification, http://www.dow.com/liquidseps/prod/xle_440.htm.

[3] Dow Water & Process Solutions NF90-400 Product Specification, http://www.dow.com/liquidseps/prod/nf90_400.htm.

[4] X. Zhu, M. Elimelech, Colloidal fouling of reverse osmosis membranes: measurements and fouling mechanisms, Environmental Science and Technology, 31 (1997) 3654-3662.

[5] R.J. Petersen, Composite reverse osmosis and nanofiltration membranes, Journal of Membrane Science, 83 (1993) 81-150.

[6] R.A. Kudva, H. Keskkula, D.R. Paul, Compatibilization of nylon 6/ABS blends using glycidyl methacrylate/methyl methacrylate copolymers, Polymer, 39 (1998) 2447-2460.

[7] W.E. Mickols, Composite Membrane with Polyalkylene Oxide Modified Polyamide Surface, U.S. Patent 6,280,853 B1, 2001.

[8] E.V. Anslyn, D.A. Dougherty, Modern Physical Organic Chemistry, 10th ed., University Science Books, Sausalito, CA, 2006.

[9] R.E. Parker, N.S. Isaacs, Mechanisms of epoxide reactions, Chemical Reviews, 59 (1959) 737-799.

[10] J.A. Veil, M.G. Puder, D. Elcock, R.J. Redweik, A White Paper Describing Produced Water from Production of Crude Oil, Natural Gas, and Coal Bed Methane, Contract No. W-31-109-Eng-38; U.S. Department of Energy National Energy Technology Laboratory, Argonne National Laboratory, 2004.

[11] R.W. Baker, Membrane Technology and Applications, 2nd ed., John Wiley & Sons Ltd., West Sussex, 2004.

[12] V.L. Snoeyink, D. Jenkins, Water Chemistry, John Wiley & Sons, New York, 1980.

[13] J. Gilron, S. Belfer, P. Vaisanen, M. Nystrom, Effects of surface modification on antifouling and performance properties of reverse osmosis membranes, Desalination, 140 (2001) 167-179.

[14] W.E. Mickols, Dow Water & Process Solutions, personal communication, 2008.

[15] H. Choi, K. Zhang, D.D. Dionysiou, D.B. Oerther, G.A. Sorial, Effect of permeate flux and tangential flow on membrane fouling for wastewater treatment, Separation and Purification Technology, 45 (2005) 68-78.

[16] F. Wang, V.V. Tarabara, Pore blocking mechanisms during early stages of membrane fouling by colloids, Journal of Colloid and Interface Science, 328 (2008) 464-469.

[17] V. Freger, J. Gilron, S. Belfer, TFC polyamide membranes modified by grafting of hydrophilic polymers: an FT-IR/AFM/TEM study, Journal of Membrane Science, 209 (2002) 283-292.

4 COMMERCIAL REVERSE OSMOSIS MEMBRANE PERFORMANCE CHARACTERIZATION[†]

4.1 Abstract

Crossflow filtration experiments were performed to characterize the water flux and NaCl rejection of the two commercial polyamide reverse osmosis (RO) membranes chosen for study (LE and XLE from Dow Water & Process Solutions). Thorough cleaning of the crossflow system, combined with following the manufacturer's recommended pretreatment and test conditions (i.e., feed pressure, flowrate, temperature, feed pH, and feed filtration) resulted in measured performance values consistent with manufacturer benchmarks. Correction for the effect of concentration polarization also proved important. The influence of feed pH and continuous feed filtration on water flux and salt rejection was characterized. While rejection was strongly affected by feed pH, water flux was essentially unaffected. Continuous filtration of the feed led to higher water flux and lower salt rejection than that observed in experiments with unfiltered feed, suggesting fouling of the membrane surfaces by unfiltered feed. The flux and rejection of these membranes obeyed a general tradeoff relation: membranes that exhibited higher flux had lower rejection and vice versa.

4.2 Motivation

The ultimate goal of this research is to modify the surface of commercial polyamide-based interfacial composite membranes to increase their fouling resistance, using approaches building upon those reported previously in the literature [1, 2]. As a first step in this process, the influence of feed pH and crossflow conditions on the flux and rejection of small coupons from unmodified flat-sheet reverse osmosis membranes was characterized.

In principle, one might use literature values of flux and rejection in the unmodified flat-sheet membranes as a starting point for membrane modification studies. In this regard, Table 4.1 presents results from several flat-sheet membrane coupon (i.e., not module) characterization studies on modern commercial polyamide-based desalination membranes during the last decade [2-5]. For reference, the manufacturers' test conditions (feed pressure, pH, temperature, and NaCl concentration in the feed) and membrane performance (flux, rejection, and permeance) are recorded in boldface type directly above the literature data for each membrane [6-11]. Water permeance (A) values, calculated as flux divided by (Δp-$\Delta\pi$), where Δp and $\Delta\pi$ are the differences between feed and permeate pressure and osmotic pressure, respectively, are included since some literature data were

[†] This chapter has been adapted with permission from: E.M. Van Wagner, A.C. Sagle, M.M. Sharma, B.D. Freeman, Effect of crossflow testing conditions, including feed pH and continuous feed filtration, on commercial reverse osmosis membrane performance, Journal of Membrane Science, 345 (2009) 97-109.

reported at operating pressures or NaCl concentrations (i.e., osmotic pressures) other than those used by the manufacturers. As indicated in Table 4.1, for each membrane, there are variations in flux and rejection values from different literature studies (see, e.g., the BW30 data in Table 4.1) and differences between the literature results and the manufacturer's results. Rejection values reported in the literature studies are invariably lower than the manufacturer's data, and permeance values are generally, but not always, lower in the literature studies than those reported by the manufacturers. While some of this variation might be due to changes in membrane performance over time, since the manufacturer's values reported in Table 4.1 are for current generation membranes, it is also possible that some of the observed variations resulted from differences in experimental conditions among the various studies.

Table 4.1. Comparison of reported membrane performance to manufacturer benchmark values for several commercial reverse osmosis membranes.

Membrane	Δp (bar)	pH	Temperature (^oC)	NaCl feed concentration (mg/L)	Water flux[a] ($L/(m^2h)$)	Water permeance ($L/(m^2h\ bar)$)	Minimum NaCl rejection[a] (%)
BW30 [6]	**15.5**	**8**	**25**	**2000**	**45**	**3.3**	**99.0**
BW30 [2][b]	15.5	Nr	nr	1500	42	2.9	94.8
BW30 [3][c]	15.5	Nr	21	2000	48	3.5	96.5
BW30 [4]	13.8	7	25	585	49	3.7	97.9
SW30HR [7]	**55.2**	**8**	**25**	**32000**	**27**	**1.1**	**99.6**
SWHR [5][b]	12.4	Nr	20	2000	10	0.9	92.0
XLE [8]	**6.9**	**8**	**25**	**500**	**49**	**7.7**	**98.0**
XLE [5][b]	12.4	Nr	20	2000	66	6.0	93.0
ESPA1 [9]	**10.3**	**6.5-7**	**25**	**1500**	**51**	**5.6**	**99.0**
ESPA [3][c]	10.3	Nr	21	1500	39	4.3	97.0
ESPA3 [10]	**10.3**	**6.5-7**	**25**	**1500**	**59**	**6.5**	**98.5**
ESPA3 [4]	13.8	7	25	585	83	6.2	94.9
CPA2 [11]	**15.5**	**6.5-7**	**25**	**1500**	**47**	**3.3**	**99.5**
CPA2 [2][b]	15.5	Nr	nr	1500	36	2.5	95.5
CPA2 [3][c]	15.5	Nr	21	1500	34	2.4	95.6

nr = not reported

Manufacturers' conditions and performance are recorded in boldface type directly above the literature data for each membrane.

[a]The range of acceptable flux values around the manufacturer benchmark value is +25/-15% [8, 9], but rejections only differ by ~ 1-2 % [12].

[b]Tests conducted in stirred (dead-end batch) cells. Results from all other experiments reported in this table (including manufacturers' testing) were obtained using crossflow filtration.

[c]Water used in these experiments was RO permeate passed through a deionizing column and a UF filter.

The observed differences between the literature data and the manufacturer's data prompted the study of the influence of desalination membrane test conditions on the measured flux and rejection of current commercial membranes. The objective was to develop flat-sheet membrane test protocols that permit facile and reliable interlaboratory comparisons of data and permit the generation of laboratory data that is coherent with results reported by the manufacturers.

The literature studies summarized in Table 4.1 used small, flat-sheet membrane coupons, whereas the manufacturers' results are often derived from the performance of large spiral-wound modules. Manufacturers report that flux (and, therefore, permeance) may vary by approximately +25/-15% from one small area of membrane to another due to normal variations in the membrane production process [8, 9], but the effect of these variations is minimized by the large area of membrane contained in a typical spiral-wound module. NaCl rejection values are only expected to vary by 1-2%, with lower rejection values indicating defective membrane samples [12]. Examination of the data in Table 4.1 reveals that the permeance values reported in the literature are often within the acceptable range of the manufacturers' specifications, and are, therefore, reasonable considering the expected variability. However, the reported salt rejection values are, in most cases, well below the manufacturers' specifications. The literature studies were, for the most part, not conducted at the same conditions used by the manufacturers, and these differences in protocol may influence the results. One objective of this study was to explore the sensitivity of these modern, commercially available membranes to laboratory test conditions.

Concentration polarization (i.e., the buildup of salt at the membrane surface) may also influence the data reported in Table 4.1 [13-16]. A few of the experiments in Table 4.1 were conducted using dead end filtration, where concentration polarization might be expected to be particularly severe and where overall salt concentration in the feed solution increases with time. Both of these factors could contribute to the low rejection values observed in those cases.

Most of the results reported in Table 4.1 were conducted using crossflow filtration, which maintains nearly constant feed composition over time (since the amount of permeate produced is typically kept small relative to the feed solution volume, and the permeate product is often recycled to the feed tank). However, although polarization effects can be minimized in crossflow mode by operating at lower pressure and higher crossflow velocity, they can never be completely eliminated and should be accounted for to find the true salt rejection capacity of a reverse osmosis membrane. None of the studies included in Table 4.1 reported the flow conditions or accounted for concentration polarization, which might contribute to the low reported salt rejections.

Cadotte's results suggested that his noncellulosic thin-film composite membranes (i.e., interfacial polyamide membranes on polysulfone ultrafiltration supports) were resistant to compaction (i.e., an initial reduction in water flux with time due, presumably, to pressure-

induced densification or collapse of the membrane support structure) [17]. However, the literature contains reports of initial flux decline in RO membranes, often attributing the flux decline to compaction [4, 5]. In 1985, researchers at Osmonics (now GE Water and Process Technologies) studied this issue to determine whether this flux decline was due to compaction or fouling; they compared the flux as a function of time for ultrafiltration (UF) and RO membranes tested in 2000 mg/L NaCl feed solutions with and without continuous feed filtration through a UF element [18]. They also recognized the possibility that biological fouling could cause flux decline, and they added formaldehyde to the feed water to prevent biogrowth. Membranes tested with continuous UF filtration showed much less flux decline with time than those tested in unfiltered feeds. For example, the flux of a cellulose acetate RO membrane (Δp = 41.4 bar, T = 25°C) decreased by 35% over 1000 hours when the feed was unfiltered, but the flux only decreased by 5.5% over the same time period when the feed was continuously filtered through the UF element before contacting the RO membrane. This result was taken to suggest that fouling caused most of the observed flux decline typically attributed to compaction.

Building upon the results noted above, in this study it was demonstrated that RO flat-sheet membrane performance values closely matching those of the manufacturer can be achieved with careful attention to membrane storage and handling protocols, crossflow system cleaning procedures, and experimental conditions. In addition, the impact of feed pH and continuous feed filtration on membrane performance was determined. The sensitivity of RO membranes to their environment highlights the importance of attention to experimental detail when studying such highly selective, high flux membranes.

4.3 Detailed Measurement Protocol

All characterization experiments were conducted at 150 psig feed pressure (Δp = 10.3 bar). Concentration polarization experiments (Experiments 1 and 2) included four different flowrates: 1, 2, 3, and 4 L/min, corresponding to Reynolds numbers of 600, 1100, 1700, and 2200, respectively. The channel height (3 mm) was used as the characteristic length in Reynolds number calculations, according to the parallel plate approximation for channels with large aspect ratios (width/height > 3-4) [19]. However, the feed moves through a 90° bend to enter the test channel, so the flow is likely turbulent at all flowrates yielding Re>1000 [20]. A mass transfer correlation analysis performed using the experimental data also indicated turbulent flow conditions, as is explained further below. Additionally, the flow was not fully developed because the channel length is only 82 mm. The feed was continuously passed through the carbon and particle filter (to maintain more constant performance during the course of the experiments, as will be explained further below), and feed pH was buffered to the manufacturer-suggested value (pH ~ 8 [8, 21]) using $NaHCO_3$, to mimic the natural adsorption of CO_2 from air [22, 23]. The concentration of $NaHCO_3$ required to achieve these pH values contributes negligibly to the osmotic pressure (5.0×10^{-4} M (0.025 bar)). Pure water flux was first measured at each flowrate in random order, then 2000 mg/L NaCl was added to the feed solution, and water flux as well as bulk feed and permeate salt concentrations were measured for the

same series of flowrates. Samples were collected after 20 minutes of operation at each flowrate to ensure that measured flux and permeate concentration were steady state values. A handheld conductivity meter was used to measure the conductivity of the collected permeate and bulk feed solutions. The concentration polarization model discussed in Chapter 2 was then used to calculate the true rejection and concentration polarization modulus (M) at each flowrate [24].

Next, a set of experiments (Experiments 3 and 4) was performed to determine the effect of feed pH on membrane performance (water flux and salt rejection). The feed was also continuously filtered in these experiments, the flowrate was set to 4 L/min, and pure water flux was measured just before adding 2000 mg/L NaCl, to allow calculation of the concentration polarization modulus at the start of each experiment. Feed pH was randomly adjusted to lower or higher values by adding 1 M HCl or 5 % (w) (1.2 M) NaOH to the feed tank, respectively. The amount of acid and base required to achieve these pH values has a negligible effect on feed concentration and osmotic pressure (i.e., causes less than 5% increase in feed conductivity).

Filtration tests (Experiments 5 and 6) were then performed to determine the flux and rejection properties of the membranes as a function of time, using the manufacturer's specified operating conditions. Dow Water & Process Solutions' specifications are based on using an unfiltered feed containing 2000 mg/L NaCl at pH 8 with a feed pressure of 150 psig (Δp = 10.3 bar), and a flowrate corresponding to 15-20% polarization (M = 1.15-1.20) [8, 12, 21]. The permeate pressure was atmospheric, and feed pH was achieved using $NaHCO_3$ as a buffer. An additional set of experiments (Experiments 7 and 8) was performed at the same conditions, but with a continuously filtered feed, to demonstrate the effect of this variable on membrane performance.

In each of these experiments (Experiments 5-8), pure water flux was first measured before adding 2000 mg/L NaCl. Then, water flux and NaCl rejection were monitored for 24 hours. True rejection was calculated based on the polarization modulus measured at the start of each experiment (using the pure water flux and the first flux and rejection measurements in 2000 mg/L NaCl).

In each experiment, the permeate stream from each cell was continuously recycled to the feed tank, except during sample collection for flux and rejection measurements. Three membrane samples cut from the same area of each membrane roll were used in each experiment to gauge the variability between samples. The results presented are average values obtained for the three samples, and the reported uncertainty is one standard deviation of the experimental results for the three samples.

Table 4.2 summarizes the conditions used for each experiment, and may be used as a reference for the following discussion.

Table 4.2. Summary of experimental conditions for the LE and XLE characterization studies (24-25°C and 150 psig feed pressure (Δp = 10.3 bar) maintained for all experiments).

Experiment	Membrane	Flowrate (L/min)	Continuous feed filtration	Feed pH
1	LE	1, 2, 3, 4	Y	7.7
2	XLE	1, 2, 3, 4	Y	7.8
3	LE	4	Y	4.5-9.0
4	XLE	4	Y	5.0-9.0
5	LE	4	N	7.9
6	XLE	4	N	7.8
7	LE	4	Y	7.8
8	XLE	4	Y	7.8

4.4 Results and Discussion

4.4.1 Concentration Polarization

The results of the concentration polarization experiments for the LE and XLE membranes (Experiments 1 and 2) are presented in Figures 4.1 and 4.2, respectively. The measured quantities (i.e., pure water flux, water flux in 2000 mg/L NaCl, and apparent NaCl rejection) are shown in Figures 4.1(a) and 4.2(a). The apparent salt rejection increased with increasing flowrate for both membranes, but the XLE membrane had less sample-to-sample variability than the LE membrane. The standard deviation of water flux in 2000 mg/L NaCl, reflecting sample-to-sample variability among the three samples run simultaneously during the experiments for each membrane, was in the range 0.3-0.5 LMH for the XLE membrane, compared to 1.3-1.4 LMH for the LE membrane. Similarly, the standard deviation of apparent NaCl rejection was in the range 0.08-0.1% for the XLE membrane, while it was 0.3-0.4% for the LE membrane (compare error bars in Figures 4.1(a) and 4.2(a)).

The bulk feed and permeate salt concentrations (i.e., the apparent rejection), pure water flux, and water flux in 2000 mg/L NaCl feed were then used to determine the salt concentration at the membrane surface ($c_{so(m)}$ or $\pi_{so(m)}$), true salt rejection (R_{true}) and concentration polarization modulus (M) at each feed flowrate, using the model discussed in Chapter 2 [24]. The apparent and true rejections, as well as the polarization moduli, are shown in Figures 4.1(b) and 4.2(b). The trend of decreasing polarization modulus with increasing flowrate was common to both membranes. This behavior was expected, since a higher feed flowrate tangential to the membrane surface is expected to give better mixing and less salt buildup at the membrane surface, thus reducing the salt boundary layer thickness [13]. The polarization modulus values were used to calculate mass transfer coefficients and Sherwood numbers, and a plot of the natural logarithm of Sherwood number versus the natural logarithm of Reynolds number yielded a line with

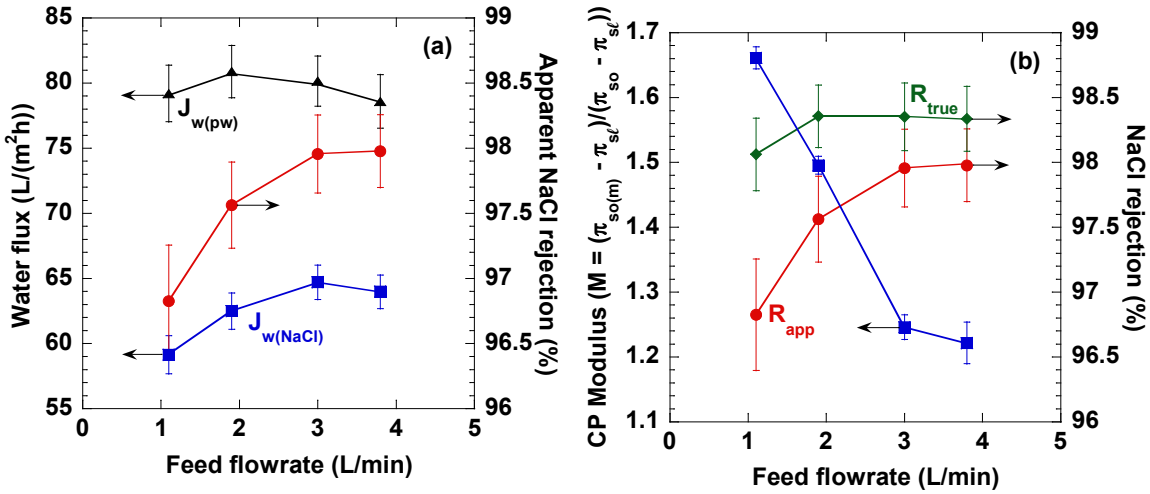

Figure 4.1. *(a) Pure water flux, water flux in 2000 mg/L NaCl feed, and apparent NaCl rejection for the LE membrane as a function of feed flowrate. (b) Apparent NaCl rejection, concentration polarization modulus (M), and true NaCl rejection for the LE membrane as a function of feed flowrate. Experiment 1 conditions: T = 24-25°C, Δp = 10.3 bar, feed passed continuously through a carbon and particle filter, feed pH 7.7. Error bars in the figure represent one standard deviation of the experimental results for the three samples tested in this experiment.*

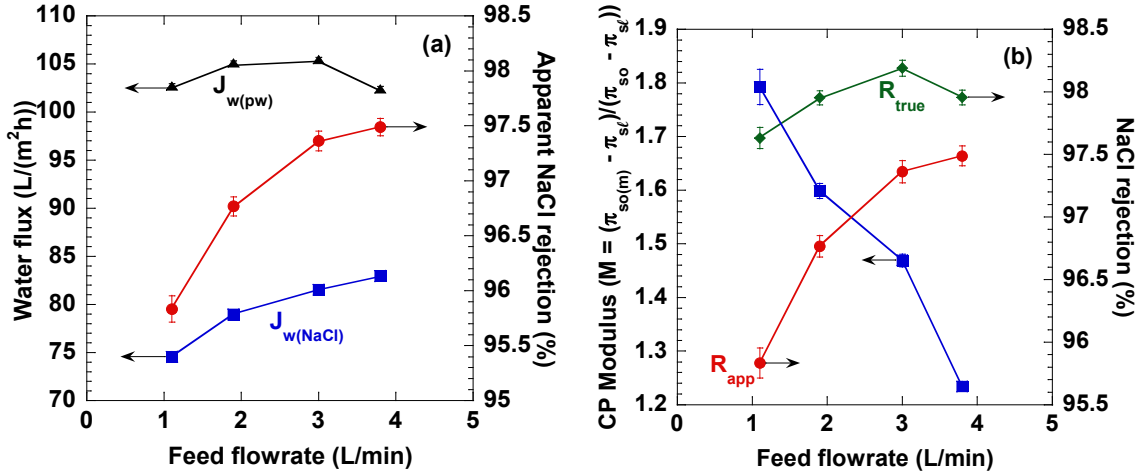

Figure 4.2. *(a) Pure water flux, water flux in 2000 mg/L NaCl feed, and apparent NaCl rejection for the XLE membrane as a function of feed flowrate. (b) Apparent NaCl rejection, concentration polarization modulus (M), and true NaCl rejection for the XLE membrane as a function of feed flowrate. Experiment 2 conditions: T = 24-25°C, Δp = 10.3 bar, feed passed continuously through a carbon and particle filter, feed pH 7.8. Error bars in the figure represent one standard deviation of the experimental results for the three samples tested in this experiment.*

slope greater than 0.8 for both membranes, indicating the crossflow system was operating in a turbulent flow regime [24].

Table 4.3 presents the concentration polarization-corrected (i.e., calculated using surface concentration rather than the bulk feed concentration) water permeance (A) and salt permeance (B) values for both membranes, averaged for all feed flowrates tested. As evidenced by the small standard deviations seen in Table 4.3, water and salt permeance values were essentially constant with flowrate. Dow Water & Process Solutions' target water and salt permeance values (corrected for 15-20% polarization [12]) are included for comparison. Measured water and salt permeance values were higher than the manufacturer's target values for both membranes. Discrepancies with the manufacturer's values may be explained, at least in part, by differences between the testing conditions of these experiments and those of the manufacturer (i.e., use of the carbon and particle filter). This possibility will be examined further in the following sections.

Table 4.3. Comparison of concentration polarization-corrected water permeance and salt permeance values[a] of LE and XLE membranes to manufacturer specifications.

Membrane	**Water permeance (A) (LMH/bar)[d]**	**Dow's specified water permeance (A) (LMH/bar)[e]**	**Salt permeance (B) (LMH)[d]**	**Dow's specified salt permeance (B) (LMH)[e]**
LE[b]	7.7 ± 0.1	5.9 (5.0-7.4)	1.1 ± 0.05	0.51 (0.43-0.63)
XLE[c]	10.0 ± 0.2	7.7 (6.5-9.6)	1.7 ± 0.1	1.3 (1.1-1.7)

[a] $A = \dfrac{J_{w(NaCl)}}{\left[\Delta p - \left(\pi_{so(m)} - \pi_{s\ell}\right)\right]}$ (cf. Equation 2.32)

$B = \dfrac{J_{w(NaCl)}\pi_{s\ell}}{\left(\pi_{so(m)} - \pi_{s\ell}\right)}$ (cf. Equations 2.23 and 2.24; note that osmotic pressure is directly proportional to concentration and osmotic pressure at the membrane surface, $\pi_{so(m)}$, is used in place of bulk feed osmotic pressure, π_{so})

[b] T = 24-25°C, Δp = 10.3 bar, feed passed continuously through a carbon and particle filter, pH 7.7 (experiment 1).

[c] T = 24-25°C, Δp = 10.3 bar, feed passed continuously through a carbon and particle filter, pH 7.8 (experiment 2).

[d] Water and salt permeance values are average values for all four feed flowrates (1, 2, 3, and 4 L/min).

[e] Values were calculated using the manufacturer's minimum NaCl rejection. Range in parentheses accounts for acceptable range of water flux around target value (+25/-15%) [8, 21]. Values have been corrected for concentration polarization using the 15-20% polarization specified by the manufacturer [12].

As shown in Figures 4.1(b) and 4.2(b), polarization has a significant effect on salt rejection, especially at low flowrates. Although the effect diminishes as flowrate increases (i.e., the difference between apparent and true rejection decreases), correcting for polarization still increases true rejection by several tenths of a percent above the apparent rejection, which is significant in these highly selective membranes. In the limit of no polarization (i.e., $c_{so} = c_{so(m)}$) the concentration polarization modulus must, by definition, approach a value of one [13, 24, 25]. Figure 4.1(b) indicates that the polarization modulus may be beginning to level off and approach a value of one at feed flowrates greater than 3 L/min for the LE membrane. However, as seen in Figure 4.2(b), the polarization modulus decreases continuously with increasing feed flowrate, even at a feed flowrate of 4 L/min, for the XLE membrane. The XLE membrane has a higher water flux than the LE membrane, so it is reasonable to expect that a higher feed flowrate would be required to observe a similar effect on the polarization modulus.

To match the 15-20% polarization conditions specified by Dow Water & Process Solutions for operation of their flat-sheet membranes [12], a flowrate of 4 L/min was chosen for use in all subsequent experiments.

4.4.2 Effect of Feed pH on Membrane Performance

The water flux and true NaCl rejection as a function of feed pH for the LE and XLE membranes are presented in Figures 4.3(a) and (b), respectively (experiments 3 and 4). While water flux was independent of feed pH over the pH range considered, rejection increased fairly linearly with increasing feed pH (note: the amount of HCl and NaOH added to adjust the feed pH had a negligible effect on feed concentration, so flux and rejection were calculated without correction for the additional ions). The fact that rejection depends on pH in normal solution pH range emphasizes the necessity of careful pH control, since a difference of only one pH unit can change true rejection by nearly 0.5%. Cadotte noted the independence of water flux and dependence of rejection on feed pH for the FT-30 membrane [26], and recent work with other aromatic polyamide membranes has also shown a similar trend of increasing rejection with increasing feed pH [27]. One possible explanation for the increase in rejection seen with increasing pH from pH 5 to pH 9 is the increasingly negative charge of the polyamide membrane surface over this pH range, as indicated by increasingly negative zeta potential values [28]. The numbers on Figures 4.3(a) and (b) indicate the order of the measurements (i.e., the history of the imposed pH changes), emphasizing that the effect of feed pH on rejection was reversible under the conditions of this study. That is, following short periods of exposure to lower pH, the rejection of both membranes increased as pH increased, indicating the membranes sustained no permanent change in properties due to pH cycling for the short exposure periods considered in this investigation. This phenomenon was also observed by Cadotte during his original investigation into the properties of the FT-30 membrane [26].

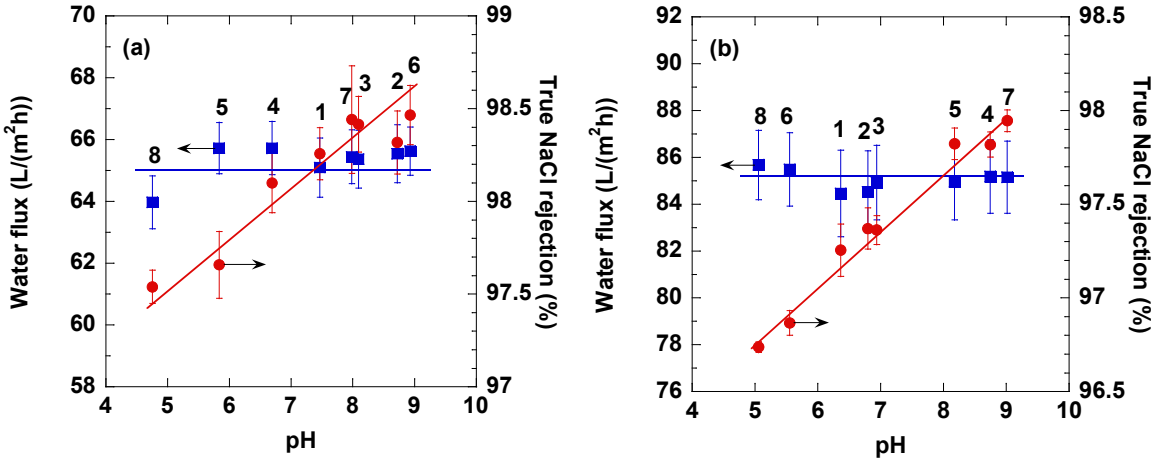

Figure 4.3. *Average water flux and true NaCl rejection as a function of feed pH (T = 24-25oC, Δp = 10.3 bar, flowrate = 4 L/min, feed passed continuously through a carbon and particle filter, feed pH adjusted using 1 M HCl or 5% NaOH). (a) LE membranes (M = 1.09-1.22, experiment 3). (b) XLE membranes (M = 1.16-1.29, experiment 4). Error bars in the figures represent one standard deviation of the experimental results for the three samples tested. Note: numbers 1-8 indicate the order of the measurements, and demonstrate the reversibility of the pH/rejection phenomenon. The lines were drawn to follow trends suggested by the data, and should be used to guide the eye.*

4.4.3 Performance at Manufacturer's Specified Conditions

After determining the optimum flowrate for testing, the performance of the LE and XLE membranes was measured over 24 hours using the conditions used by Dow Water & Process Solutions in their flat-sheet characterization studies. The performance of the LE membrane as a function of time (experiment 5; T = 24-25°C, Δp = 10.3 bar, flowrate = 4 L/min, unfiltered feed, feed pH 7.9) is presented in Figure 4.4. Figure 4.4(a) shows the average values of water flux and apparent and true NaCl rejections for the three LE samples tested in this experiment. During the 24 hour experiment, water flux decreased by 10 LMH, and true NaCl rejection increased by 0.5%. Figure 4.4(b) includes the water flux of each membrane sample and Figure 4.4(c) gives the apparent and true NaCl rejection for each sample (data in these figures were used to calculate average values shown in Figure 4.4(a)). While the three samples had fluxes within 2 LMH of each other, one sample (cell 1) had significantly higher rejection than the other two samples (~ 0.6% higher near the start of the experiment, decreasing to ~ 0.3% higher after 24 hours). A propagation of errors analysis revealed the uncertainty inherent in the water flux measurement (due to ability to accurately measure permeate mass, active membrane area and permeate collection time) to be ± 1.5-2 LMH for the RO membranes considered in this study [29]. Thus, the flux discrepancy depicted in Figure 4.4(b) may be due to

inherent limitations of the experimental measurement. A similar analysis performed for NaCl rejection gave an inherent uncertainty of ± 0.1-0.2%, so the difference in rejection between the sample in cell 1 and the other two cells reflects an actual difference in salt rejection of these membrane samples. Membrane modules typically have over 20,000 times the area of the membrane samples tested in the laboratory-scale crossflow system (400 ft^2 (37 m^2) vs. 1.82×10^{-3} m^2). Thus, membrane variations which are averaged out over the area of a module can easily become significant in the small samples tested in the laboratory, as indicated by the variability in membrane rejection shown in Figure 4.4(c).

The average water flux, apparent rejection and true rejection of the XLE membrane as a function of time are shown in Figure 4.5 (experiment 6; T = 24-25°C, Δp = 10.3 bar, flowrate = 4 L/min, unfiltered feed, feed pH 7.8). The behavior of the XLE membrane mimicked that of the LE membrane (cf. Figures 4.4(a) and 4.5), with a steadily declining water flux that fell 10 LMH over 24 hours while the true rejection increased by 0.5%. The standard deviation of the measured water flux (2.4-3.8 LMH) was slightly higher than the uncertainty inherent in the measurement (1.5-2 LMH), indicating some variability between the three XLE membrane samples tested.

The time at which flux and rejection are reported is another consideration when attempting to match the manufacturer's specifications. The time dependence of flux and rejection depicted in Figures 4.4 and 4.5 provides evidence of the importance of matching the manufacturer's specified time at which data are to be reported. Dow Water & Process Solutions recommends measurement of LE and XLE membrane coupon performance after 20 minutes of filtration [12]. Table 4.4 compares the water flux, water permeance, true rejection, and salt permeance of each membrane with the corresponding values reported by the manufacturer. For this comparison, the data are reported at the time suggested by the manufacturer. That is, the values in the table come from the points on Figures 4.4(a) and 4.5 corresponding to 20 minutes of operation. Both the experimentally determined and manufacturer's target water and salt permeances have been corrected for the effects of concentration polarization.

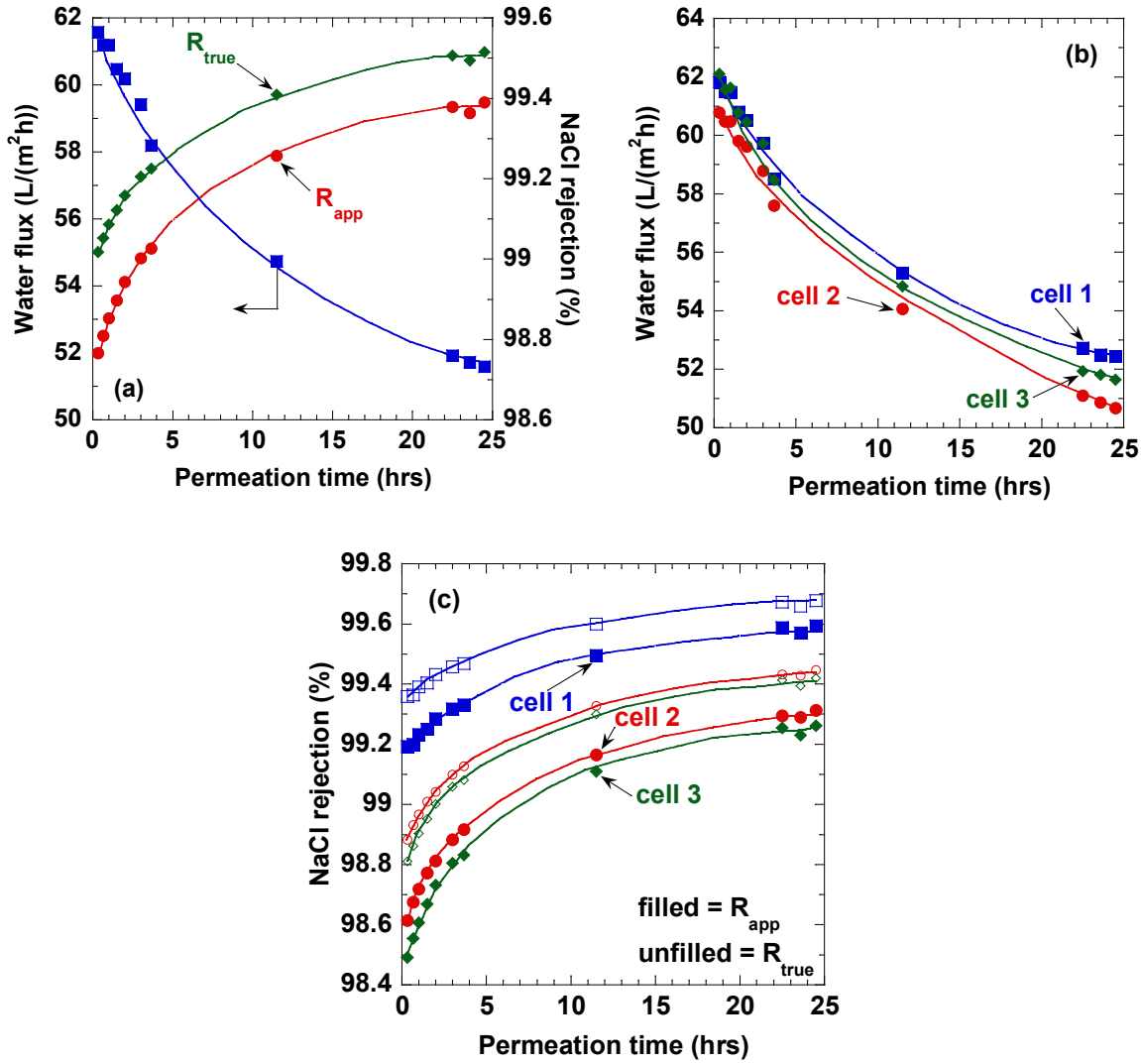

Figure 4.4. (a) Average water flux, apparent NaCl rejection and true NaCl rejection as a function of time for three LE membranes tested at Dow Water & Process Solutions' specified conditions (T = 24-25°C, Δp = 10.3 bar, flowrate = 4 L/min, unfiltered feed, feed pH 7.9, M = 1.26, experiment 5). Note: uncertainty in water flux ~ 0.5-0.9 LMH, uncertainty in R_{app} ~ 0.2-0.4%, uncertainty in R_{true} ~ 0.1-0.3%. (b) Water flux and (c) Apparent and true NaCl rejection as a function of time for each of the three LE membranes.

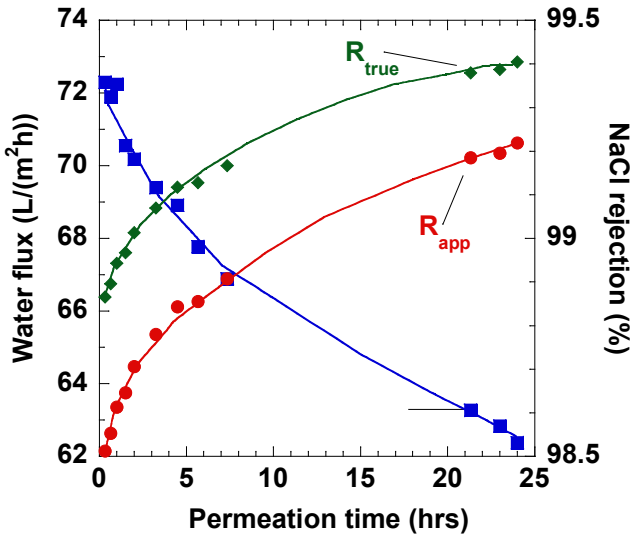

Figure 4.5. Average water flux, apparent NaCl rejection and true NaCl rejection as a function of time for XLE membranes tested at Dow Water & Process Solutions' specified conditions (T = 24-25°C, Δp = 10.3 bar, flowrate = 4 L/min, unfiltered feed, feed pH 7.8, M = 1.31, experiment 6). Note: uncertainty in water flux ~ 2.4-3.8 LMH, uncertainty in R_{app} ~ 0.07-0.2%, uncertainty in R_{true} ~ 0.04-0.1%.

Examination of the data in Table 4.4 shows that the measured water flux and concentration polarization-corrected water permeance of the XLE and LE membranes were within the manufacturer's target ranges. In addition, the true salt rejection values were in good agreement with those of the manufacturer, reaching at least the minimum target values after the specified 20 minute run time. The concentration polarization-corrected salt permeance values fell slightly above the upper end of Dow's target range for the LE membrane. However, considering the uncertainty in the measured values, the measured salt permeance values are consistent with the values specified by the manufacturer. For the XLE membrane, the salt permeance (0.83 LMH) fell below Dow's target range. Calculation of salt permeance (using Equations 2.23 and 2.24) is influenced by water flux as well as salt rejection, which explains why the LE membrane, whose water fluxes fell near the upper end of the manufacturer's target range, had a salt permeance value that fell above the manufacturer's target range. In addition, the water flux of the XLE membrane (72 LMH) was very near Dow's target value (65 LMH) while its true salt rejection after 20 minutes (98.9%) was much higher than Dow's specified minimum salt rejection (98.0%, used to calculate the manufacturer's specified salt permeance), which explains why the salt permeance of the XLE membrane fell below the manufacturer's target range. It is important to note that the manufacturer's salt permeance value given is a maximum acceptable value. As salt rejection increases from the minimum value to the stabilized value, salt permeance decreases. Since the XLE membranes tested had NaCl rejections near the stabilized value, their salt permeance values were lower than the maximum acceptable values stated by the manufacturer.

Table 4.4. Comparison of measured membrane performance to manufacturer benchmark values (test conditions matching those of manufacturer).

Membrane	Water flux (LMH)	Dow's specified water flux (LMH)[c]	Water permeance (A) (LMH/bar)[d]	Dow's specified water permeance (A) (LMH/bar)[e]	R_{true} (%)	Dow's specified R_{true} (minimum and stabilized) (%)	Salt permeance (B) (LMH)[d]	Dow's specified salt permeance (B) (LMH)[e]
LE[a]	62 ± 1	50 (42-62)	7.4 ± 0.1	5.9 (5.0-7.4)	99.0 ± 0.3	99.0-99.3	0.61 ± 0.2	0.51 (0.43-0.63)
XLE[b]	72 ± 4	65 (55-81)	8.9 ± 0.5	7.7 (6.5-9.6)	98.9 ± 0.1	98.0-99.0	0.83 ± 0.1	1.3 (1.1-1.7)

[a]Δp = 10.3 bar, feed flowrate = 4 L/min, T = 24-25°C, unfiltered feed, pH 7.9, measurement taken after 20 minutes (experiment 5) [12, 21].
[b]Δp = 10.3 bar, feed flowrate = 4 L/min, T = 24-25°C, unfiltered feed, pH 7.8, measurement taken after 20 minutes (experiment 6) [8, 12].
[c]Range of numbers in parentheses indicates acceptable range of water flux around target value (+25/-15%) [8, 21].
[d]Values were corrected for effects of concentration polarization (osmotic pressure at the membrane surface, $\pi_{so(m)}$, was used in place of bulk feed osmotic pressure, π_{so}).
[e]Values were calculated using the manufacturer's minimum NaCl rejection. Range in parentheses accounts for acceptable range of water flux around target value (+25/-15%) [8, 21]. Values have been corrected for concentration polarization using the 15-20% polarization specified by the manufacturer [12].

4.4.4 Influence of Continuous Feed Filtration on Membrane Performance

The influence of continuous feed filtration on membrane performance is presented in Figures 4.6(a) and (b) for the LE and XLE membranes, respectively. The only condition that was changed in experiments 7 and 8 (as compared to experiments 5 and 6) was that the feed was continuously filtered. In this way, the effect of continuous feed filtration on membrane performance could be isolated and studied. Figure 4.6(a) compares the flux and true rejection performance of the LE membranes from experiments 5 and 7, and Figure 4.6(b) compares the results of experiments 6 and 8 for the XLE membranes. For both membranes, water flux was much more stable with time when the feed was continuously filtered. The water flux of the LE and XLE membranes increased slightly over the first 3-4 hours before starting to decrease. After 24 hours, the water flux of the XLE membrane had decreased to its initial value, while the flux of the LE membrane had decreased by 1 LMH (1.5%), well within the inherent uncertainty of the measurement (1.5-2 LMH). On the other hand, twenty-four hours of operation with unfiltered feed led to flux declines of 16% for the LE and 14% for the XLE membranes. Irrespective of the time-dependent trends, water flux was always higher and true rejection was always lower in continuous filtration experiments than in unfiltered feed experiments for both membranes.

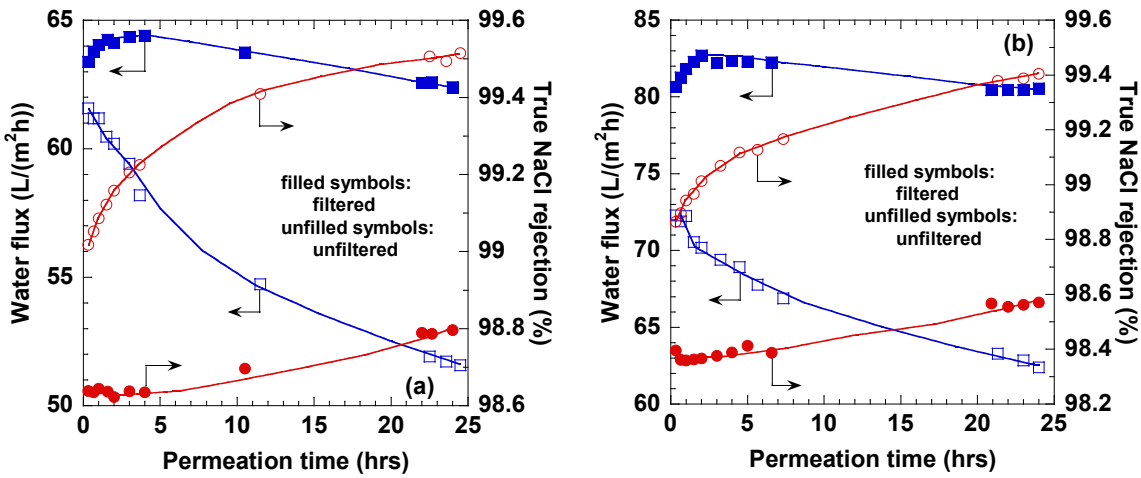

Figure 4.6. Comparison of average water flux and true NaCl rejection (T = 24-25°C, Δp = 10.3 bar, flowrate = 4 L/min) as a function of time. (a) LE membranes tested in unfiltered feed (experiment 5, feed pH 7.9, M = 1.26, unfilled symbols) and continuously filtered feed (experiment 7, feed pH 7.8, M = 1.14, filled symbols). Note: experiment 5 uncertainty given in Figure 4.4(a); experiment 7 uncertainty in water flux ~ 0.6-1.0 LMH, uncertainty in R_{true} ~ 0.07-0.1%. (b) XLE membranes tested in unfiltered feed (experiment 6, feed pH 7.8, M = 1.31, unfilled symbols) and continuously filtered feed (experiment 8, feed pH 7.8, M = 1.21, filled symbols). Note: experiment 6 uncertainty given in Figure 4.5; experiment 8 uncertainty in water flux ~ 2.2-2.5 LMH, uncertainty in R_{true} ~ 0.08-0.1%.

Figures 4.6(a) and (b) demonstrate that the true salt rejection of the LE and XLE membranes only increased by ~ 0.2% over 24 hours using continuously filtered feed, significantly less than the 0.5% increase observed in unfiltered feed. The larger increase in true salt rejection and decline in water flux in the unfiltered feed experiments (versus the rather stable flux and rejection behavior in the continuously filtered feed experiments) for these membranes could be explained as the result of fouling. Although no obvious foulants were added to the system and

ultrapure water was used as the feed water, there could be particulate matter in the water, introduced either from dust and particulate matter found normally in air (the feed tank cover was not air-tight) or from the wetted stainless steel parts of the crossflow system. Biofouling is another possibility. Passing the feed continuously through the carbon and particle filter presumably removes much of any particulate matter found in the feed and acts to prevent biological growth in the system. Without continuous filtration, the feed may pick up enough contaminants to cause the sensitive reverse osmosis membranes to foul, blocking surface area and resulting in lower water flux and higher NaCl rejection. Over time, additional foulant buildup would cause the flux to decrease and the rejection to increase. In contrast, the carbon and particle filter continuously removes foulants, resulting in more stable flux and rejection values over time, as well as higher flux and lower rejection due to the lack of foulants. These results also give insight into Dow Water & Process Solutions' choice of a run time of 20 minutes before taking flux and rejection measurements, to report performance values before the effects of fouling become significant (since their protocol does not employ continuously filtered feed water). Thus, in these membranes at least, there is little evidence for pressure-induced compaction. This result is in agreement with the GE findings that the majority of the initial flux decline observed in the literature may well be attributed to low levels of membrane fouling [18], as was observed in experiments using unfiltered feed water.

4.4.5 Permeance/Salt Passage Tradeoff

Finally, data from experiments 1-8 are presented in Figure 4.7 as a tradeoff plot of water/salt permeability selectivity (A/B) as a function of water permeance (used as a rough indicator of membrane permeability). For the same selectivity, the XLE membranes had higher water permeance than the LE membranes. For both membranes, water permeance and water/salt selectivity values obtained in experiments using unfiltered feed (experiments 5 and 6 for the LE

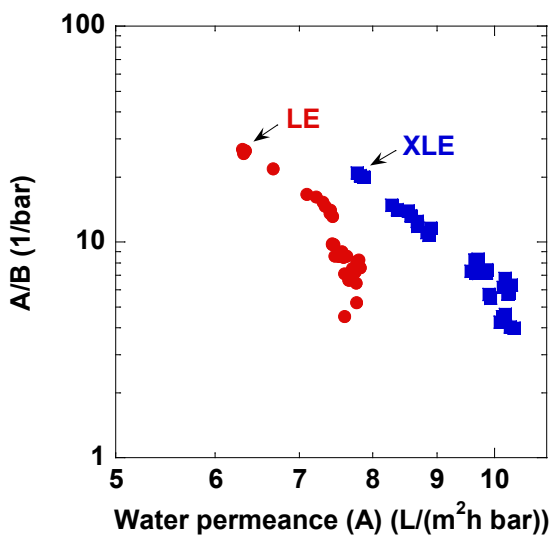

Figure 4.7. Permeance/selectivity tradeoff plot for LE and XLE membranes (experiments 1-8). Water and salt permeance values have been corrected for the effects of concentration polarization (osmotic pressure at the membrane surface, $\pi_{so(m)}$, used in place of bulk feed osmotic pressure, π_{so}).

and XLE membranes, respectively) fell further to the upper left corner of the plot than those values obtained in the continuous feed filtration experiments (experiments 7 and 8 for the LE and XLE membranes, respectively), possibly due to surface fouling by the unfiltered feed, which resulted in decreased water permeance and increased selectivity for water over salt.

In gas separation membranes, permeability and selectivity are known to be inversely correlated [30, 31]. However, it is rare to find the data for desalination membranes presented in such a fashion. A significant difference between the permeability/selectivity tradeoff plots used in gas separations and the permeance/selectivity tradeoff plot presented in Figure 4.7 is that permeability is a material property, independent of the thickness of the membrane being tested, while permeance, on the other hand, is inversely proportional to membrane thickness. The data for the desalination membranes are presented in terms of permeance rather than permeability because the thickness of these interfacial composite desalination membranes is not reported. Thus, the permeance axis of Figure 4.7 is influenced by the thickness of the membranes. In the future, it is hoped that more data will be available where the membrane thickness is known, so that plots of water/salt permeability selectivity as a function of water permeability can be constructed to understand where the upper bound should be drawn for desalination membranes.

4.5 Conclusions

Measured performance values of commercial RO flat-sheet membrane coupons were sensitive to crossflow testing conditions. Water flux and salt rejection values matching the manufacturer benchmarks were achieved through careful matching of their pretreatment and testing conditions. Continuous feed filtration eliminated the flux decline observed in unfiltered feed, suggesting that the initial flux decline often observed in the literature is due to modest fouling of the membrane rather than pressure-induced compaction of the membrane or support. Additionally, salt rejection was found to be linearly dependent on feed pH in the pH range from 5 to 9. Water permeance and water/salt selectivity appeared to be inversely correlated, suggesting the existence of a tradeoff relationship between water transport and water/salt selectivity in desalination membranes. The manufacturer's operating conditions, including pressure, flowrate, temperature, and feed pH, should be followed when performing experiments on their membranes in order to achieve flux and rejection values similar to those reported by the manufacturer. Although Dow Water & Process Solutions does not report data from experiments employing continuous feed filtration, their experiments are very short (e.g., one hour or less), and fouling plays a minor role on this timescale. Therefore, when longer tests are performed, continuous feed filtration can be used to avoid fouling.

4.6 Acknowledgements

The author would like to thank Dr. Bill Mickols of Dow Water & Process Solutions for sharing his laboratory testing protocols.

4.7 References

[1] W.E. Mickols, Composite Membrane with Polyalkylene Oxide Modified Polyamide Surface, U.S. Patent 6,280,853 B1, 2001.

[2] S. Belfer, Y. Purinson, R. Fainshtein, Y. Radchenko, O. Kedem, Surface modification of commercial composite polyamide reverse osmosis membranes, Journal of Membrane Science, 139 (1998) 175-181.

[3] J. Gilron, S. Belfer, P. Vaisanen, M. Nystrom, Effects of surface modification on antifouling and performance properties of reverse osmosis membranes, Desalination, 140 (2001) 167-179.

[4] C.Y. Tang, Y.-N. Kwon, J.O. Leckie, Fouling of reverse osmosis and nanofiltration membranes by humic acid - effects of solution composition and hydrodynamic conditions, Journal of Membrane Science, 290 (2007) 86-94.

[5] B.-H. Jeong, E.M.V. Hoek, Y. Yan, A. Subramani, X. Huang, G. Hurwitz, A.K. Ghosh, A. Jawor, Interfacial polymerization of thin film nanocomposites: a new concept for reverse osmosis membranes, Journal of Membrane Science, 294 (2007) 1-7.

[6] Dow Water & Process Solutions BW30-400 Product Specification, http://www.dow.com/liquidseps/prod/bw30_400.htm.

[7] Dow Water & Process Solutions SW30HR-380 Product Specification, http://www.dow.com/liquidseps/prod/sw30hr_380.htm.

[8] Dow Water & Process Solutions XLE-440 Product Specification, http://www.dow.com/liquidseps/prod/xle_440.htm.

[9] Nitto Denko Hydranautics ESPA 1 Product Specification, http://www.membranes.com/docs/8inch/ESPA1.pdf.

[10] Nitto Denko Hydranautics ESPA 3 Product Specification, http://www.membranes.com/docs/8inch/ESPA3.pdf.

[11] Nitto Denko Hydranautics CPA 2 Product Specification, http://www.membranes.com/docs/8inch/CPA2.pdf.

[12] W.E. Mickols, Dow Water & Process Solutions, personal communication, 2008.

[13] R.W. Baker, Membrane Technology and Applications, 2nd ed., John Wiley & Sons Ltd., West Sussex, 2004.

[14] R.F. Probstein, Physicochemical Hydrodynamics: An Introduction, 2nd ed., John Wiley & Sons, Inc., New York, 1994.

[15] U. Merten, H.K. Lonsdale, R.L. Riley, Boundary-layer effects in reverse osmosis, I & EC Fundamentals, 3 (1964) 210-213.

[16] T.K. Sherwood, P.L.T. Brian, R.E. Fisher, L. Dresner, Salt concentration at phase boundaries in desalination by reverse osmosis, I & EC Fundamentals, 4 (1965) 113-118.

[17] J.E. Cadotte, R.J. Petersen, Thin-film composite reverse-osmosis membranes: origin, development, and recent advances, in Synthetic Membranes: Desalination, A.F. Turbak (Ed.), ACS Symposium Series, 153rd ed., Vol. 1, American Chemical Society, 1981, pp. 305-326.

[18] B.J. Rudie, T.A. Torgrimson, D.D. Spatz, Reverse-osmosis and ultrafiltration membrane compaction and fouling studies using ultrafiltration pretreatment, in Reverse Osmosis and Ultrafiltration, S. Sourirajan, T. Matsuura (Eds.), ACS Symposium Series, 281st ed., American Chemical Society, 1985, pp. 403-414.

[19] R.W. Fox, A.T. McDonald, P.J. Pritchard, Introduction to Fluid Mechanics, 6th ed., John Wiley and Sons, Hoboken, 2004.

[20] M. Asai, J.M. Floryan, Certain aspects of channel entrance flow, Physics of Fluids, 16 (2004) 1160-1163.

[21] Dow Water & Process Solutions LE-400 Product Specification, http://www.dow.com/liquidseps/prod/le_400.htm.

[22] V.L. Snoeyink, D. Jenkins, Water Chemistry, John Wiley & Sons, New York, 1980.

[23] X. Zhu, M. Elimelech, Colloidal fouling of reverse osmosis membranes: measurements and fouling mechanisms, Environmental Science and Technology, 31 (1997) 3654-3662.

[24] I. Sutzkover, D. Hasson, R. Semiat, Simple technique for measuring the concentration polarization level in a reverse osmosis system, Desalination, 131 (2000) 117-127.

[25] P.L.T. Brian, Concentration polarization in reverse osmosis desalination with variable flux and incomplete salt rejection, I & EC Fundamentals, 4 (1965) 439-445.

[26] J.E. Cadotte, R.J. Petersen, R.E. Larson, E.E. Erickson, A new thin-film composite seawater reverse osmosis membrane, Desalination, 32 (1980) 25-31.

[27] S. Kim, H. Ozaki, J. Kim, Effect of pH on the rejection of inorganic salts and organic compound using nanofiltration membrane, Korean Journal of Chemical Engineering, 23 (2006) 28-33.

[28] M. Elimelech, W.H. Chen, J.J. Waypa, Measuring the zeta (electrokinetic) potential of reverse osmosis membranes by a streaming potential analyzer, Desalination, 95 (1994) 269-286.

[29] P.R. Bevington, D.K. Robinson, Data Reduction and Error Analysis for the Physical Sciences, 2nd ed., McGraw Hill, New York, 1992.

[30] L.M. Robeson, Correlation of separation factor versus permeability for polymeric membranes, Journal of Membrane Science, 62 (1991) 165-185.

[31] B.D. Freeman, Basis of permeability/selectivity tradeoff relations in polymeric gas separation membranes, Macromolecules, 32 (1999) 375-380.

This page is intentionally left blank

5 SURFACE CHARACTERIZATION OF A COMMERCIAL REVERSE OSMOSIS MEMBRANE

5.1 Abstract

In addition to characterizing the performance (i.e., water flux and NaCl rejection) of commercial reverse osmosis membranes, surface properties of these polyamide materials were also investigated. ATR-FTIR and XPS were employed to characterize the chemical composition of the polyamide membrane, while surface roughness, hydrophilicity and charge were characterized using AFM, contact angle and zeta potential measurements, respectively. Membrane characterization, including both performance and surface properties, is essential for future comparison with the properties of modified membranes, to identify any changes resulting from surface modification.

5.2 Results and Discussion

5.2.1 ATR-FTIR

The ATR-FTIR absorbance spectrum of a commercial XLE membrane is presented in Figure 5.1. The entire mid-infrared region is shown in Figure 5.1(a), while the region 1000-1800 cm^{-1} is enlarged in Figure 5.1(b). Characteristic peaks in the spectra of aromatic polyamide composite membranes are labeled in Figure 5.1(b): the amide I peak representative of the C=O stretch (1), the amide II peak representative of the N-H bend (3), and peaks due to the underlying polysulfone support layer (2 and 4) [1]. The polysulfone support layer appears in the spectra because the 1 μm penetration depth of ATR-FTIR is greater than the polyamide layer thickness (0.1 μm) [1].

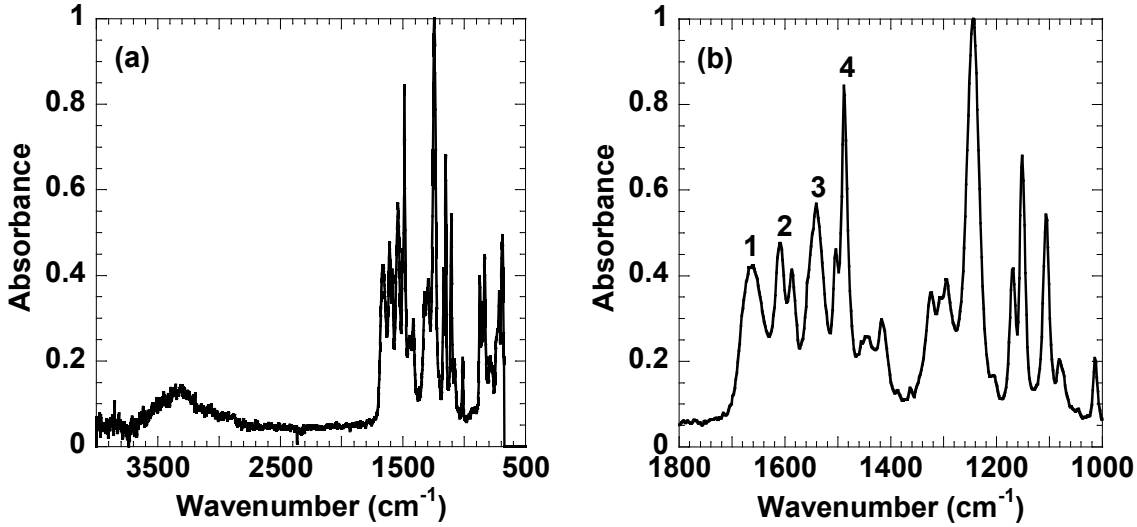

Figure 5.1. ATR-FTIR spectrum of a Dow Water & Process Solutions XLE composite polyamide membrane. (a) mid-infrared region (500-4000 cm^{-1}) and (b) view of 1000-1800 cm^{-1} region, where peaks characteristic of composite aromatic polyamide membranes are labeled 1-4.

The ATR-FTIR spectrum of poly(ethylene glycol) diglycidyl ether (PEGDE) is presented in Figure 5.2. The ether C-O peak at 1100 cm^{-1} is the largest peak associated with PEGDE, and although there are other peaks in this region for the polyamide membrane, it may be possible to observe an increase in intensity upon PEGDE modification. Thus, ATR-FTIR could be used to verify the presence of PEGDE on the membrane surface.

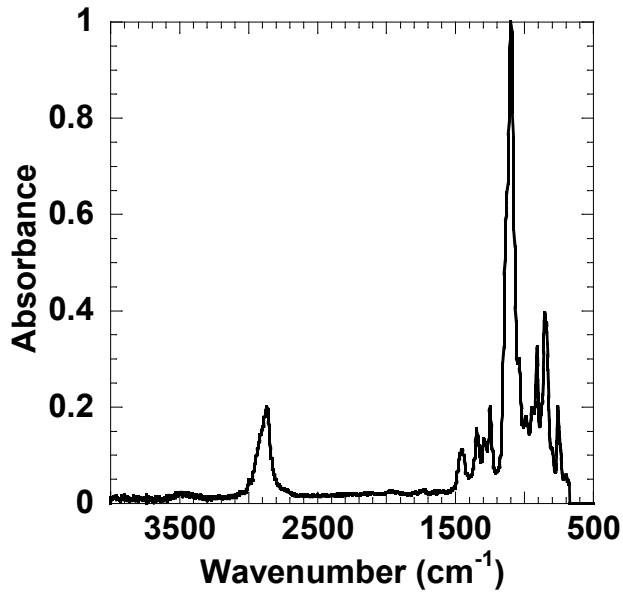

Figure 5.2. ATR-FTIR spectrum of MW 200 poly(ethylene glycol) diglycidyl ether.

5.2.2 XPS

The theoretical compositions of a fully crosslinked and uncrosslinked aromatic polyamide formed from *m*-phenylene diamine and trimesoyl chloride were calculated according to the repeat structures shown in Figure 5.3(a) and (b), respectively. Table 5.1 includes the calculated elemental composition of both theoretical structures, along with the measured composition of an XLE membrane determined from XPS. The oxygen to nitrogen ratio (O/N) included in Table 5.1 is often used for making comparisons between samples, since it minimizes the impact of ubiquitous adventitious carbon contamination that may affect measured carbon composition [2]. Comparing theoretical fully uncrosslinked and fully crosslinked O/N ratios (2.01 and 1.00, respectively) to the experimentally determined ratio (1.17), the XLE membrane appears to be approximately 83% crosslinked. That is, all three of the acid chloride groups have reacted with an amine group of *m*-phenylene diamine for approximately 83% of the trimesoyl chloride molecules, while for the remaining 17%, only two acid chloride groups have reacted, leaving the final acid chloride group to undergo hydrolysis to form a pendant carboxylic acid group. For comparison, characterization of an FT-30 membrane by Cadotte suggested that the polyamide was approximately 72% crosslinked [3]. Processing conditions and any hydrolysis of trimesoyl chloride occurring before the interfacial polymerization may play a role in observed sample-to-sample variability [3].

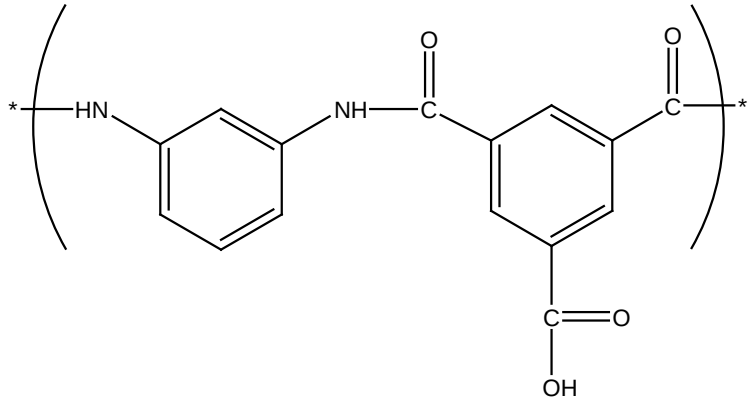

(a)

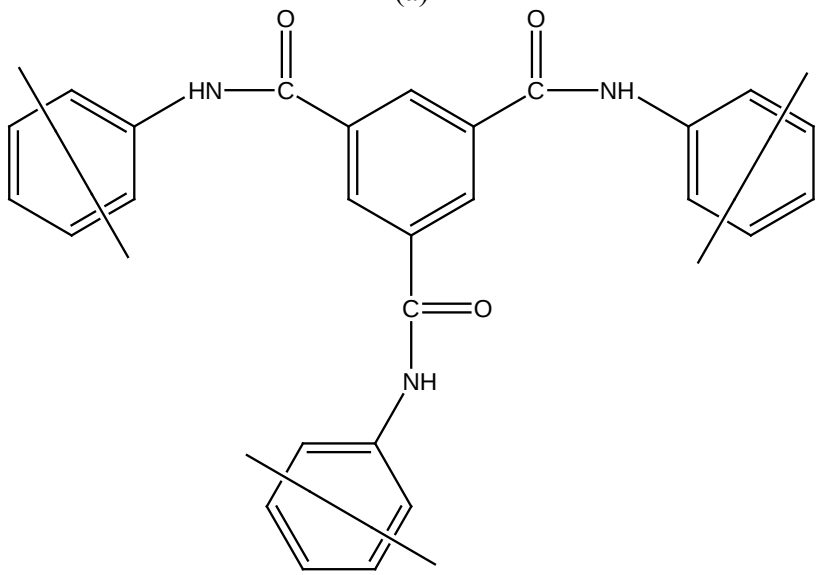

(b)

Figure 5.3 *Repeat chemical structures for (a) uncrosslinked ($C_{12}O_4N_2H_{10}$) and (b) crosslinked ($C_{18}O_3N_3H_{12}$) aromatic polyamides.*

Table 5.1. *Theoretical and measured polyamide elemental composition (atomic concentration).*

	O (%)	**N (%)**	**C (%)**	**O/N**
Uncrosslinked polyamide (theoretical)	19.1	9.5	71.4	2.01
Crosslinked polyamide (theoretical)	12.5	12.5	75.0	1.00
XLE	13.1	11.2	75.7	1.17

5.2.3 Surface Roughness and Hydrophilicity

The surface roughness and hydrophilicity of an XLE membrane were determined using AFM and contact angle measurements, respectively. The tapping mode was employed to prevent distortion of the delicate polyamide surface by the AFM tip, and analysis of 5 μm × 5 μm squares gave an RMS surface roughness of 58 ± 5 nm, in agreement with typical values reported for aromatic polyamide membranes [4, 5]. The aromatic amine used in the interfacial polymerization is thought to cause the ridge-and-valley surface structure of aromatic polyamides [3]. Other membranes, such as cellulose acetate membranes, have relatively smooth surfaces compared to aromatic polyamides (e.g., the roughness of a cellulose acetate membrane is on the order of 1 nm) [4].

The captive bubble method, using *n*-decane as the oil, was used to measure the oil in water contact angle of the XLE membrane. An image of an *n*-decane droplet on an XLE membrane submerged in water is given in Figure 5.4. The average contact angle (measured through the water phase) is 35 ± 2°, so the XLE membrane is already fairly hydrophilic (a smaller water phase contact angle indicates a more hydrophilic surface).

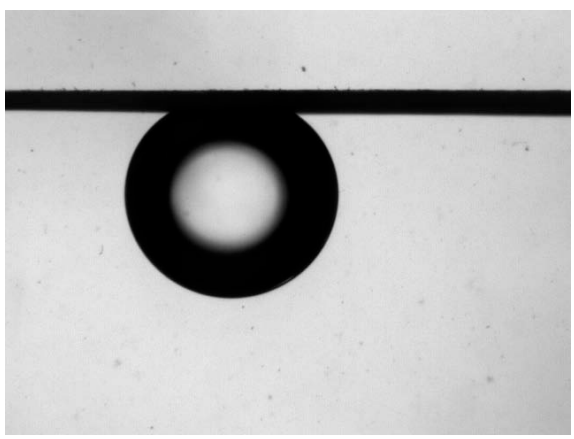

Figure 5.4 Image of an n-decane droplet on an inverted XLE membrane submerged in water, using the captive bubble method for contact angle measurement.

5.2.4 Surface Charge

Zeta potential was calculated from the measured streaming potential using the Fairbrother-Mastin approximation, as described in Chapter 3. The zeta potential as a function of pH for an XLE membrane is presented in Figure 5.5. The membrane surface is positively charged at low pH values, due to the protonated NH_3^+ groups, and negatively charged at high pH values, due to the deprotonated COO^- groups [6, 7]. The isoelectric point, or point of zero net surface charge, occurs at a pH of 4.3, in agreement with values reported in the literature for similar materials [7-9].

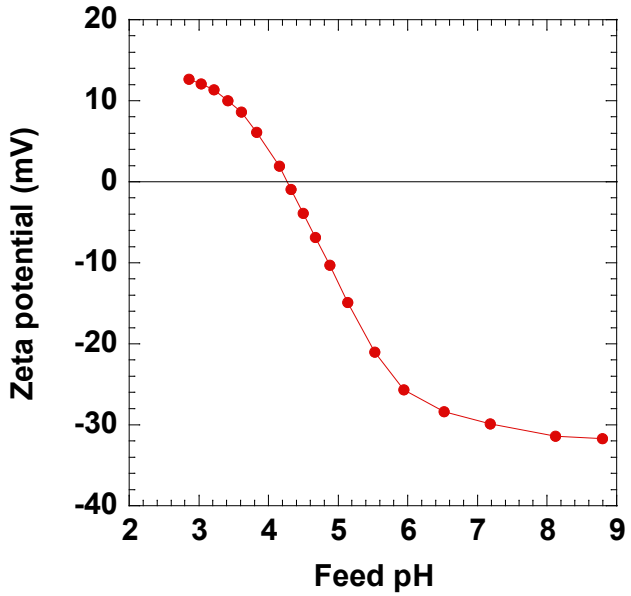

Figure 5.5. Zeta potential versus feed pH for an XLE membrane (0.01 M NaCl background electrolyte).

The charged nature of the polyamide membrane is responsible, at least in part, for its ability to reject salts such as sodium chloride. NaCl rejection increases linearly with increasing feed pH in the pH range 5 – 9 (cf. Figure 4.3). The change in rejection was fairly small over this pH range, corresponding to an increase in negative charge as indicated by the zeta potential measurements (cf. Figure 5.5). Figure 5.6 presents the apparent NaCl rejection as a function of pH for an XLE membrane, measured over a wider pH range (i.e., 3 – 9). In addition to overall rejection (determined from measured conductivity), individual ion rejections were also measured, using inductively coupled plasma mass spectroscopy (ICP-MS) to measure Na^+ concentration and ion chromatography to measure Cl^- concentration. Above pH 6, rejection increased slowly with pH, as was observed earlier (cf. Figure 4.3), and the overall and individual ion rejections were the same. As pH was decreased below 5, rejection decreased sharply. This was expected due to the positive charge on the membrane surface at low pH. However, the difference between the Na^+ and Cl^- rejections may indicate preferential permeation of hydronium ions over sodium ions with chloride ions to maintain electroneutrality. There was an excess of hydronium and chloride ions present at lower feed pH values due to the amount of added HCl required to reach those pH values, and acid transport has been suggested to explain the decrease in rejection below pH values of 5 [3]. Additionally, the discrepancy between overall rejection and individual ion (i.e., Na^+ and Cl^-) rejections at low pH may be due to H^+ and OH^- ion rejections, which were not measured individually, but would be included in the measured solution conductivity.

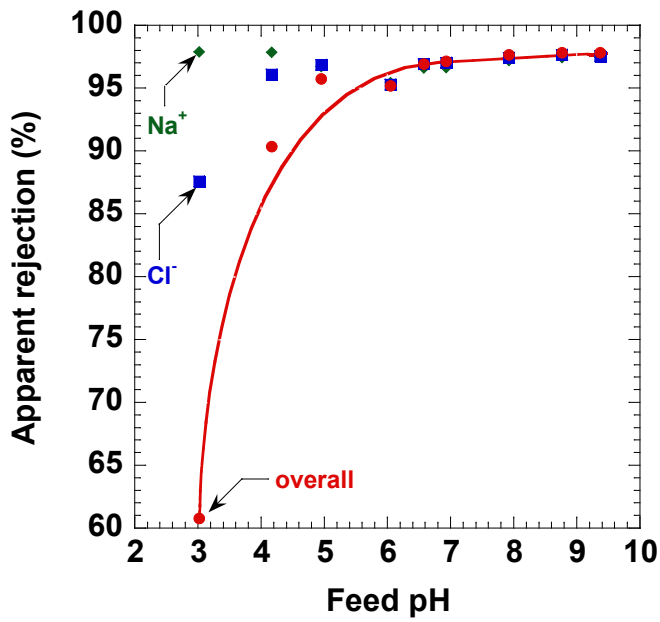

Figure 5.6. Apparent NaCl rejection as a function of feed pH for an XLE membrane. Overall rejection was determined from measuring solution conductivity, Na^+ rejection was determined using ICP-MS, and Cl^- rejection was determined using ion chromatography.

Using the expression for surface charged density, σ_s (C/m^2), given in Equation 2.39, the concentration of charged sites, [CS] (mol/m^2), may be written as follows:

$$[CS] = \left|\frac{\sigma_s}{eN_A}\right| = \left|\frac{1}{eN_A}\left(8RT\varepsilon\varepsilon_o c \times 10^3\right)^{1/2} \sinh\left(\frac{zF\varphi_w}{2\times 10^3 RT}\right)\right| \tag{5.1}$$

where e is the charge on an electron (1.602×10^{-19} C/electron) and N_A is Avogadro's number (6.023×10^{23} molecules/mol).

The measured zeta potential, ζ (mV), may be used to estimate the value of surface potential, φ_w (mV) (cf. Figure 2.8). Assuming that potential decays exponentially with distance from the membrane surface, the Stern potential, φ_s (i.e., the potential at the Stern plane, approximated by the Na^+ hydrated ion radius, 0.22 nm), is roughly 80% of the surface potential [6, 10]. Since the Stern potential is approximately equal to the zeta potential [10], the surface potential may be approximated by 1.25ζ. Substituting this approximation into Equation 5.1 yields:

$$[CS] = \left|\frac{\sigma_s}{eN_A}\right| = \left|\frac{1}{eN_A}\left(8RT\varepsilon\varepsilon_o c \times 10^3\right)^{1/2} \sinh\left(\frac{1.25zF\zeta}{2\times 10^3 RT}\right)\right| \tag{5.2}$$

The zeta potential data in Figure 5.5 were used in Equation 5.2 to calculate the concentration of charged sites as a function of pH.

For surface modification studies, it would be desirable to know the number of surface reactive groups (i.e., amine and carboxylic acid) present on the membrane surface, but this information is

not readily available. A model based on the pKa values of the COOH and NH_2 groups on an aromatic polyamide membrane surface was developed to allow estimation of the number of each type of group as well as the overall concentration of charged sites. The surface concentrations of carboxylic acid and amine groups that give the minimum difference between the calculated and measured (i.e., determined from zeta potential data) concentration of charged sites approximate the number of each group present on the membrane surface.

The equilibrium between protonated and deprotonated surface amine groups is given by:

$$RNH_3^+ + H_2O \leftrightarrow RNH_2 + H_3O^+ \tag{5.3}$$

The associated equilibrium constant is given by:

$$K_{RNH_3^+} = \frac{[RNH_2][H_3O^+]_s}{[RNH_3^+]} = 10^{-3.97} \tag{5.4}$$

where the pKa was estimated using an experimental pKa calculator [11]. $[H_3O^+]_s$ is used to distinguish the surface concentration from the bulk concentration, $[H_3O^+]_b$, and these two concentrations are related by:

$$[H_3O^+]_s = [H_3O^+]_b \exp\left(\frac{-1.25ze\zeta}{kT}\right) \tag{5.5}$$

where k is Boltzmann's constant (1.38×10^{-23} J/K), and the zeta potential has been used to estimate the surface potential. The bulk hydronium ion concentration is related to the pH of the electrolyte by:

$$[H_3O^+]_b = 10^{-pH} \tag{5.6}$$

The total concentration of amines on the membrane surface at any pH is equal to the sum of the concentrations of protonated and deprotonated amines:

$$[RNH_2]_{tot} = [RNH_3^+] + [RNH_2] \tag{5.7}$$

Equations 5.4 – 5.7 may be combined to give an expression for the concentration of protonated amine groups on the membrane surface:

$$[RNH_3^+] = [RNH_2]_{tot} \frac{10^{(3.97-pH)} \exp\left(\frac{-1.25ze\zeta}{kT}\right)}{1 + 10^{(3.97-pH)} \exp\left(\frac{-1.25ze\zeta}{kT}\right)} \tag{5.8}$$

The equilibrium between protonated and deprotonated surface carboxylic acid groups is given by:

$$RCOOH + H_2O \leftrightarrow RCOO^- + H_3O^+ \tag{5.9}$$

The associated equilibrium constant is given by:

$$K_{COOH} = \frac{[RCOO^-][H_3O^+]_s}{[RCOOH]} = 10^{-3.74} \tag{5.10}$$

where the pKa was again estimated using the experimental pKa calculator [11]. The total concentration of carboxylic acids on the membrane surface at any pH is equal to the sum of the concentrations of protonated and deprotonated carboxylic acids:

$$[RCOOH]_{tot} = [RCOOH] + [RCOO^-] \tag{5.11}$$

Equations 5.5 – 5.6 and 5.10 – 5.11 may be combined to give an expression for the concentration of deprotonated carboxylic acid groups on the membrane surface:

$$[RCOO^-] = [RCOOH]_{tot} \frac{10^{(pH-3.74)} \exp\left(\frac{1.25ze\zeta}{kT}\right)}{1 + 10^{(pH-3.74)} \exp\left(\frac{1.25ze\zeta}{kT}\right)} \tag{5.12}$$

The net concentration of charged sites, [CS] (mol/m^2), is given by:

$$[CS] = \left| [RNH_3^+] - [RCOO^-] \right| \tag{5.13}$$

where $[RNH_3^+]$ and $[RCOO^-]$ are given by Equations 5.8 and 5.12, respectively. Using the zeta potential data as a function of pH (cf. Figure 5.5) in Equations 5.8 and 5.12, the values of $[RNH_2]_{tot}$ and $[RCOOH]_{tot}$ that give the minimum difference between the concentration of charged sites calculated from Equation 5.13 and the previously determined experimental concentration of charged sites (cf. Equation 5.2) are 0.650×10^{-7} mol/m^2 and 1.03×10^{-7} mol/m^2, respectively.

In the interfacial polymerization reaction used to form the polyamide membrane, the polysulfone support is first soaked in an aqueous *m*-phenylene diamine solution before being contacted with an organic trimesoyl chloride solution [3]. Thus, there should be an excess of surface carboxylic acid groups compared to surface amine groups [12], so a 60% greater concentration of surface carboxylic acid groups, as calculated in the previous paragraph, is not unreasonable. Figure 5.7 presents the concentration of charged sites as a function of feed pH calculated from the model (Equation 5.13) using the optimum values of $[RNH_2]_{tot}$ and $[RCOOH]_{tot}$, and also from Equation 5.2 (i.e., using experimental zeta potential data). The fit over the entire pH range is poor, perhaps due to discrepancies between the pKa values used in the model (i.e., 3.97 for the amines and 3.74 for the carboxylic acids) and the actual pKa values of the carboxylic acid and amine groups on the surface of the polyamide membrane sample whose zeta potential was measured (i.e., sample-to-sample variability).

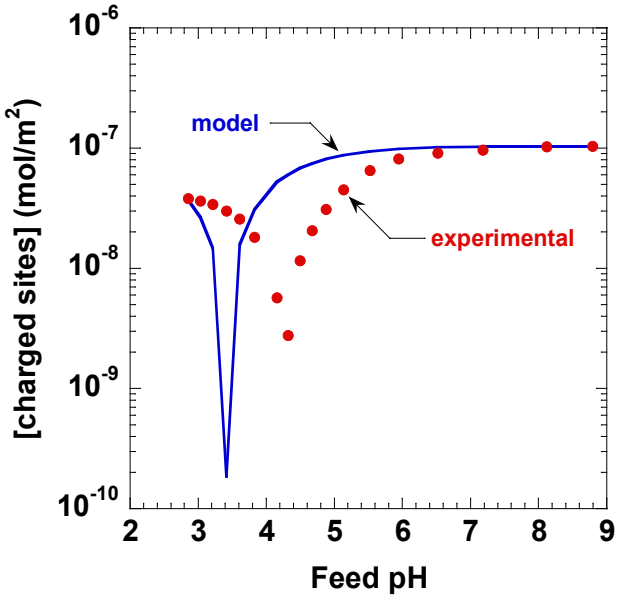

Figure 5.7 Surface concentration of charged sites as a function of feed pH, calculated from the model (Equation 5.13), with $[RNH_2]_{tot}$ = 0.650 × 10^{-7} mol/m^2 and $[RCOOH]_{tot}$ = 1.03 × 10^{-7} mol/m^2, and from Equation 5.2 (i.e., using experimental zeta potential data).

Since the pKa values of the two charged groups are very similar [13], they may be approximated as having the same value, so that the pKa value may be adjusted along with the $[RNH_2]_{tot}$ and $[RCOOH]_{tot}$ values to give the best fit between the experimental concentration of charged sites and the model prediction. Figure 5.8 presents the concentration of charged sites calculated from the experimental zeta potential data (Equation 5.2) and from the model (Equation 5.13) using the optimum values of pKa, $[RNH_2]_{tot}$ and $[RCOOH]_{tot}$. The pKa, $[RNH_2]_{tot}$ and $[RCOOH]_{tot}$ values used in Equation 5.13 are 4.6, 0.475 × 10^{-7} mol/m^2 and 1.03 × 10^{-7} mol/m^2, respectively. These concentrations correspond to a total of approximately 0.1 amine and carboxylic acid groups per nm^2 of membrane surface. The fit between the predicted (i.e., model) and experimental concentration of charged sites as a function of feed pH is very good over the entire pH range, and the ratio of carboxylic acid to amine groups is 2.2, indicating there are approximately twice as many surface carboxylic acid groups as amine groups.

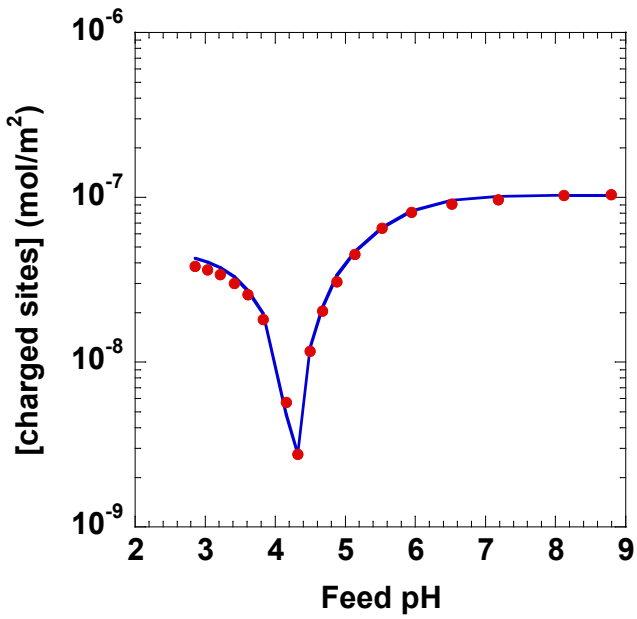

Figure 5.8. Surface concentration of charged sites as a function of feed pH, calculated from the model (Equation 5.13), with pKa = 4.6 for the amines and carboxylic acids, $[RNH_2]_{tot}$ = 0.475 × 10^{-7} mol/m^2 and $[RCOOH]_{tot}$ = 1.03 × 10^{-7} mol/m^2, and from Equation 5.2 (i.e., using experimental zeta potential data).

5.3 Conclusions

The chemical composition of an XLE polyamide membrane was characterized using ATR-FTIR and XPS, and its surface properties, including roughness, hydrophilicity, and charge, were measured. The XLE membrane presented the typical peaks associated with aromatic polyamides, and its chemical composition was indicative of a highly crosslinked polyamide. The membrane was hydrophilic and had a relatively rough surface. The surface charge and NaCl rejection of the XLE membrane were strongly dependent on feed pH. A model developed to estimate the surface concentration of carboxylic acid and amine groups suggested that there were approximately twice as many carboxylic acid groups as amine groups on the polyamide membrane surface.

5.4 References

[1] V. Freger, J. Gilron, S. Belfer, TFC polyamide membranes modified by grafting of hydrophilic polymers: an FT-IR/AFM/TEM study, Journal of Membrane Science, 209 (2002) 283-292.

[2] H. Celio, Texas Materials Institute, The University of Texas at Austin, personal communication, 2009.

[3] R.J. Petersen, Composite reverse osmosis and nanofiltration membranes, Journal of Membrane Science, 83 (1993) 81-150.

[4] M. Elimelech, X. Zhu, A.E. Childress, S. Hong, Role of membrane surface morphology in colloidal fouling of cellulose acetate and composite aromatic polyamide reverse osmosis membranes, Journal of Membrane Science, 127 (1997) 101-109.

[5] S.-Y. Kwak, S.G. Jung, Y.S. Yoon, D.W. Ihm, Details of surface features in aromatic polyamide reverse osmosis membranes characterized by scanning electron and atomic force microscopy, Journal of Polymer Science: Part B: Polymer Physics, 37 (1999) 1429-1440.

[6] W. Stumm, Chemistry of the Solid-Water Interface: Processes at the Mineral-Water and Particle-Water Interface in Natural Systems, John Wiley & Sons, Inc., New York, 1992.

[7] M. Elimelech, W.H. Chen, J.J. Waypa, Measuring the zeta (electrokinetic) potential of reverse osmosis membranes by a streaming potential analyzer, Desalination, 95 (1994) 269-286.

[8] A.E. Childress, M. Elimelech, Effect of solution chemistry on the surface charge of polymeric reverse osmosis and nanofiltration membranes, Journal of Membrane Science, 119 (1996) 253-268.

[9] G. Hurwitz, G.R. Guillen, E.M.V. Hoek, Probing polyamide membrane surface charge, zeta potential, wettability, and hydrophilicity with contact angle measurements, Journal of Membrane Science, 349 (2010) 349-357.

[10] R.F. Probstein, Physicochemical Hydrodynamics: An Introduction, 2nd ed., John Wiley & Sons, Inc., New York, 1994.

[11] W.E. Mickols, Dow Water & Process Solutions, personal communication, 2008.

[12] G.E. Zaikov, A.L. Iordanskii, V.S. Markin, Diffusion of Electrolytes in Polymers, VSP BV, Utrecht, 1988.

[13] E.V. Anslyn, D.A. Dougherty, Modern Physical Organic Chemistry, 10th ed., University Science Books, Sausalito, CA, 2006.

This page is intentionally left blank

6 SURFACE MODIFICATION USING POLY(ETHYLENE GLYCOL) DIGLYCIDYL ETHER TO ENHANCE MEMBRANE FOULING RESISTANCE

6.1 Abstract

To improve fouling resistance, polyamide reverse osmosis (XLE) and nanofiltration (NF90) membranes were modified by grafting poly(ethylene glycol) (PEG) diglycidyl ether (PEGDE) to their top surfaces from aqueous solution. The effect of PEG molecular weight (200 vs. 1000) and treatment solution concentration (1% (w/w) vs. 15% (w/w)) on water flux and NaCl rejection was measured. XLE membranes were treated with both molecular weight PEGDEs, while NF90 membranes were only treated with the higher molecular weight PEGDE. PEGDE grafting density as well as surface properties of modified and unmodified membranes, including charge, hydrophilicity and roughness, were measured and compared. The fouling resistance of modified membranes to charged surfactants (i.e., sodium dodecyl sulfate (SDS) and dodecyltrimethylammonium bromide (DTAB)) and emulsions of *n*-decane and these charged surfactants was compared to that of unmodified membranes. In general, modified membranes exhibited improved fouling resistance and an improved ability to be cleaned after fouling compared to unmodified membranes. Fouling resistance increased with increasing PEG molecular weight, but showed little dependence on treatment solution concentration, suggesting that further improvements in membrane fouling resistance might be obtained by using lower concentrations of higher molecular weight PEG for surface modification.

6.2 Results and Discussion

6.2.1 Characterization of PEGDE on the Modified Membrane Surfaces via FTIR and XPS

ATR-FTIR and XPS were used to qualitatively verify the presence of PEGDE on the membrane surface following the surface grafting protocol. Figures 6.1 (a) and 6.1 (b) present ATR-FTIR spectra in the range of 1000 to 1200 cm^{-1} for the modified and unmodified XLE and NF90 membranes, respectively. The polyamide membrane has several peaks in this region [1], including those at 1080, 1105, 1150 and 1170 cm^{-1} attributed to the C-C stretch of the aromatic rings [2]. The largest peak for PEG, attributed to the ether C-O stretch as well as the C-C stretch, occurs around 1100 cm^{-1} [3], and may be expected to cause a noticeable change in absorbance for the PEGDE-modified membranes, as was observed by Kang et al. for membranes modified with MPEG-NH_2 [4]. Figures 6.1(a) and 6.1(b) reveal an increase in absorbance around 1100 cm^{-1} (i.e., between 1080 and 1130 cm^{-1}) with increasing PEG molecular weight and concentration of the aqueous PEGDE treatment solution. Peaks at 1150 and 1170 cm^{-1} do not exhibit a systematic increase in absorbance upon PEGDE modification, as expected since PEGDE has minimal absorbance at these wavenumbers. The penetration depth of ATR-FTIR is approximately 1 μm [5], so the fact that the peaks of the polyamide membrane are visible after PEGDE modification indicates that the PEGDE graft layer is thinner than 1 μm.

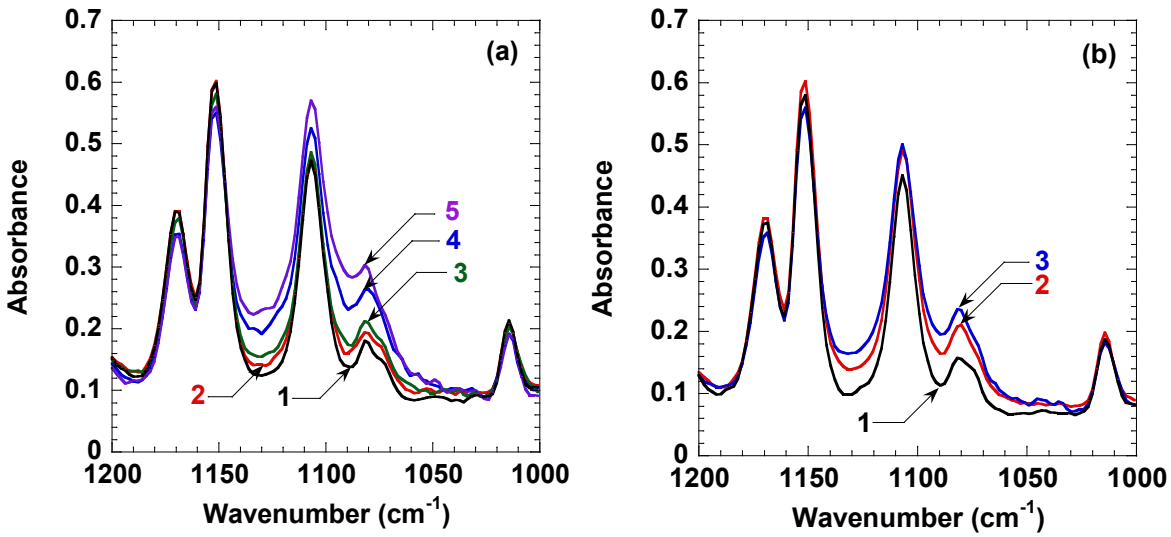

Figure 6.1. ATR-FTIR spectra in the range 1000 – 1200 cm^{-1} for (a) the unmodified XLE membrane (1) and XLE membranes modified with 1% (w/w) MW 200 PEGDE (2), 1% (w/w) MW 1000 PEGDE (3), 15% (w/w) MW 200 PEGDE (4), and 15% (w/w) MW 1000 PEGDE (5), and (b) the unmodified NF90 membrane (1) and NF90 membranes modified with 1% (w/w) MW 1000 PEGDE (2) and 15% (w/w) MW 1000 PEGDE (3).

Table 6.1 presents atomic concentration data from XPS analysis of an unmodified XLE membrane and XLE membranes modified with 1% (w/w), 15% (w/w), and 100% (w/w) MW 1000 PEGDE. Since PEGDE contains oxygen but not nitrogen (excluding hydrogen, PEGDE contains 67% carbon and 33% oxygen), the observed increases in oxygen content and decreases in nitrogen content upon PEGDE modification are expected, and the ratio of oxygen to nitrogen on the membrane surface increases. Additionally, the carbon content of an XLE membrane, 75.7%, is higher than that in PEGDE (67%), so the observed decrease in carbon content with increasing concentration of PEGDE in the surface treatment solution (and, presumably, increasing amounts of PEGDE on the membrane surface), is consistent with the oxygen and nitrogen results. These trends (i.e., decreasing nitrogen and carbon content and increasing oxygen content and oxygen to nitrogen ratio) have also been observed by Kang et al. [4] and Sagle et al. [6] for polyamide membranes modified with PEG-based materials, so the changes in composition observed here are reasonable within the context of the previous work done in this area. Furthermore, these XPS results are qualitatively consistent with the ATR-FTIR results.

Table 6.1 XPS measurements of surface atomic concentration (%) of oxygen, nitrogen and carbon measured for an unmodified XLE membrane and XLE membranes modified with MW 1000 PEGDE.

Membrane	O (%)	N (%)	C (%)	O/N
XLE	13.1	11.2	75.7	1.17
1% (w/w) MW 1000 XLE	13.7	10.7	75.6	1.28
15% (w/w) MW 1000 XLE	15.6	10.3	74.1	1.51
100% (w/w) MW 1000 XLE	17.6	10.4	72.0	1.69

Interestingly, even an XLE membrane treated with 100% (w/w) MW 1000 PEGDE (i.e., no water used in the treatment solution) still has a sizeable nitrogen content according to XPS. This result indicates that the PEGDE layer is thinner than the photoelectron escape depth. In general, the photoelectron escape depth is approximately 10 nm (at 0° takeoff angle) [6], and the 45° takeoff angle used here is expected to probe an even thinner surface layer. However, Sagle et al. reported that a 2 µm thick layer of crosslinked poly(ethylene glycol) diacrylate on a polyamide membrane still resulted in significant nitrogen content as measured by XPS [6], so XPS may not be a good indicator of PEG layer thickness, or the grafted layer may not be uniform over the region of membrane probed by XPS. However, XPS does provide qualitative evidence of the presence of PEGDE on the membrane surface.

6.2.2 Graft Density of PEGDE on the Modified Membrane Surface

Figure 6.2 presents the dependence of graft density on the concentration of PEGDE in the aqueous treatment solution. Graft density increased with increasing PEGDE concentration, and, at least for membranes modified with 15% (w/w) PEGDE, graft density was larger for membranes modified with higher molecular weight PEGDE. The graft density data are also qualitatively consistent with the ATR-FTIR and XPS results presented above (i.e., higher graft density corresponds to higher absorbance in the range of 1080 to 1130 cm^{-1} and higher oxygen to nitrogen ratio).

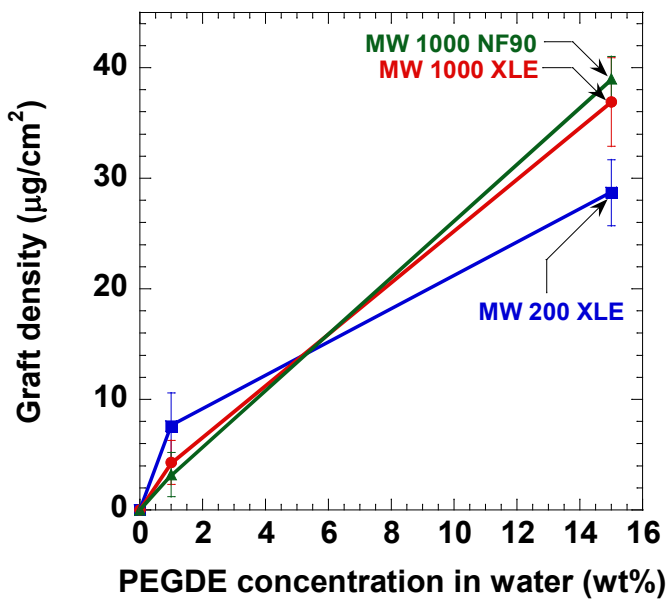

Figure 6.2. Graft density for XLE membranes modified with 1% (w/w) and 15% (w/w) MW 200 and MW 1000 PEGDE, and NF90 membranes modified with 1% (w/w) and 15% (w/w) MW 1000 PEGDE. The unmodified XLE and NF90 membranes (i.e., 0% (w/w) PEGDE concentration in water) are shown on this figure at zero graft density. Error bars associated with graft density indicate the standard deviation of the results for at least three membrane samples.

The apparent effective PEGDE thickness on the membrane surface may be estimated from the measured graft densities (μg/cm^2) and the density of PEGDE (the density of MW 1000 PEGDE is not reported by the supplier, so the density of MW 200 PEGDE, 1.15 g/cm^3 is used as an estimate). The range of graft densities observed (3 – 39 μg/cm^2) corresponds to thicknesses of 26 – 339 nm. Previous work by Belfer et al. reported a grafting layer thickness of 20 nm for a semi-aromatic piperazine-based polyamide nanofiltration membrane grafted with polyacrylic acid [5], while Louie et al. reported a coating thickness of 0.3 μm (300 nm) for a commercial polyamide reverse osmosis membrane coated with PEBAX® 1657 [7], so the layer thicknesses due to PEGDE grafting appear to be similar to those reported earlier. Using the measured graft densities and the molecular weight of PEGDE, and approximating the membrane surface as a flat sheet, the number of PEGDE molecules per unit area can also be estimated. The measured graft densities suggest the presence of 15 to over 500 PEGDE molecules per nm^2 of membrane, depending on the molecular weight and concentration of PEGDE. Based on estimation of surface charge density from zeta potential analysis (cf. Chapter 5), the total number of reactive amine and carboxylic acid groups present on the same area of polyamide membrane surface (~ 0.1 amine and carboxylic acid groups per nm^2 of membrane) is likely to be two to three orders of magnitude smaller than the number of PEGDE molecules present [8]. Thus, the amount of PEGDE attached to a membrane surface is apparently not strictly limited by the number of surface amine and carboxylic acid groups, which suggests that additional PEGDE may also adsorb onto the membrane surface, perhaps filling surface defects, in addition to grafting to the reactive groups on the membrane surface.

The membrane modification procedure was altered in the graft density experiments to accommodate the sample size required for use in the magnetic suspension balance. Small samples (1 in^2) were required to fit in the sample pail, making isolation of the top surface of each of the membranes impractical, so the membranes were treated by submersion, using as little PEGDE solution as possible to cover all twelve samples. Water flux is lower for membranes modified by submersion versus top surface isolation, but the post-modification isopropanol soak and water rinses are expected to remove unreacted PEGDE. However, it is possible that not all unreacted PEGDE was removed (e.g., PEGDE could be adsorbed to the reinforcing fabric backing). The magnetic suspension balance would detect any residual PEGDE, resulting in apparent grafting density values somewhat higher than those obtained in samples that were only modified by exposure of the top surface of the membrane to PEGDE. Thus, the reported graft densities are upper bounds of the graft density for samples used for fouling characterization (i.e., membranes treated by top surface isolation). Additionally, 70 grams of solution were required to completely cover the surface of all twelve 1 in^2 membrane samples (0.9 grams of solution/cm^2 membrane), versus the 10 grams used to treat the membranes in all other experiments (where a single continuous area of membrane was modified in a 10 cm diameter casting ring; 0.1 grams of solution/cm^2 membrane). However, decreasing the amount of treatment solution as much as possible (to 0.6 grams of solution/cm^2 membrane) revealed no measurable difference in graft density, indicating this difference in treatment procedure had negligible effect on graft density. Finally, mass measurements were done in air, so measured graft densities may include not only grafted PEGDE, but also water absorbed by the highly hydrophilic PEGDE. Performing the measurements under vacuum did not result in lower graft densities, so it appears that the amount of absorbed water is negligible compared to the amount of PEGDE grafted to the membrane.

6.2.3 Surface Charge, Hydrophilicity, and Roughness

The measured surface properties of unmodified and modified XLE and NF90 membranes, as well as those of the unmodified LE membrane, are presented in Table 6.2. The LE membrane is included because it has lower water flux than the XLE and NF90 membranes, and its fouling behavior will be compared to that of the modified XLE and NF90 membranes. This strategy permits a comparison of fouling properties in modified and unmodified membranes having approximately the same initial flux. The unmodified LE, XLE and NF90 membranes all have essentially the same zeta potential at pH 8 (~ -32 mV). At the same pH (pH 8) and using the same background electrolyte (i.e., 10 mM NaCl), zeta potential values between -10 and -40 mV have previously been reported for polyamide desalination membranes [6, 9, 10]. The zeta potential of modified XLE membranes is essentially equal to that of an unmodified XLE membrane. In contrast, the modified NF90 membranes have slightly less negative zeta potentials than the unmodified NF90 membrane. Since PEGDE is a neutral molecule, it is expected to lower the magnitude of the membrane's surface charge, but the charge of the underlying polyamide is dominant for the modified membranes. Sagle et al. reported that polyamide membranes coated with 2 µm thick PEG-based hydrogel layers experienced a 25% decrease in surface charge [6], so it is reasonable that the PEG layer thicknesses estimated here (26 – 339 nm) would have minimal effect on surface charge.

Table 6.2. Surface properties (charge, hydrophilicity and roughness) of unmodified and PEGDE-modified membranes.

Membrane	Zeta potential at pH 8 (mV)	Oil-in-water contact angle (^{o})	RMS surface roughness (nm)
LE	-32.2 ± 0.6	33 ± 2	55 ± 3
XLE	-31.2 ± 1.3	35 ± 2	58 ± 5
1% (w/w) MW 200 XLE	-30.8 ± 1.0	-	-
15% (w/w) MW 200 XLE	-31.3 ± 0.4	37 ± 2	70 ± 4
1% (w/w) MW 1000 XLE	-29.8 ± 1.4	-	-
15% (w/w) MW 1000 XLE	-29.8 ± 0.3	32 ± 2	77 ± 3
NF90	-32.4 ± 1.1	30 ± 3	47 ± 5
1% (w/w) MW 1000 NF90	-26.4 ± 0.3	-	-
15% (w/w) MW 1000 NF90	-26.3 ± 0.5	32 ± 6	56 ± 1

The contact angles for unmodified and highly modified (i.e., 15% (w/w) PEGDE treatment solution concentration) membranes showed no measurable difference, and the low contact angle values (approximately 30°) indicated all the membranes were hydrophilic. Louie et al. reported that coating a commercial polyamide reverse osmosis membrane with PEBAX® 1657 had a negligible effect on contact angle, although the actual contact angle values reported for the modified and unmodified membranes (~ 60 ^{o}) were higher, possibly due to differences in measurement conditions (i.e., measurement of air-in-water contact angle versus the oil-in-water contact angle measured here) [7].

The surface roughness values in Table 6.2 indicate PEGDE modification may cause a slight increase in roughness, perhaps indicating conformation of PEGDE to the polyamide ridge-and-valley surface structure during grafting. Polyamide membrane surface roughness is typically reported to be approximately 50-100 nm [4, 5, 7, 11], in agreement with the values measured here for the unmodified LE, XLE and NF90 polyamide membranes. Reports of the effect of surface modification on surface roughness vary. While Louie et al. and Belfer et al. reported decreases in surface roughness upon modification with PEBAX® 1657 and PEGMA, respectively, of up to 65% [5, 7], Kang et al. observed a 60% increase in surface roughness upon modification with MPEG-NH_2 [4]. Thus, the slight increase in surface roughness observed here upon PEGDE modification (~ 19 – 33%) is reasonable considering the range of results reported previously. Overall, PEGDE modification appears to cause minimal changes in surface charge, hydrophilicity and roughness.

6.2.4 Water Flux and NaCl Rejection of Modified Membranes

The water flux and true NaCl rejection in 2000 mg/L NaCl feed of the PEGDE-modified and unmodified XLE and NF90 membranes are presented in Figures 6.3(a) and 6.3(b), respectively. The data were collected from the initial NaCl feed portion of the fouling experiments (cf. Figure 3.7(a), t = 30 min – 1 hr). Modification of the XLE membrane with 1% (w/w) MW 200 PEGDE caused a 15% decrease in water flux and no change in NaCl rejection, while treatment with a 15% (w/w) MW 200 PEGDE solution produced a modified XLE membrane with 31% lower water flux and 0.2% higher NaCl rejection than the unmodified XLE membrane. Modification of the XLE membrane with MW 1000 PEGDE resulted in a larger decrease in water flux and increase in NaCl rejection than that obtained with the MW 200 PEGDE. However, there was minimal change in performance due to modification with a 15% (w/w) MW 1000 PEGDE solution relative to modification with a 1% (w/w) MW 1000 PEGDE solution (44% vs. 37% decrease in water flux and 0.4% vs. 0.3% increase in NaCl rejection compared to the unmodified XLE membrane, respectively). Thus, it appears that, at least for the higher molecular weight PEGDE, after initially grafting PEGDE to the membrane surface, treatment with higher concentration PEGDE solutions has less impact on membrane performance. Surface modifications causing decreases in water flux similar to those observed for PEGDE modification have been reported by Sagle et al. (~ 35 – 40% decrease in water flux observed for PEG hydrogel-coated membranes) [6] and Belfer et al. (up to 30 % decrease in water flux for membranes grafted with PEGMA) [12], although much larger reductions in water flux due to surface modification have also been reported (e.g., Louie et al. reported up to an 80% decrease in water flux for membranes coated with PEBAX® 1657 [7] and Mickols observed a 75% decrease in water flux for a reverse osmosis membrane treated by submersion in a 1% (w/w) MW 200 PEGDE solution [13]). Additionally, surface modifications that reduce flux often increase rejection [6, 7, 12, 13], so the increase in rejection accompanying surface modification with PEGDE is reasonable. Increasing rejection could be explained as the result of plugging surface defects in the polyamide membrane by PEGDE, or possibly as the result of PEGDE interacting with and influencing the transport properties of the polyamide membrane [6, 14].

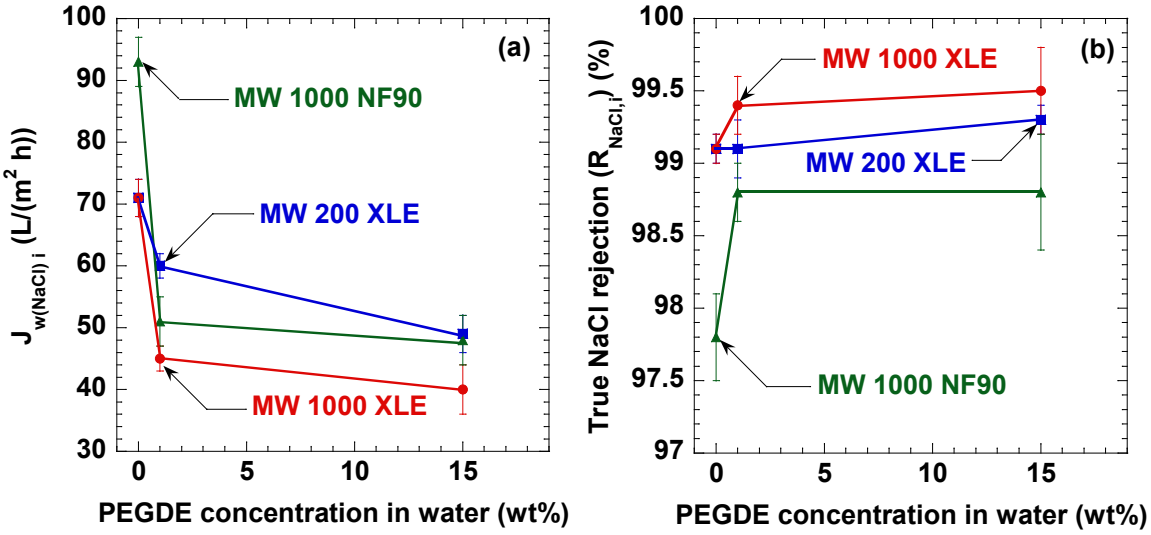

Figure 6.3. *(a) Water flux and (b) true NaCl rejection in 2000 mg/L NaCl feed, for unmodified XLE and NF90 membranes (i.e., 0% (w/w) PEGDE concentration in water), XLE membranes modified with 1% (w/w) and 15% (w/w) MW 200 and MW 1000 PEGDE, and NF90 membranes modified with 1% (w/w) and 15% (w/w) MW 1000 PEGDE. Error bars in the figures indicate the standard deviation of the performance of at least six membrane samples.*

Plugging of minute surface defects in the unmodified polyamide membrane by PEGDE could also help explain the minimal difference in performance for membranes modified with low (1% (w/w)) and high (15% (w/w)) concentrations of PEGDE. Although PEG is a much more permeable material than the polyamide layer in desalination membranes, it is still far less permeable than a defect, so plugging defects with even small amounts of PEGDE could result in substantial decreases in water flux (e.g., the 37% flux decline observed for XLE membranes treated with 1% (w/w) MW 1000 PEGDE) and contribute to an increase in rejection. However, PEGDE grafted onto the dense, defect-free polyamide surface, which presumably constitutes the vast majority of the membrane surface, would have a much smaller effect on water flux, since the permeability of the polyamide is believed to be much lower than that of PEGDE (e.g., the 7% further flux decline caused by grafting 15% (w/w) MW 1000 PEGDE onto the XLE membrane surface).

The increase in NaCl rejection observed for XLE membranes modified with MW 1000 PEGDE inspired the use of NF90 membranes for modification. PEGDE modification always decreases water flux, but using the higher flux NF90 membranes and leveraging the NaCl rejection enhancement observed upon modification could lead to higher flux modified membranes with NaCl rejection values similar to those of the XLE membranes. Although modification led to larger relative declines in water flux for the NF90 membranes than the XLE membranes (e.g. 45% vs. 37% decrease in water flux for membranes modified with 1% (w/w) MW 1000 PEGDE, which may indicate a larger number of defects in the less-selective NF90 membranes), NF90 membranes modified with MW 1000 PEGDE did have higher water flux than the comparable

modified XLE membranes (cf. Figure 6.3(a), 51 vs. 45 L/(m^2 h) (LMH) and 48 vs. 40 LMH for membranes modified with 1% (w/w) and 15% (w/w) PEGDE solutions, respectively). However, the modified NF90 membranes did not quite reach the same level of NaCl rejection as the modified XLE membranes (cf. Figure 6.3(b)), although their NaCl rejection increased enough (from 97.8% to 98.8%) to fall within the manufacturer's target range for the XLE membranes (98.0 – 99.0%, cf. Table 3.1). The water flux of the unmodified NF90 membrane (93 LMH) was near the lower end of the manufacturer's target range (91 – 134 LMH), while its NaCl rejection (97.8%) exceeded the expected range (85 - 95%) [15]. Lower water flux is typically accompanied by increased NaCl rejection due to the inverse relationship between permeability and selectivity [16-18], so the unmodified NF90 performance falls in line with this tradeoff, suggesting that this particular roll of NF90 membrane was simply more selective than an average NF90 membrane.

Figure 6.4 presents the dependence of water flux on PEGDE grafting density measured using the magnetic suspension balance. The behavior for all modified membranes (MW 200 and MW 1000 XLE and MW 1000 NF90) followed similar trends to those observed in Figure 6.3(a), where water flux was presented as a function of PEGDE treatment solution concentration. For XLE and NF90 membranes modified with MW 1000 PEGDE, a large decrease in water flux was observed at low grafting densities (i.e., membranes treated with 1% (w/w) MW 1000 PEGDE solution), and a subsequent large increase in grafting density resulted in little additional decrease in water flux (i.e., membranes treated with 15% (w/w) MW 1000 PEGDE solution). XLE membranes modified with MW 200 PEGDE, on the other hand, exhibited a more gradual decline in water flux with increasing grafting density, similar to the observed dependence of water flux on PEGDE treatment solution concentration for these membranes.

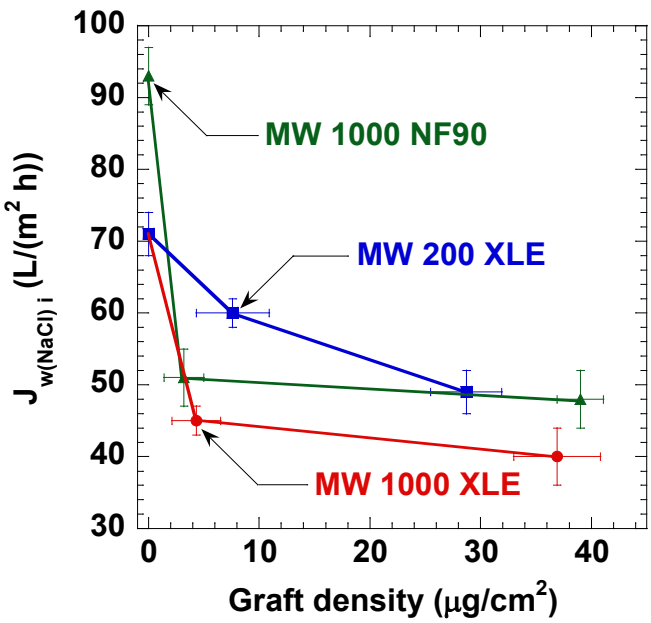

Figure 6.4. *Water flux in a 2000 mg/L NaCl feed versus graft density measured using the magnetic suspension balance, for XLE membranes modified with 1% (w/w) and 15% (w/w) MW 200 and MW 1000 PEGDE, and NF90 membranes modified with 1% (w/w) and 15% (w/w) MW 1000 PEGDE. The unmodified XLE and NF90 membranes (i.e., 0% (w/w) PEGDE concentration in water) are shown on this figure at zero graft density. Error bars associated with $J_{w(NaCl)i}$ are defined in Figure 6.3; error bars associated with graft density are defined in Figure 6.2.*

6.2.5 Fouling Resistance and Flux Recovery in Surfactant Fouling Tests

Figure 6.5 illustrates representative results from fouling experiments. In this example, the fouling of unmodified LE and XLE membranes as well as an XLE membrane modified with 1% (w/w) MW 1000 PEGDE by SDS is presented. Figure 6.5(a) presents water flux as a function of time, where the first point for each membrane corresponds to $J_{w(NaCl)i}$ in Figure 3.7(b). The water flux data up to t = 24 hrs represents the fouling portion of the test (the water flux at t = 24 hrs corresponds to $J_{w(foul)}$ in Figure 3.7(b)), and the time period t = 27 – 30 hrs monitors the flux recovery after cleaning the membranes (the water flux at t = 30 hrs is $J_{w(NaCl)f}$ in Figure 3.7(b)). The modified XLE membrane had lower water flux than the unmodified XLE membrane throughout the entire experiment, but it is difficult to compare the performance of these two membranes directly because modification decreased the initial water flux ($J_{w(NaCl)i}$) by 34%. Initial water flux may impact the extent of fouling observed, since a higher flux membrane will process (i.e., permeate) a larger volume of feed water (and therefore, be exposed to a larger amount of the foulant) during a given time period than a lower flux membrane. An increase in fouling rate with increasing water flux has been observed previously for reverse osmosis membranes [19].

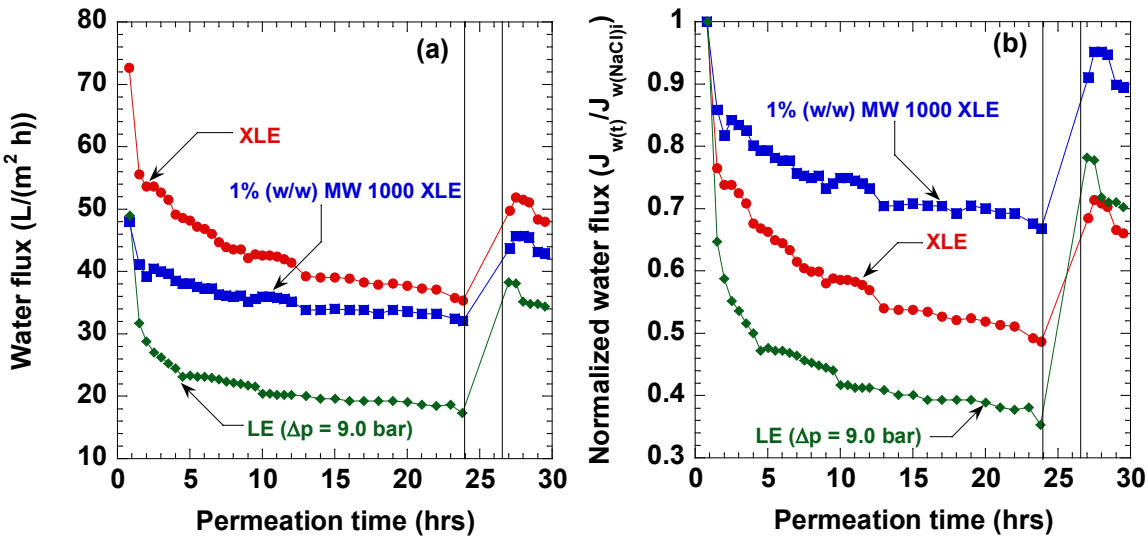

Figure 6.5. Typical fouling behavior observed in all fouling tests, using SDS fouling results obtained for unmodified LE and XLE membranes and an XLE membrane modified with 1% (w/w) MW 1000 PEGDE. (a) Water flux and (b) normalized water flux, as a function of time.

One means of minimizing the effect of water flux on fouling rate is to compare the performance of modified membranes with that of unmodified membranes of similar initial water flux. Since all three membranes chosen for study (i.e., LE, XLE and NF90) share approximately the same polyamide chemistry, they are expected to exhibit similar fouling behavior. Figure 6.5(a) also includes the performance of an unmodified LE membrane, operated at a lower transmembrane pressure difference (i.e., $\Delta p = 9.0$ bar vs. $\Delta p = 10.3$ bar used for the other membranes) to closely match the initial water flux of the modified XLE membrane. During the fouling experiment, the modified XLE membrane had higher water flux than the unmodified LE membrane. That is, the modified XLE membrane demonstrated better fouling resistance, and flux recovery after cleaning, than an unmodified LE membrane with nearly identical initial water flux.

In Figure 6.5(b), the data from Figure 6.5(a) are presented in terms of normalized water flux, determined by dividing the water flux at time t (i.e., $J_{w(t)}$) by $J_{w(NaCl)i}$. Flux normalization allows comparison of membranes with dissimilar initial water fluxes (e.g., the unmodified XLE membrane and XLE membrane modified with 1% (w/w) MW 1000 PEGDE). Although it is difficult to determine which of these two membranes has better fouling resistance in Figure 6.5(a), Figure 6.5(b) demonstrates that the modified XLE membrane retained more of its initial water flux than the unmodified XLE membrane (70% vs. 50%, respectively), and the modified XLE membrane also regained more of its lost flux after cleaning (90% vs. 66%, respectively).

Figures 6.6 (a) and 6.6 (b) give the water flux and normalized water flux, respectively, as a function of volumetric throughput during the SDS fouling test (i.e., up to t = 24 hours), rather than the presentation in Figures 6.5(a) and 6.5(b), where the same flux data were presented as a function of permeation time. Volumetric throughput, or the total permeate volume produced per unit area of membrane in a given time, is another important indicator of membrane performance. Although it is unclear in Figure 6.5, Figure 6.6 clearly demonstrates that the unmodified XLE membrane produces the most permeate during the 24 hour fouling test (~ 1.1 m^3/m^2 membrane),

followed by the XLE membrane modified with 1% (w/w) MW 1000 PEGDE (~ 0.9 m^3/m^2 membrane) and, finally, the unmodified LE membrane operated at lower transmembrane pressure difference (Δp = 9.0 bar) to match the initial water flux of the modified XLE membrane (~ 0.6 m^3/m^2 membrane). Thus, the XLE membrane modified with 1% (w/w) MW 1000 PEGDE had higher water flux and volumetric throughput than the unmodified LE membrane with nearly identical initial water flux.

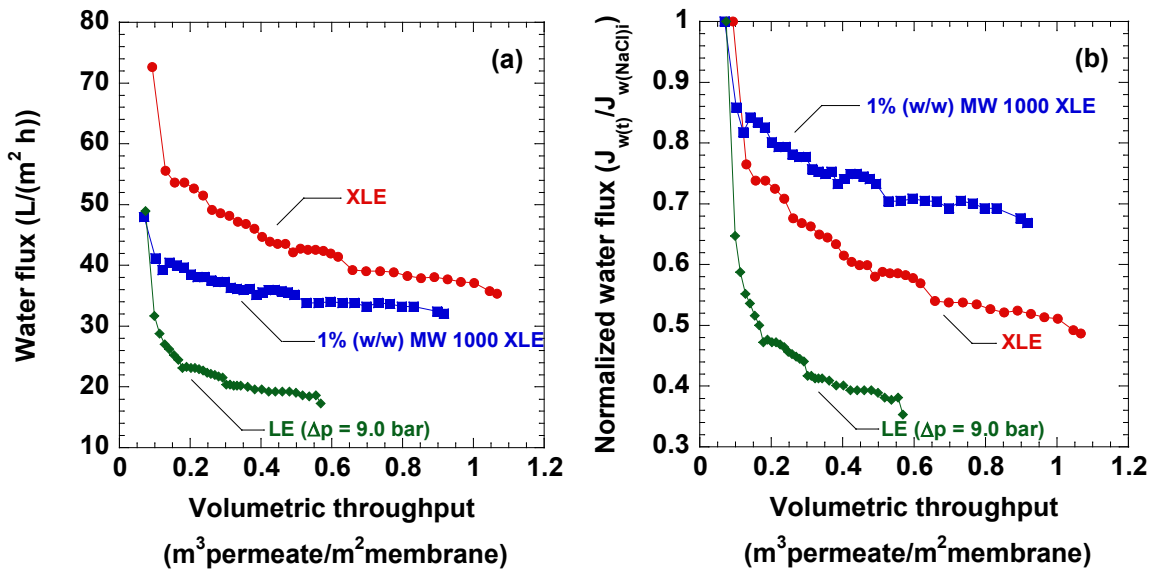

Figure 6.6. Typical fouling behavior observed in all fouling tests, using SDS fouling results obtained for unmodified LE and XLE membranes and an XLE membrane modified with 1% (w/w) MW 1000 PEGDE. (a) Water flux and (b) normalized water flux, as a function of volumetric throughput.

In addition to water flux and volumetric throughput, the salt rejection capability of the membranes should also be considered when comparing their performance. The initial NaCl rejection values of the XLE, 1% (w/w) MW 1000 PEGDE XLE and LE membranes were 99.1%, 99.4% and 99.1%, respectively, and at the end of the 24 hour fouling test, the NaCl rejection had increased to 99.9% for all three membranes. Using linear interpolation between the initial and final rejection values to calculate the amount of NaCl permeated reveals the XLE membrane produced twice as much salt as either the XLE membrane modified with 1% (w/w) MW 1000 PEGDE or the LE membrane during the 24 hour fouling test. Thus, although the XLE membrane had slightly higher water flux than the XLE membrane treated with 1% (w/w) MW 1000 PEGDE at the end of the 24 hour fouling test (35 vs. 32 LMH, cf. Figure 6.5(a) or Figure 6.6(a)), it also permeated twice as much salt. In addition, the LE and 1% (w/w) MW 1000 XLE membranes had similar initial water fluxes and produced similar amounts of salt during the 24 hour test, but the modified XLE membrane had higher water flux (32 vs. 17 LMH) and higher volumetric throughput (0.9 m^3 permeate/m^2 membrane vs. 0.6 m^3 permeate/m^2 membrane) than the LE membrane at the end of the 24 hour fouling test (cf. Figure 6.6(a)).

In the following figures, fouling results are presented in terms of flux retained after fouling ($J_{w(foul)}/J_{w(NaCl)i}$) and regained after cleaning ($J_{w(NaCl)f}/J_{w(NaCl)i}$) (i.e., the normalized water flux at t = 24 hrs and at t = 30 hrs, respectively, cf. Figure 6.5(b)) as a function of initial water flux ($J_{w(NaCl)i}$), to account, at least approximately, for the effect of initial water flux on fouling behavior.

The SDS fouling data for all modified XLE and NF90 membranes as well as unmodified LE, XLE and NF90 membranes are summarized in Figures 6.7(a) and 6.7(b), showing the fraction of flux retained after fouling and the fraction of flux regained after cleaning, respectively. In these and subsequent figures presenting summaries of fouling data, the filled symbols represent results from modified membranes, and the unfilled symbols represent results from unmodified membranes. LE membranes were tested at three different transmembrane pressures to allow comparison of modified XLE and NF90 membrane behavior to the behavior of unmodified membranes with similar initial water fluxes. Comparison of modified and unmodified membrane performance at the same initial water flux demonstrates that several modified membranes had better fouling resistance in SDS tests, based upon fraction of flux retained after fouling and flux recovery after cleaning (i.e., fraction of flux regained), than the unmodified membranes. For example, the XLE membranes modified with 1% (w/w) MW 1000 PEGDE retained and regained approximately 20 – 25% more of their initial flux than did the LE membranes of similar initial water flux (~ 45 LMH). Similar improvements in SDS fouling resistance (i.e., flux retention) were observed by Sagle et al. for polyamide membranes coated with PEG-based hydrogels [6].

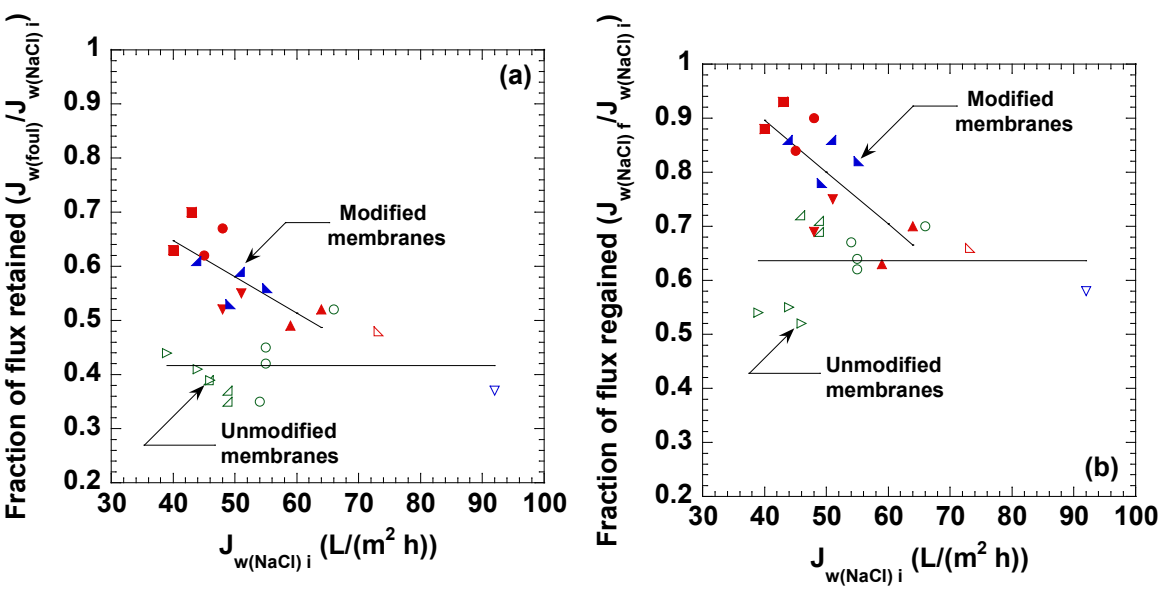

Figure 6.7. *(a) Fraction of flux retained after fouling with 150 mg/L SDS and (b) fraction of flux regained after fouling and cleaning, as a function of initial water flux. Definition of symbols: ○ LE, ◿ LE (Δp = 9.0 bar), ▷ LE (Δp = 8.6 bar), ◺ XLE, ▽ NF90, ▲ 1% (w/w) MW 200 XLE, ▼ 15% (w/w) MW 200 XLE, ● 1% (w/w) MW 1000 XLE, ■ 15% (w/w) MW 1000 XLE, ◣ 1% (w/w) MW 1000 NF90, and ◢ 15% (w/w) MW 1000 NF90. Lines have been drawn through the modified and unmodified membrane data to guide the eye.*

In general, membranes modified with MW 1000 PEGDE demonstrated better fouling resistance and flux recovery in SDS tests than membranes modified with MW 200 PEGDE, which could be explained as the result of steric hindrance (i.e., the longer PEG chains of MW 1000 PEGDE may provide more of a steric barrier than the shorter PEG chains of MW 200 PEGDE). The difference in molecular weight between MW 200 and MW 1000 PEGDE (i.e., 330 g/mol vs. 1130 g/mol) also means that the molar concentration of MW 200 PEGDE is 3.4 times larger than that of MW 1000 PEGDE at the same mass concentration (e.g., 1% (w/w)), so MW 200 PEGDE has 3.4 times as many epoxide endgroups as MW 1000 PEGDE. Since the measured PEGDE graft densities exceeded the number of surface amine and carboxylic acid groups on the membrane (perhaps indicating PEGDE adsorption as well as grafting), most of the epoxide endgroups will be left unreacted. The endgroups are not expected to improve membrane fouling resistance, so the higher concentration of endgroups in MW 200 PEGDE could play a role in the observed dependence of fouling behavior on PEGDE molecular weight. However, fouling resistance was less dependent on PEGDE treatment solution concentration, since membranes modified with 1% (w/w) and 15% (w/w) PEGDE treatment solutions had similar fouling resistance.

Within the scatter of the data points, the fraction of flux retained and regained in the SDS fouling tests was essentially independent of initial water flux for the unmodified membranes and decreased with increasing initial water flux for the modified membranes (cf. Figure 6.7). Using a series-resistance approach [14, 20], the pressure-normalized water flux (i.e., the permeance) during fouling is given by:

$$A = \left(\frac{1}{A_m} + \frac{1}{A_f} \right)^{-1} \tag{6.1}$$

where A_m is the membrane permeance during fouling (assumed to be equivalent to the membrane permeance in the absence of fouling) and A_f is the permeance of the deposited foulant layer. The fraction of flux retained during fouling (i.e., $J_{w(foul)}/J_{w(NaCl)i}$) may be expressed as the ratio of the permeance during fouling to the permeance in the absence of fouling (i.e., A_m):

$$\frac{J_{w(foul)}}{J_{w(NaCl)i}} = \frac{1}{A_m \left(\frac{1}{A_m} + \frac{1}{A_f} \right)} = \frac{1}{1 + \frac{A_m}{A_f}} \tag{6.2}$$

Figure 6.8 presents the ratio A_f/A_m as a function of initial water flux, $J_{w(NaCl)i}$. For the modified membranes, this ratio decreases with increasing initial water flux, indicating the growth of a thicker or less permeable fouling layer (i.e., decreasing A_f) with increasing water flux, which is reasonable since fouling extent is expected to increase with increasing initial water flux [19]. However, for the unmodified membranes, the ratio A_f/A_m remains nearly constant with increasing initial water flux, which, if A_m is not influenced by the fouling, would indicate an increase in A_f, which is not expected. One possible explanation is that the permeance of the unmodified membranes is affected by fouling, i.e., the foulant may interact with the membrane. The larger extent of fouling observed for the unmodified membranes as compared to the modified membranes would support the possibility of interactions between the unmodified

membranes and the foulant which are absent, or at least weaker, in the modified membranes, whose PEG chains may prevent foulants from closely approaching their surfaces.

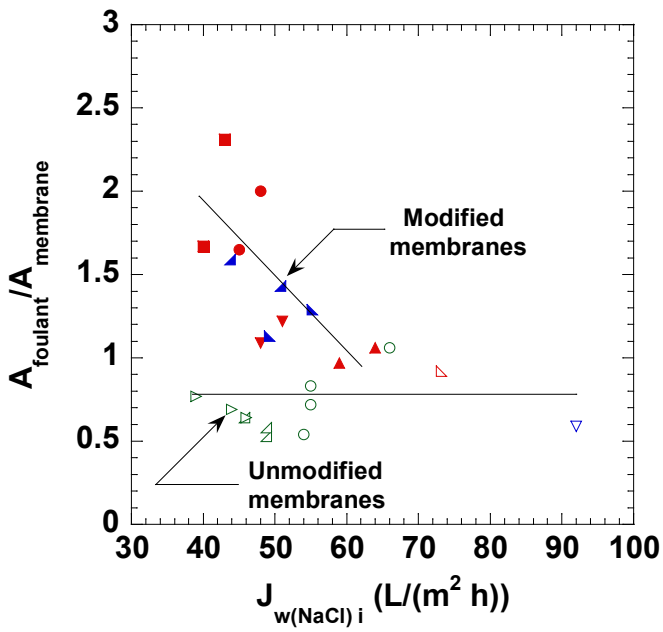

Figure 6.8 *Ratio of foulant layer permeance to membrane permeance as a function of initial water flux during fouling with 150 mg/L SDS. Definition of symbols: ○ LE, ◿ LE (Δp = 9.0 bar), ▷ LE (Δp = 8.6 bar), ◺ XLE, ▽ NF90, ▲ 1% (w/w) MW 200 XLE, ▼ 15% (w/w) MW 200 XLE, ● 1% (w/w) MW 1000 XLE, ■ 15% (w/w) MW 1000 XLE, ◣ 1% (w/w) MW 1000 NF90, and ◢ 15% (w/w) MW 1000 NF90. Lines have been drawn through the modified and unmodified membrane data to guide the eye.*

The DTAB fouling results presented in Figures 6.9(a) and 6.9(b) are similar to those in Figures 6.7(a) and 6.7(b) for SDS fouling, in that fouling resistance and flux recovery were better for membranes modified with higher molecular weight PEGDE, and fouling resistance and flux recovery were better in many of the modified membranes than in unmodified membranes of similar initial water flux. As in the case of SDS fouling, the unmodified membranes' fouling resistance was relatively independent of initial water flux, suggesting possible interactions between DTAB and the unmodified membrane surfaces. The improvement in DTAB fouling resistance demonstrated by PEGDE-modified membranes was similar to that observed by Sagle et al. for polyamide membranes coated with PEG-based hydrogels (~ 10 – 15%) [6]. Mickols and Kang et al. also reported similar increases in DTAB fouling resistance during short, 2 – 3 hour fouling tests, for reverse osmosis membranes modified by submersion in a 0.3% (w/w) MW 200 PEGDE solution and by treatment with a 5% (w/w) MPEG-NH_2 solution, respectively [4, 13]. Comparison of the SDS and DTAB fouling behavior of PEGDE-modified membranes to surfactant fouling reports in the literature indicates PEGDE modification is at least as effective as other modifications. Additionally, the strategy employed here, to compare the performance of modified and unmodified membranes with similar initial water flux, may provide a clearer picture of the effect of surface modification on fouling behavior.

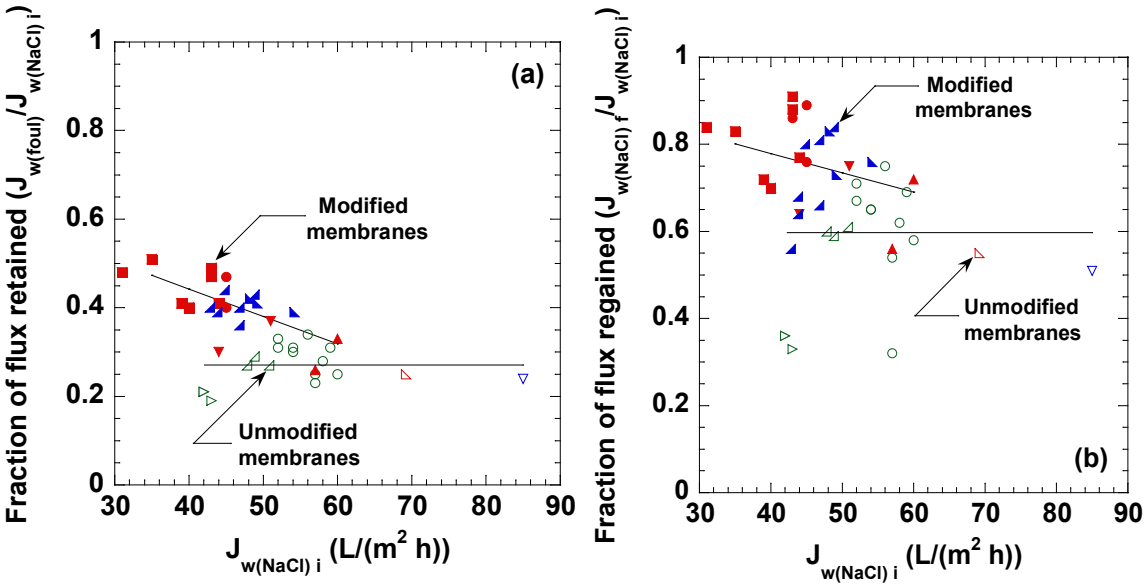

Figure 6.9. *(a) Fraction of flux retained after fouling with 150 mg/L DTAB and (b) fraction of flux regained after fouling and cleaning, as a function of initial water flux. Definition of symbols: ○ LE, ◿ LE (Δp = 9.0 bar), ▷ LE (Δp = 8.6 bar), ◺ XLE, ▽ NF90, ▲ 1% (w/w) MW 200 XLE, ▼ 15% (w/w) MW 200 XLE, ● 1% (w/w) MW 1000 XLE, ■ 15% (w/w) MW 1000 XLE, ◣ 1% (w/w) MW 1000 NF90, and ◢ 15% (w/w) MW 1000 NF90. Lines have been drawn through the modified and unmodified membrane data to guide the eye.*

Fouling was more extensive with DTAB than with SDS for all membranes (cf. Figures 6.9(a) and 6.7(a)), which may result from electrostatic interactions. The membrane surfaces are negatively charged at the pH of operation (pH 8, cf. Table 6.2), so cationic DTAB is attracted to the oppositely charged membrane surface. Anionic SDS has unfavorable electrostatic interactions with the membrane surface, yet still fouled the membrane, indicating the attractive hydrodynamic force (i.e., the water flux through the membrane that brings foulants in close contact with the membrane surface) was stronger than the repulsive electrostatic force. However, although DTAB caused extensive fouling, much of this fouling was reversible, similar to the case of SDS (cf. Figures 6.9(b) and 6.7(b)).

6.2.6 Fouling Resistance and Flux Recovery in Emulsion Fouling Tests

Figures 6.10(a) and 6.10(b) present fouling results for membranes tested in an emulsion containing *n*-decane and SDS. While several modified membranes retained similar fractions of their initial flux in the emulsion and surfactant tests, there was more sample-to-sample variability in *n*-decane:SDS tests than in SDS tests, and the unmodified membranes' fouling resistance showed a dependence on initial water flux in the emulsion tests that was absent in the tests using only the surfactant (cf. Figures 6.10(a) and 6.7(a)), which may indicate that SDS is less likely to interact with the unmodified membrane surfaces when it is emulsified with *n*-decane. The cleaning procedure was also much less effective in the emulsion fouling tests than in the surfactant tests. For example, XLE membranes modified with 15% (w/w) MW 1000 PEGDE recovered 90% of their initial flux in the SDS test (cf. Figure 6.7(b)), while they only recovered 60% of their initial flux after fouling and cleaning in the *n*-decane:SDS emulsion test.

Considering that these membranes retained approximately 60% of their initial flux after fouling, the cleaning procedure had a negligible effect on flux recovery. Thus, emulsion fouling was essentially entirely irreversible while surfactant fouling was at least somewhat reversible. In general, higher molecular weight PEG (i.e., MW 1000 vs. MW 200) gave modified membranes with better resistance to fouling by emulsions of *n*-decane and SDS, similar to the behavior observed in the surfactant fouling tests.

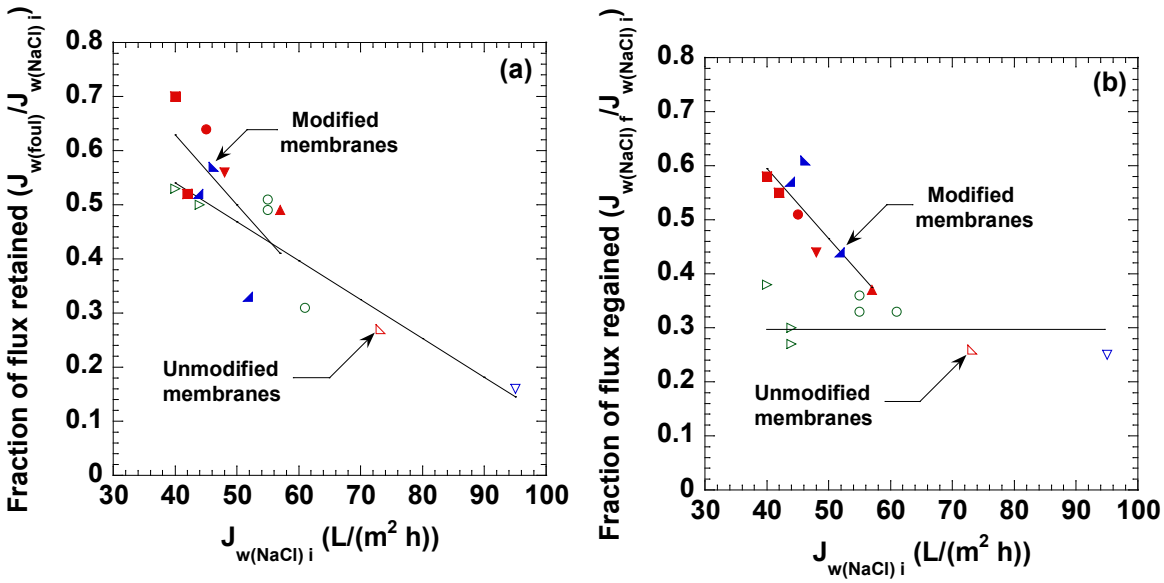

Figure 6.10. (a) Fraction of flux retained after fouling with a 150 mg/L 9:1 n-decane:SDS emulsion and (b) fraction of flux regained after fouling and cleaning, as a function of initial water flux. Definition of symbols: ○ LE, ▷ LE (Δp = 8.6 bar), ◺ XLE, ▽ NF90, ▲ 1% (w/w) MW 200 XLE, ▼ 15% (w/w) MW 200 XLE, ● 1% (w/w) MW 1000 XLE, ■ 15% (w/w) MW 1000 XLE, ◣ 1% (w/w) MW 1000 NF90, and ◢ 15% (w/w) MW 1000 NF90. Lines have been drawn through the modified and unmodified membrane data to guide the eye.

The fouling results for emulsions of *n*-decane and DTAB are given in Figures 6.11 (a) and 6.11(b). The fouling resistance behavior observed for the unmodified membranes was similar to that observed in the SDS and DTAB surfactant tests (i.e., fouling resistance was fairly independent of initial water flux), suggesting the possibility of interactions between the *n*-decane:DTAB emulsion and the unmodified membrane surfaces. Unlike the SDS emulsion tests, the extent of fouling in the DTAB emulsion tests was larger than that observed in the surfactant tests (cf. Figures 6.11 (a) and 6.9(a)). Fouling was also much more severe in DTAB emulsion tests than in SDS emulsion tests (e.g., XLE membranes modified with 15% (w/w) MW 1000 PEGDE retained 30% and 60% of their initial fluxes, respectively, cf. Figures 6.11(a) and 6.10(a)). Thus, DTAB is a stronger foulant for these membranes than SDS, and the addition of *n*-decane appears to exacerbate fouling. These fouling results are different from those observed by Sagle et al. for PEG hydrogel-coated polyamide membranes, where *n*-decane:SDS fouling was much more extensive than SDS fouling (i.e., 75% flux decline in emulsion tests vs. less than 25% flux decline in surfactant tests), and also slightly more extensive than *n*-decane:DTAB

fouling (i.e., 75% flux decline in *n*-decane:SDS vs. 60% flux decline in *n*-decane:DTAB) [6]. However, reports of this type are limited, and further investigation is required to fully understand the expected fouling behavior of surface-modified polyamide membranes in emulsions of *n*-decane and charged surfactants.

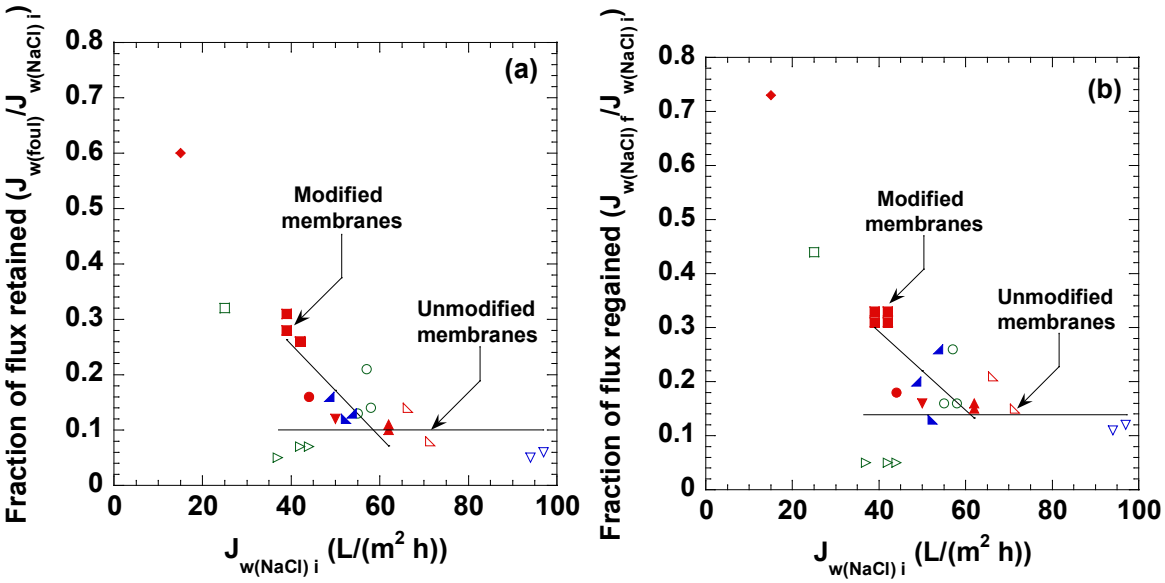

Figure 6.11. *(a) Fraction of flux retained after fouling with a 150 mg/L 9:1 n-decane:DTAB emulsion and (b) fraction of flux regained after fouling and cleaning, as a function of initial water flux. Definition of symbols: ○ LE, ▷ LE (Δp = 8.6 bar), □ LE (Δp = 5.5 bar), ◺ XLE, ▽ NF90, ▲ 1% (w/w) MW 200 XLE, ▼ 15% (w/w) MW 200 XLE, ● 1% (w/w) MW 1000 XLE, ■ 15% (w/w) MW 1000 XLE, ◣ 1% (w/w) MW 1000 NF90, ◢ 15% (w/w) MW 1000 NF90, and ◆ 15% (w/w) MW 1000 XLE (Δp = 5.5 bar). Lines have been drawn through the modified and unmodified membrane data (excluding data obtained for Δp = 5.5 bar) to guide the eye.*

There was very little difference in performance between PEGDE-modified and unmodified membranes in the DTAB emulsion tests, with the exception of the XLE membrane modified with 15% (w/w) MW 1000 PEGDE, which did retain more of its initial flux after fouling than the unmodified LE membrane operated at similar initial water flux (30% flux retention versus less than 10% flux retention), although the cleaning procedure did not result in sharp gains in flux, consistent with results from the SDS emulsion tests. Testing this modified membrane at a lower transmembrane pressure difference (Δp = 5.5 bar, giving an initial water flux of 15 LMH, rather than the initial water flux of 40 LMH obtained at Δp = 10.3 bar) revealed significantly higher flux retention than that of an unmodified LE membrane operated at the same transmembrane pressure difference (60% flux retention versus 32% flux retention) (cf. Figure 6.11(a)). Additionally, at lower transmembrane pressure difference, the cleaning procedure had a positive effect on flux recovery (e.g., an increase of 13%, from 60% of flux retained after fouling to 73% of flux regained after cleaning for the 15% (w/w) MW 1000 PEGDE-modified XLE membrane) (cf. Figure 6.11(b)).

Fouling rate has been reported to increase with increasing water flux [19]. The initial fouling test performed here at significantly lower transmembrane pressure difference and thus, much lower initial water flux, indicates that fouling rate also decreases with decreasing water flux, as expected. For highly fouling feeds such as the emulsion of *n*-decane and DTAB, fouling may occur so quickly that, beyond the first several minutes of fouling, the observed fouling behavior is indicative of transport through a foulant layer on the membrane surface that acts as the limiting resistance to mass transfer. In this case, the transport properties of the membrane, whether unmodified or modified, have little effect on the observed fouling behavior. Operation at lower transmembrane pressure difference, and thus lower water flux (decreasing the rate at which the foulant is brought to the membrane surface) could slow the rate of fouling enough to allow the fouling resistance of the membrane, not a foulant layer, to determine the observed fouling behavior. The preliminary experiment performed here confirms the feasibility of such an approach to limit hydrodynamic fouling effects and focus on the effects of surface modification in fouling tests. Other approaches, such as increasing the crossflow shear rate (i.e., increasing the feed flowrate to sweep foulants away from the membrane surface more effectively), have also been suggested to decrease the fouling rate [21, 22]. Although these approaches were initially proposed as a means of reducing commercial (i.e., unmodified) membrane fouling, they could also allow comparison of modified and unmodified membrane fouling behavior at conditions that emphasize the membrane properties, instead of those of a foulant layer.

6.2.7 NaCl and Organic Rejection in Fouling Tests

Table 6.3 presents the true NaCl rejection for each of the membranes at the end of the fouling portion of the test (i.e., at t = 24 hrs) for the four fouling conditions studied (i.e., SDS, DTAB, *n*-decane:SDS, and *n*-decane:DTAB), and it compares these values to the initial true NaCl rejection of each membrane (i.e., measured in 2000 mg/L NaCl feed). NaCl rejection increased for all membranes when they were fouled with SDS or DTAB. Following *n*-decane:SDS fouling, most membranes experienced an increase in NaCl rejection, with the exception of the unmodified NF90 membrane, whose NaCl rejection decreased. For the case of the *n*-decane:DTAB emulsion, however, all the membranes experienced a decrease in NaCl rejection upon fouling, although the NF90 membranes (unmodified and modified) were affected more than the XLE (unmodified and modified) and LE (unmodified) membranes (NaCl rejection of NF90 membranes decreased by several percent versus 1% or less for XLE and LE membranes). These results suggest in feeds containing an emulsion, modified XLE membranes have similar or better fouling resistance compared to modified NF90 membranes, with less negative impact on NaCl rejection.

Table 6.3. Initial NaCl rejection and NaCl rejection in the presence of each foulant (measured at t = 24 hrs).[1]

Membrane	$R_{NaCl,i}$ (%)	R_{SDS} (%)	R_{DTAB} (%)	$R_{n\text{-decane:SDS}}$ (%)	$R_{n\text{-decane:DTAB}}$ (%)
LE	99.1 ± 0.2	99.9	99.7 ± 0.2	99.8 ± 0.1	98.9 ± 0.2
XLE	99.1 ± 0.1	99.9	99.8	99.4	98.2 ± 0.4
1% (w/w) MW 200 XLE	99.1 ± 0.2	99.9	99.6 ± 0.2	99.7	98.1 ± 0.2
15% (w/w) MW 200 XLE	99.3 ± 0.1	99.9	99.7 ± 0.1	99.7	98.4
1% (w/w) MW 1000 XLE	99.4 ± 0.2	99.9	99.7 ± 0.1	99.8	98.4
15% (w/w) MW 1000 XLE	99.5 ± 0.3	99.9 ± 0.1	99.6 ± 0.3	99.8	98.8 ± 0.4
NF90	97.8 ± 0.3	99.8	99.8	96.3	91.7 ± 0.8
1% (w/w) MW 1000 NF90	98.8 ± 0.2	99.8	99.4 ± 0.1	99.2	94.8
15% (w/w) MW 1000 NF90	98.8 ± 0.4	99.9 ± 0.1	99.4 ± 0.2	99.0 ± 0.1	92.5 ± 3.7

[1]NaCl rejection has been corrected for the effects of concentration polarization, and is, therefore, the true NaCl rejection.

During fouling, deposition of a foulant layer on the membrane surface may further increase the surface NaCl concentration (i.e., beyond the increase resulting from concentration polarization [23-25]), due to hindered back diffusion of NaCl through the foulant layer to the bulk feed solution [22]. This phenomenon, referred to as cake-enhanced osmotic pressure, leads to higher NaCl concentration at the membrane surface, higher salt flux through the membrane, and, therefore, lower NaCl rejection [22]. The effect of cake-enhanced osmotic pressure increases with increasing foulant layer thickness (i.e., increasing extent of fouling) [22]. Therefore, since all the membranes were severely fouled by the *n*-decane:DTAB emulsion (flux retention was 30% or less for all membranes) and the unmodified NF90 membrane was also severely fouled by

the *n*-decane:SDS emulsion (16% flux retention), it is reasonable that decreased NaCl rejection was observed in these cases. NaCl rejection increased after fouling in cases where fouling was less severe (i.e., in SDS and DTAB tests for all membranes and in *n*-decane:SDS tests for all membranes except the unmodified NF90 membrane), which suggests that the fouling layer thicknesses were not large enough for the cake-enhanced osmotic pressure effect, which tends to decrease rejection, to overcome the effect of surface defect plugging, which tends to increase rejection.

The final true NaCl rejection values (i.e., after fouling and cleaning) of the membranes are compared to their initial true NaCl rejection values in Table 6.4. While the final NaCl rejection values were generally lower than the corresponding values measured during fouling (for the tests with SDS, DTAB and *n*-decane:SDS (cf. Tables 6.3 and 6.4)), they were still generally higher than the initial NaCl rejections, suggesting that while some of the adsorbed foulant (which potentially plugged surface defects, causing an increase in NaCl rejection during fouling) was removed by cleaning, there was also irreversible adsorption of foulant. Observed flux recoveries of less than 100% after fouling and cleaning also corroborate the hypothesis of some level of irreversible fouling. The final NaCl rejections measured in the *n*-decane:DTAB tests (and in the *n*-decane:SDS test for the unmodified NF90 membrane) were generally lower than the initial rejection values, which suggests that the foulant layer was not removed by the cleaning procedure (i.e., the cake-enhanced osmotic pressure effect was significant even after cleaning). Negligible flux recovery in these tests supports the hypothesis that a relatively thick foulant layer was still present on the membrane surface after cleaning.

Within the detection limits of the TOC analyzer, organic rejection was essentially 100% in all fouling tests. Organic rejection greater than 95% has been documented previously for polyamide membranes (i.e., unmodified and coated with PEG-based hydrogels) tested with the same organic foulants [6].

Table 6.4 Initial NaCl rejection and final NaCl rejection (i.e., measured after fouling and cleaning, at t = 30 hrs).[1]

Membrane	$R_{NaCl,i}$ (%)	$R_{SDS,f}$ (%)	$R_{DTAB,f}$ (%)	$R_{n\text{-decane:SDS},f}$ (%)	$R_{n\text{-decane:DTAB},f}$ (%)
LE	99.1 ± 0.2	99.7 ± 0.1	99.7 ± 0.1	99.6 ± 0.1	99.2 ± 0.3
XLE	99.1 ± 0.1	99.7	99.7	99.2	98.2 ± 0.1
1% (w/w) MW 200 XLE	99.1 ± 0.2	99.7 ± 0.1	99.6 ± 0.1	99.6	98.2 ± 0.7
15% (w/w) MW 200 XLE	99.3 ± 0.1	99.7 ± 0.1	99.7 ± 0.1	99.6	97.6
1% (w/w) MW 1000 XLE	99.4 ± 0.2	99.7 ± 0.1	99.7 ± 0.1	99.7	98.9
15% (w/w) MW 1000 XLE	99.5 ± 0.3	99.7	99.7 ± 0.1	99.6 ± 0.1	98.9 ± 0.1
NF90	97.8 ± 0.3	99.2	99.3	95.5	94.6 ± 0.5
1% (w/w) MW 1000 NF90	98.8 ± 0.2	99.3 ± 0.1	99.2 ± 0.3	98.7	95.5
15% (w/w) MW 1000 NF90	98.8 ± 0.4	99.3 ± 0.1	99.1 ± 0.3	98.6 ± 0.1	95.5 ± 0.1

[1]NaCl rejection has been corrected for the effects of concentration polarization, and is, therefore, the true NaCl rejection.

6.3 Conclusions

An aqueous top surface treatment method was employed to graft poly(ethylene glycol) diglycidyl ether (PEGDE) to the surfaces of commercial reverse osmosis (XLE) and nanofiltration (NF90) membranes. Water flux decreased due to this surface modification, as expected, and NaCl rejection increased. However, in many cases, the initial large decrease in water flux observed for low grafting density (i.e., for membranes treated with 1% (w/w) MW 1000 PEGDE) was followed by a much smaller decrease in water flux and larger increase in grafting density (i.e., for membranes treated with 15% (w/w) MW 1000 PEGDE), suggesting that after a small amount

of PEGDE is grafted to the membrane surface, additional PEGDE has much less of an impact on membrane performance. Membranes modified with PEGDE generally demonstrated improved fouling resistance to charged surfactants and emulsions containing *n*-decane and a charged surfactant, but experienced minimal changes in surface properties (e.g., surface charge, hydrophilicity and roughness). The observed effects could be related, in part, to steric hindrance imparted by the PEG chains, preventing foulants from closely approaching the membrane surface. Comparison of the fouling behavior of modified membranes to that of unmodified membranes of similar initial water flux indicated the observed improvements in fouling resistance were not due to the decrease in initial water flux caused by PEGDE modification. PEGDE molecular weight had a stronger influence on fouling resistance than did PEGDE treatment concentration, suggesting modification with lower concentrations (i.e., less than 1% (w/w)) of higher molecular weight (i.e., greater than 1000) PEGDE may be a means of optimizing the balance between water flux and fouling resistance for modified membranes.

6.4 Acknowledgements

The author would like to thank Dr. Bill Mickols of Dow Water & Process Solutions for helpful discussions, Dr. Hugo Celio of the Center for Nano and Molecular Science & Technology at the University of Texas at Austin for performing the XPS analysis, and Dr. Young-Hye Na of the IBM Almaden Research Center for performing the AFM analysis.

6.5 References

[1] S. Belfer, Y. Purinson, O. Kedem, Surface modification of commercial polyamide reverse osmosis membranes by radical grafting: an ATR-FTIR study, Acta Polymerica, 49 (1998) 574-582.

[2] L.G. Wade, Organic Chemistry, 4th ed., Prentice-Hall, Inc., Upper Saddle River, New Jersey, 1999.

[3] Y.S. Park, J. Won, Y.S. Kang, Preparation of poly(ethylene glycol) brushes on polysulfone membranes for olefin/paraffin separation, Langmuir, 16 (2000) 9662-9665.

[4] G. Kang, M. Liu, B. Lin, Y. Cao, Q. Yuan, A novel method of surface modification on thin-film composite reverse osmosis membrane by grafting poly(ethylene glycol), Polymer, 48 (2007) 1165-1170.

[5] V. Freger, J. Gilron, S. Belfer, TFC polyamide membranes modified by grafting of hydrophilic polymers: an FT-IR/AFM/TEM study, Journal of Membrane Science, 209 (2002) 283-292.

[6] A.C. Sagle, E.M. Van Wagner, H. Ju, B.D. McCloskey, B.D. Freeman, M.M. Sharma, PEG-coated reverse osmosis membranes: desalination properties and fouling resistance, Journal of Membrane Science, 340 (2009) 92-108.

[7] J.S. Louie, I. Pinnau, I. Ciobanu, K.P. Ishida, A. Ng, M. Reinhard, Effects of polyether-polyamide block copolymer coating on performance and fouling of reverse osmosis membranes, Journal of Membrane Science, 280 (2006) 762-770.

[8] W. Stumm, Chemistry of the Solid-Water Interface: Processes at the Mineral-Water and Particle-Water Interface in Natural Systems, John Wiley & Sons, Inc., New York, 1992.

[9] A.E. Childress, M. Elimelech, Effect of solution chemistry on the surface charge of polymeric reverse osmosis and nanofiltration membranes, Journal of Membrane Science, 119 (1996) 253-268.

[10] M. Elimelech, W.H. Chen, J.J. Waypa, Measuring the zeta (electrokinetic) potential of reverse osmosis membranes by a streaming potential analyzer, Desalination, 95 (1994) 269-286.

[11] S.-Y. Kwak, S.G. Jung, Y.S. Yoon, D.W. Ihm, Details of surface features in aromatic polyamide reverse osmosis membranes characterized by scanning electron and atomic force microscopy, Journal of Polymer Science: Part B: Polymer Physics, 37 (1999) 1429-1440.

[12] J. Gilron, S. Belfer, P. Vaisanen, M. Nystrom, Effects of surface modification on antifouling and performance properties of reverse osmosis membranes, Desalination, 140 (2001) 167-179.

[13] W.E. Mickols, Composite Membrane with Polyalkylene Oxide Modified Polyamide Surface, U.S. Patent 6,280,853 B1, 2001.

[14] J.M.S. Henis, M.K. Tripodi, Composite hollow fiber membranes for gas separation: the resistance model approach, Journal of Membrane Science, 8 (1981) 233-246.

[15] Dow Water & Process Solutions NF90-400 Product Specification, http://www.dow.com/liquidseps/prod/nf90_400.htm.

[16] L.M. Robeson, Correlation of separation factor versus permeability for polymeric membranes, Journal of Membrane Science, 62 (1991) 165-185.

[17] B.D. Freeman, Basis of permeability/selectivity tradeoff relations in polymeric gas separation membranes, Macromolecules, 32 (1999) 375-380.

[18] E.M. Van Wagner, A.C. Sagle, M.M. Sharma, B.D. Freeman, Effect of crossflow testing conditions, including feed pH and continuous feed filtration, on commercial reverse osmosis membrane performance, Journal of Membrane Science, 345 (2009) 97-109.

[19] X. Zhu, M. Elimelech, Colloidal fouling of reverse osmosis membranes: measurements and fouling mechanisms, Environmental Science and Technology, 31 (1997) 3654-3662.

[20] R.B. Bird, W.E. Stewart, E.N. Lightfoot, Transport Phenomena, 2nd ed., John Wiley & Sons, Inc., Hoboken, New Jersey, 2002.

[21] D. Jiao, M.M. Sharma, Mechanism of cake buildup in crossflow filtration of colloidal suspensions, Journal of Colloid and Interface Science, 162 (1994) 454-462.

[22] E.M.V. Hoek, A.S. Kim, M. Elimelech, Influence of crossflow membrane filter geometry and shear rate on colloidal fouling in reverse osmosis and nanofiltration separations, Environmental Engineering Science, 19 (2002) 357-372.

[23] T.K. Sherwood, P.L.T. Brian, R.E. Fisher, L. Dresner, Salt concentration at phase boundaries in desalination by reverse osmosis, I & EC Fundamentals, 4 (1965) 113-118.

[24] R.W. Baker, Membrane Technology and Applications, 2nd ed., John Wiley & Sons Ltd., West Sussex, 2004.

[25] I. Sutzkover, D. Hasson, R. Semiat, Simple technique for measuring the concentration polarization level in a reverse osmosis system, Desalination, 131 (2000) 117-127.

7 CONCLUSIONS AND RECOMMENDATIONS

7.1 Conclusions

This dissertation focused on characterizing the performance of commercial aromatic polyamide reverse osmosis membranes and modifying the surfaces of aromatic polyamide reverse osmosis and nanofiltration membranes to improve their resistance to fouling by representative contaminants in produced water streams. Poly(ethylene glycol) diglycidyl ether (PEGDE) was used to modify the membrane surface, and surface properties and fouling behavior of the modified membranes were measured.

7.1.1 Reverse Osmosis Membrane Characterization

The performance (i.e., water flux and NaCl rejection) of commercial aromatic polyamide reverse osmosis membranes was sensitive to crossflow testing conditions. Concentration polarization and feed pH had a strong effect on NaCl rejection, but did not affect water flux. The use of continuous feed filtration led to higher water flux and lower NaCl rejection than was observed for similar tests performed using unfiltered feed. Additionally, the use of continuous feed filtration eliminated the flux decline observed in unfiltered feed, suggesting fouling occurs in ultrapure, unfiltered feed water. A tradeoff between water permeance and water/salt selectivity was observed for these membranes, similar to the tradeoff relationship between permeability and selectivity often observed in gas separation membranes. Water flux and salt rejection values matching the manufacturer benchmarks were achieved by matching the pretreatment and test conditions specified by the manufacturer. The ability to reliably measure commercial membrane performance was a crucial first step before undertaking surface modification studies, so that differences in performance due to modification could be separated from the effects of the testing conditions.

7.1.2 Surface Modification Using Poly(ethylene glycol) Diglycidyl Ether

An aqueous top surface treatment method was employed to graft poly(ethylene glycol) diglycidyl ether (PEGDE) to the surfaces of commercial aromatic polyamide reverse osmosis and nanofiltration membranes. Water flux decreased and NaCl rejection increased with increasing graft density, although in many cases, an initial large change in performance for low grafting densities was followed by a relatively small change in performance for much higher graft densities, suggesting that only a small amount of PEGDE is needed to cause maximum impact on membrane performance. The measured graft densities corresponded to PEGDE layer thicknesses in the range of 30 – 300 nm, which indicates significantly more PEGDE molecules on the membrane surface than the number of surface carboxylic acid or amine groups estimated from zeta potential. Plugging surface defects with PEGDE could partially explain the observed graft densities, and the increase in NaCl rejection upon modification also suggests plugging of defects, particularly for nanofiltration membranes. The surface properties of PEGDE-modified membranes (i.e., hydrophilicity, roughness and charge) were very similar to those of unmodified analogs.

7.1.3 Fouling Resistance

Membranes modified with PEGDE generally demonstrated improved fouling resistance and flux recovery in charged surfactant fouling tests compared to unmodified membranes of similar initial water flux. Comparison of modified and unmodified membranes of similar initial water flux indicated the observed improvements in fouling resistance were not due to a decrease in initial water flux caused by PEGDE modification. Since the surface properties of the modified and unmodified membranes were similar, the observed improvements in fouling resistance of PEGDE – modified membranes could be due to steric hindrance of the PEG chains preventing foulants from closely approaching the membrane surface. In general, cationic dodecyltrimethylammonium bromide (DTAB) caused more extensive fouling than did anionic sodium dodecyl sulfate (SDS), which was expected due to electrostatic attraction between the negatively charged membrane surface and positively charged DTAB. However, SDS also caused fouling, and since electrostatic repulsion between the membrane and surfactant would tend to prevent fouling, hydrodynamic forces could help explain the observed fouling.

Emulsions of *n*-decane and SDS caused similar levels of fouling as the surfactant alone, however cleaning was ineffective in removing these foulants from the membrane surface. Emulsions of *n*-decane and DTAB, on the other hand, caused more extensive fouling than the surfactant alone and could not be readily removed by cleaning. Only one of the modifications studied resulted in improved fouling resistance to *n*-decane:DTAB. Testing this membrane at approximately half the typical transmembrane operating pressure revealed even better fouling resistance and some flux recovery after cleaning, possibly due to slowing the rate of foulant deposition enough to allow transport through the modified membrane to be observed, instead of transport through a deposited foulant layer.

In all four fouling cases studied, PEGDE molecular weight had a stronger influence than grafting density on the fouling resistance of the resulting modified membranes.

7.2 Recommendations

7.2.1 Surface Modification

While a bifunctional epoxide, PEGDE, was the focus of this research, it would also be of interest to study the fouling resistance of membranes modified with monofunctional epoxides. Epoxidation of a C = C double bond may be achieved by reaction with *m*-chloroperoxybenzoic acid (MCPBA), as illustrated in Figure 7.1 [1, 2].

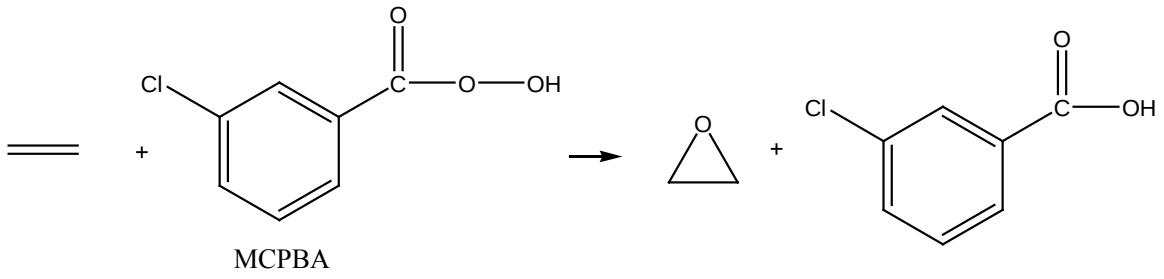

Figure 7.1. Epoxidation of a vinyl group using m-chloroperoxybenzoic acid (MCPBA).

Epoxidation of poly(ethylene glycol) acrylate (PEGA) would give a monoepoxide similar to the diepoxides used in this work. Fluorinated acrylates produced by Solvay Fluor (Houston, TX), including 2,2,2 – trifluoroethyl α – fluoroacrylate (TFEFA), 2,2,3,3,3 – pentafluoropropyl α – fluoroacrylate (PFPFA), and 2,2,3,3 – tetrafluoropropyl α – fluoroacrylate (TFPFA), could also be made into epoxides. The chemical structures of PEGA, TFEFA, PFPFA, and TFPFA are presented in Figure 7.2. Fluorine is expected to impart both oil and water – repellant properties [3-5], so a balance between water flux and fouling resistance would need to be reached. However, maintaining acceptable water flux upon modification of polyamide membranes with fouling – resistant materials is always a challenge due to the increase in mass transfer resistance imparted by adding a layer of material to the membrane surface.

Since MW 1000 PEGDE resulted in modified membranes with better fouling resistance than membranes modified with MW 200 PEGDE, it would be valuable to study the effect of higher molecular weight PEG on modified membrane fouling resistance. Poly(ethylene glycol) diacrylate (PEGDA), whose structure is also shown in Figure 7.2, is commercially available with PEG molecular weights of 2000 and 6000 (i.e., n ≈ 45 and 136, respectively). Epoxidation of the acrylate groups using MCPBA (cf. Figure 7.1) would give diepoxides with higher PEG molecular weight.

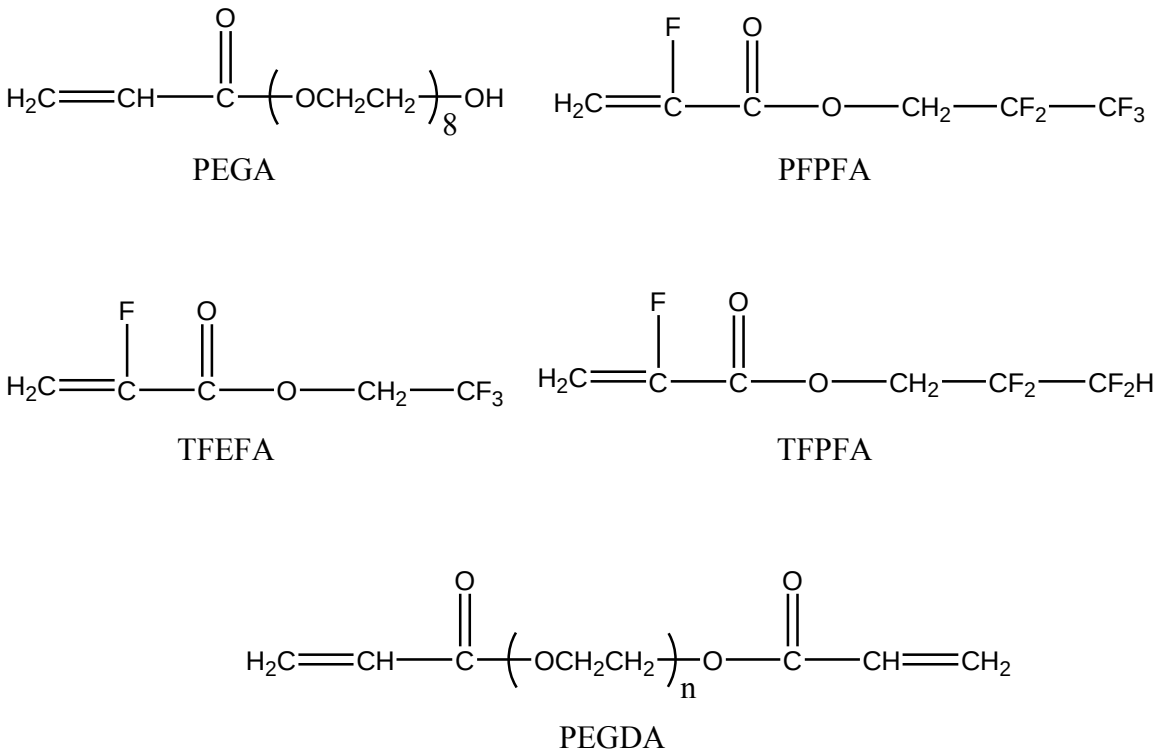

Figure 7.2. Chemical structures of potential acrylates for epoxidation and use in surface modification of polyamide membranes: poly(ethylene glycol) acrylate (PEGA), 2,2,2 – trifluoroethyl α – fluoroacrylate (TFEFA), 2,2,3,3,3 – pentafluoropropyl α – fluoroacrylate (PFPFA), 2,2,3,3 – tetrafluoropropyl α – fluoroacrylate (TFPFA), and poly(ethylene glycol) diacrylate (PEGDA).

In this work, graft density was determined from sample mass before and after PEGDE modification, and PEGDE layer thickness was then calculated from the measured graft density. Graft densities for membranes treated with 1% (w/w) and 15% (w/w) PEGDE solutions for ten minutes were easily measurable with the magnetic suspension balance, but mass changes due to modification could easily fall below the detection limit of the instrument if the effects of lower treatment concentrations or shorter reaction times were investigated. Ellipsometry would allow measurement of PEGDE layer thicknesses on the order of 1 nm [6]. The effect of conditions such as PEGDE molecular weight and treatment concentration, reaction time and temperature on layer thickness could be determined for an ideal polyamide, interfacially polymerized on a silicon wafer. However, the inherent roughness of interfacially polymerized polyamides (~ 50 nm) may make it necessary to substitute an aliphatic amine for meta-phenylene diamine, to give a smooth polyamide surface and allow detection of thickness changes on the order of 1 nm [7].

7.2.2 Membrane Fouling

The fouling studies described in this dissertation focused on one foulant concentration (150 mg/L). Investigation of the effect of foulant concentration on membrane fouling behavior would allow determination of the performance limits of these modified membranes. Also, membranes are typically cleaned periodically while in use [8], and although the effect of cleaning on flux recovery was measured, it would be valuable to perform longer fouling studies, with several fouling and cleaning cycles, to determine the long-term performance of the modified membranes. Decreasing water flux and increasing shear rate decrease the rate of foulant deposition [9-11]. Initial fouling experiments using lower transmembrane pressure drop (i.e., lower initial water flux) suggested that control of the hydrodynamic conditions could slow the rate of buildup of a mass-transfer-limiting foulant layer, and therefore emphasize differences in the modified and unmodified membranes' native fouling resistance. Operation at higher crossflow velocity (i.e., higher shear rate) could potentially give similar insight into modified membrane performance. Comparison of modified and unmodified membrane performance should include consideration of the amount of salt permeated, as well as the amount of water permeated (i.e., water flux and volumetric throughput), since both measures are important in determining the best membrane for a given application. Finally, sealing the feed tank to prevent adsorption of particulate matter from the air and coating the stainless steel tubing with polytetrafluoroethylene to prevent possible feed contamination from metal ions shed from the tubing could reduce or eliminate background fouling, so that the effects of intentionally added foulants could be separated from the background fouling experienced in crossflow tests using the current crossflow system (i.e., uncoated tubing and unsealed feed tank).

7.3 References

[1] J.D. White, R.W. Skeean, G.L. Trammell, Lewis acid and photochemically mediated cyclization of olefinic beta-keto esters, Journal of Organic Chemistry, 50 (1985) 1939-1948.

[2] T. Koerner, H. Slebocka-Tilk, R.S. Brown, Experimental investigation of the primary and secondary deuterium kinetic isotope effects for epoxidation of alkenes and ethylene with m-chloroperoxybenzoic acid, Journal of Organic Chemistry, 64 (1999) 196-201.

[3] T.W. Del Pesco, Why fluorochemicals, Journal of the American Leather Chemists Association, 90 (1995) 108-113.

[4] D.-Y. Wi, I.W. Kim, J. Kim, Water repellent cotton fabrics prepared by PTFE RF sputtering, Fibers and Polymers, 10 (2009) 98-101.

[5] B. Baradie, M.S. Shoichet, Novel fluoro-terpolymers for coatings applications, Macromolecules, 38 (2005) 5560-5568.

[6] B. Zdyrko, V. Klep, I. Luzinov, Syntheis and surface morphology of high-density poly(ethylene glycol) grafted layers, Langmuir, 19 (2003) 10179-10187.

[7] R.J. Petersen, Composite reverse osmosis and nanofiltration membranes, Journal of Membrane Science, 83 (1993) 81-150.

[8] C. Fritzmann, J. Löwenberg, T. Wintgens, T. Melin, State-of-the-art of reverse osmosis desalination, Desalination, 216 (2007) 1-76.

[9] D. Jiao, M.M. Sharma, Mechanism of cake buildup in crossflow filtration of colloidal suspensions, Journal of Colloid and Interface Science, 162 (1994) 454-462.

[10] E.M.V. Hoek, A.S. Kim, M. Elimelech, Influence of crossflow membrane filter geometry and shear rate on colloidal fouling in reverse osmosis and nanofiltration separations, Environmental Engineering Science, 19 (2002) 357-372.

[11] X. Zhu, M. Elimelech, Colloidal fouling of reverse osmosis membranes: measurements and fouling mechanisms, Environmental Science and Technology, 31 (1997) 3654-3662.

This page is intentionally left blank

APPENDIX: ADDITIONAL SURFACE MODIFICATION METHODS, SURFACE CHARGE MEASUREMENTS, AND FOULING STUDIES

Appendix A
Additional Surface Modification Methods, Surface Charge Measurements, and Fouling Studies

A.1 Additional Surface Modification Methods

A.1.1 Dip Coating

The pure water flux of XLE membranes treated with MW 200 and 1000 PEDGE by dip coating is presented in Figure A1. Membranes (d = 50 mm circles) were pretreated by soaking in a 25% (v) aqueous isopropanol solution for 20 minutes, followed by rinsing in pure water. Dip treatment was performed using a total of 200 grams of solution (including PEG and water). The water was heated to 40°C before adding the PEGDE, then the membrane was submerged in the solution for ten minutes, followed by rinsing it three times in pure water. Membranes were stored in pure water until tested. Dead end filtration was used to measure the pure water flux of the modified and unmodified membranes (Δp = 10.3 bar). Dip coating caused drastic declines in pure water flux. For example, an XLE membrane treated with 1% (w/w) MW 1000 PEGDE had a pure water flux of 28 LMH, compared to 100 LMH for an unmodified XLE membrane (i.e., submerged in 200 g of 40°C water (with no PEGDE) for 10 minutes).

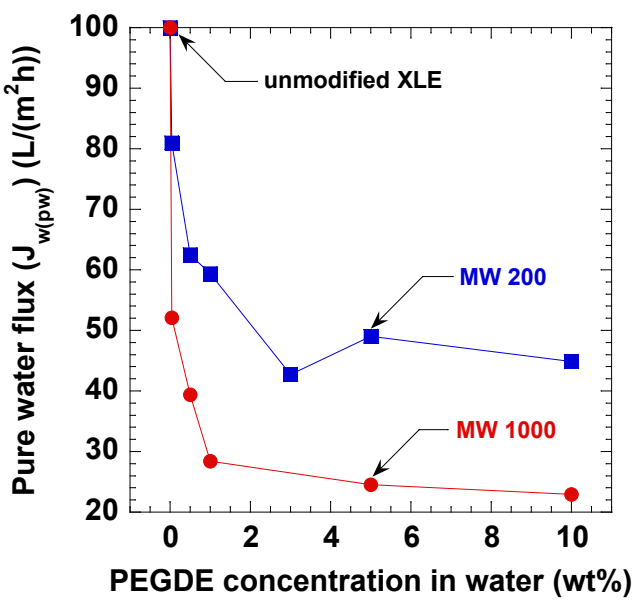

Figure A1. Pure water flux (dead end, Δp = 10.3 bar) as a function of PEGDE aqueous treatment solution concentration for XLE membranes dip coated with MW 200 and 1000 PEGDE (40°C, 10 minutes).

The effect of treatment temperature and time were determined for XLE membranes dip coated with 10% (w/w) MW 200 PEGDE. The modification procedure was identical to that described above, with the exception of the treatment temperature (i.e., 40°C or room temperature) and time

(i.e., 10 minutes or 1 minute). Table A1 gives the pure water flux of an XLE membrane treated with each of the four combinations of conditions, measured using dead end filtration and a transmembrane pressure difference of 10.3 bar. Water flux decreased with increasing treatment temperature and time, corresponding to increasing extent of PEGDE grafting.

Table A1 Pure water flux (dead end, Δp = 10.3 bar) of XLE membranes treated with 10% (w/w) MW 200 PEGDE by submersion for different times (1 minute vs. 10 minutes) and at different emperatures (room temperature vs. 40°C).

	1 minute	**10 minutes**
Room temperature	82 LMH	66 LMH
	75 LMH	45 LMH

Treatment of an XLE membrane with poly(ethylene glycol) (PEG) (cf. Figure 2.10) allowed comparison of the extent of adsorption versus grafting, since PEG has hydroxyl endgroups which are not expected to react with the carboxylic acid or amine groups on the membrane surface. Membranes were treated by submersion in 10% (w/w) MW 200 PEG or PEGDE solutions, using the standard procedure outlined above (40°C, 10 minute contact time). The surface atomic concentration (%) of each modified membrane, determined by XPS, is presented in Table A2. The XLE membranes modified with PEGDE had a much larger increase in oxygen content and decrease in nitrogen content than membranes modified with PEG, as compared to the unmodified XLE membrane composition. The oxygen to nitrogen ratio of the PEGDE-modified membranes was more than double that of the unmodified membranes, while the PEG-modified membranes had only a 25% higher oxygen to nitrogen ratio. Thus, although adsorption of PEG may occur, grafting is responsible for the majority of the effects on membrane performance seen upon PEGDE modification.

Table A2. XPS measurements of surface atomic concentration (%) of oxygen, nitrogen, carbon, and sulfur for an unmodified XLE membrane and XLE membranes modified with 10% (w/w) MW 200 PEG and PEGDE.

Membrane	**O (%)**	**N (%)**	**C (%)**	**S (%)**	**O/N**
XLE	14.3 ± 1.0	13.4 ± 0.4	72.2 ± 1.4	0.1	1.07
PEG XLE	15.6 ± 1.1	11.6 ± 0.4	72.7 ± 1.6	0.2	1.34
PEGDE XLE	19.9 ± 0.2	9.1 ± 0.3	70.9 ± 0.5	0.1	2.19

A commercially available fluorinated epoxide, (2,2,3,3,4,4,5,5,6,6,7,7,8,8,9,9,9 – heptadecafluorononyl) oxirane, whose structure is given in Figure A2, was also investigated for its potential to improve the fouling resistance of commercial polyamide membranes. Polytetrafluoroethylene (PTFE) is known to repel both water and oil, due to the high

electronegativity of fluorine [1-3]. Membrane fouling resistance could potentially be improved by grafting a fluorinated material, but the tendency to repel water would be detrimental to its application as a surface modifying agent for desalination membranes. Thus, a reasonable water flux must be maintained, perhaps by using only a small amount of fluorinated material to modify the membrane surface. XLE membranes were submerged in 300 ml of 1% (v) fluorinated epoxide in isopropanol for 1 hour (isopropanol was heated to 40°C before adding the epoxide and submerging the XLE membrane), followed by rinsing in pure water. The pure water flux of the modified membranes was typically about 75 LMH, compared to 120 LMH for the control XLE membrane, which was soaked in isopropanol for 1 hour. Soaking the XLE membrane in isopropanol increased its water flux by approximately 20% (the pure water flux of the XLE membrane is typically about 100 LMH), a phenomenon that has been observed previously [4, 5]. Initial surfactant fouling tests comparing the XLE membrane treated with fluorinated epoxide to the control XLE membrane (soaked in isopropanol) in either 20 mg/L DTAB or SDS indicated 5% higher flux retention for the membranes treated with the fluorinated epoxide.

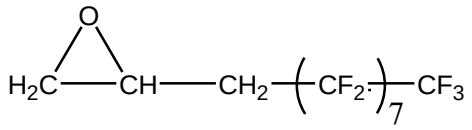

Figure A2. Chemical structure of (2,2,3,3,4,4,5,5,6,6,7,7,8,8,9,9,9 – heptadecafluorononyl) oxirane.

A.1.2 Spin Coating

Spin coating was explored as an alternative to dip coating, to prevent contact of the aqueous PEGDE solution with the nonwoven support backing of the polyamide membrane [6]. XLE membranes were spin coated with 5 ml of 10% (w/w) MW 200 PEGDE (the water was heated to 40°C before adding the PEGDE) at 1000 rpm for 20 seconds. The pure water flux of the resulting modified membranes was 87 ± 3 LMH, compared to 101 ± 4 LMH for XLE membranes that were subjected to spin coating with only water (i.e., without any PEGDE) (decrease in pure water flux of 14% due to PEGDE treatment). Spin time and solution volume were increased to 60 seconds and 50 ml, respectively, in an attempt to increase the extent of PEGDE grafting. XLE membranes spin coated with 10% (w/w) MW 200 PEGDE then had a pure water flux of 68 ± 1 LMH, compared to 88 ± 1 LMH for XLE membranes that were subjected to spin coating with only water (decrease in pure water flux of 23% due to PEGDE treatment). Although increasing contact time and amount of treatment solution did result in more PEGDE attachment, spinning for longer times was responsible for some of the observed flux decline (i.e., the XLE membranes that were subjected to spin coating with only water had 13% lower pure water flux when they were spin coated for 60 seconds versus 20 seconds, despite using a larger volume of water). Spin coating appears to dry the membrane and would also be impractical for scale-up to industrial membrane applications. The top surface treatment method was developed to leverage the main benefit of spin coating (i.e., preventing contact of the PEGDE treatment solution with the membrane backing) in a way that could be more easily applied to an existing membrane production process (e.g., incorporating a step to coat the treatment solution onto the membrane surface).

A.2 Surface Charge

The zeta potential of unmodified LE, XLE and NF90 membranes, XLE membranes modified with 1% (w/w) and 15% (w/w) MW 200 PEGDE, XLE and NF90 membranes modified with 1% (w/w) and 15% (w/w) MW 1000 PEGDE, and the XLE membrane modified with 100% (w/w) MW 1000 PEGDE are presented in Figure A3. The top surface treatment method was used to modify the membranes, and 10 mM NaCl was used as the background electrolyte. There was little difference in zeta potential between the modified and unmodified membranes, even for the XLE membrane modified with 100% (w/w) MW 1000 PEGDE, indicating there was minimal effect of PEGDE modification on surface charge.

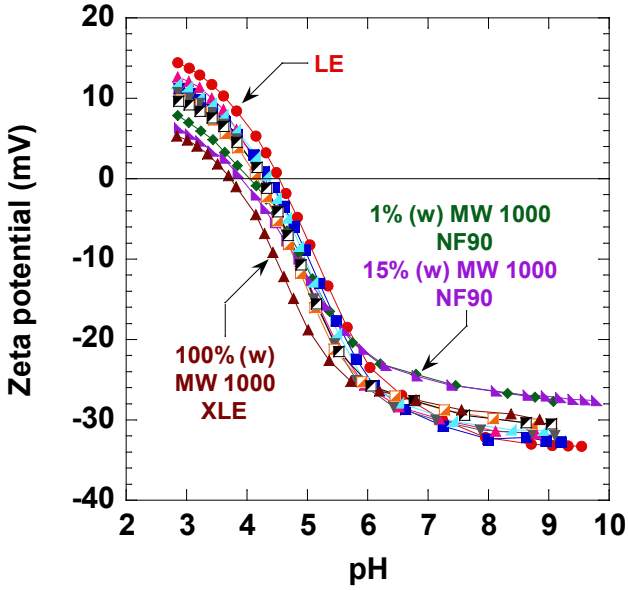

Figure A3. Zeta potential of unmodified LE, XLE and NF90 membranes and PEGDE – modified XLE and NF90 membranes in 10 mM NaCl.

Zeta potential was also measured in the presence of the charged surfactants, dodecyltrimethylammonium bromide (DTAB) and sodium dodecyl sulfate (SDS). Figure A4 gives the zeta potential of the modified and unmodified membranes in a 10 mM NaCl background electrolyte with 150 mg/L DTAB added to the solution. All membranes had positive zeta potentials over the entire pH range studied, a phenomenon which has been observed for other polyamide membranes [7]. Adsorption of DTAB to the membrane surface would presumably begin with the cationic headgroups adsorbing to the negatively charged membrane surface, leaving the hydrocarbon tails exposed. The positive surface charge indicates formation of a surfactant bilayer, where the second layer of surfactant molecules would be oriented with the charged headgroups exposed. As observed in the case of the 10 mM NaCl electrolyte, there was little difference in zeta potential between modified and unmodified membranes.

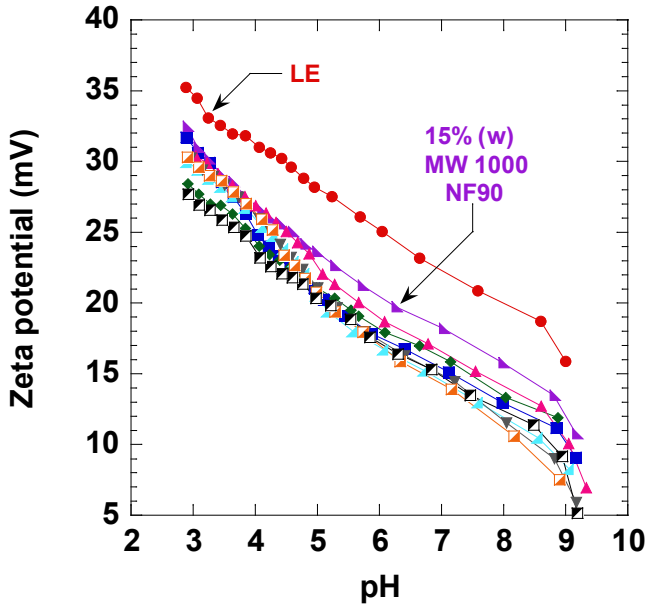

Figure A4. Zeta potential of unmodified LE, XLE and NF90 membranes and PEGDE – modified XLE and NF90 membranes in 10 mM NaCl + 150 mg/L DTAB.

Figure A5 presents the zeta potential of the modified and unmodified membranes in a 10 mM NaCl background electrolyte with 150 mg/L SDS added to the solution. As in the previous two cases (i.e., 10 mM NaCl and 10 mM NaCl + 150 mg/L DTAB), all membranes, modified and unmodified, had similar zeta potential values. The zeta potential in the presence of SDS was negative over the entire pH range studied, as has been observed for other polyamide membranes [7]. The magnitude of the increase in negative charge due to SDS was smaller than the increase in charge observed in DTAB. At pH 8, the zeta potential of all membranes was approximately -30 mV in 10 mM NaCl, -40 mV when SDS was added to the electrolyte solution (change of -10 mV), and +10 mV when DTAB was added to the electrolyte solution (change of +40 mV). Thus, SDS adsorption to the membrane surface was not as extensive as DTAB adsorption, which agrees with the larger extent of fouling observed in DTAB versus SDS fouling tests using the same surfactant concentration.

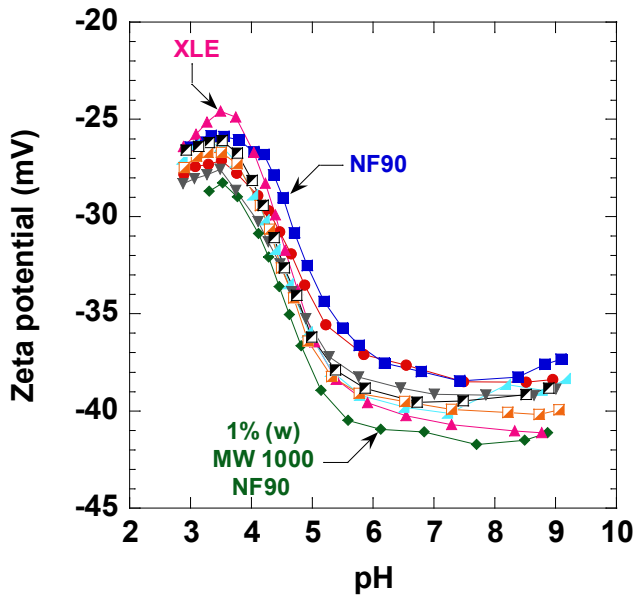

Figure A5. Zeta potential of unmodified LE, XLE and NF90 membranes and PEGDE – modified XLE and NF90 membranes in 10 mM NaCl + 150 mg/L SDS.

A.3 Fouling

Chapter 6 included the results of fouling studies using charged surfactants (i.e., SDS and DTAB) and emulsions of *n*-decane and charged surfactant as foulants. However, the observed fouling is due not only to the purposely added foulants, but also to the natural decline in flux observed in every lengthy crossflow filtration experiment where the feed solution was not continuously filtered during the course of the experiment. Particulates absorbed into the feed water from the air (i.e., dust, which is naturally attracted to water due to its high dielectric constant) are one probable cause of this background fouling. Figures A6(a) and A6(b) present the fraction of flux retained after fouling and the fraction of flux regained after fouling and cleaning for experiments in which no foulant was added to the system. The procedure was the same as in all other fouling experiments, except that no foulant was purposely added to the feed at $t = 1$ hr, when the surfactant or emulsion was typically added (cf. Figure 3.7(a)). Thus, the natural decline in water flux in 2000 mg/L NaCl feed was measured.

The trends shown in Figures A6(a) and A6(b), namely the stronger dependence of flux retention and recovery on initial flux for the modified membranes than for the unmodified membranes, and the generally better fouling resistance and flux recovery of modified versus unmodified membranes, match the trends observed for most of the foulants studied. Assuming there are no interactions between the naturally occurring and deliberately added foulants, the amount of fouling observed in a given fouling test may be reduced by the amount of fouling observed in the absence of added foulant, to determine the amount of fouling attributable to a given foulant. For example, the XLE membrane modified with 15%(w/w) MW 1000 PEGDE lost 9% of its initial water flux in the blank foulant test (i.e., it retained 91% of its initial flux), so the actual extent of fouling of this modified membrane due to SDS, DTAB, or the emulsions may be less than the observed values, which include the effects of both the naturally occurring and deliberately added foulants. However, this modified membrane regained 97% of its initial flux after fouling and

cleaning in the naturally occurring foulant test, so the naturally occurring foulants were almost entirely removed by the cleaning procedure and should therefore not impact the flux recovery observed in the surfactant or emulsion fouling tests. It should be noted that there is no experimental evidence to test the hypothesis that there are no interactions between the naturally occurring and deliberately added foulants, and an investigation of this phenomenon would be useful for understanding how much fouling is due to each of the foulants the membrane encounters.

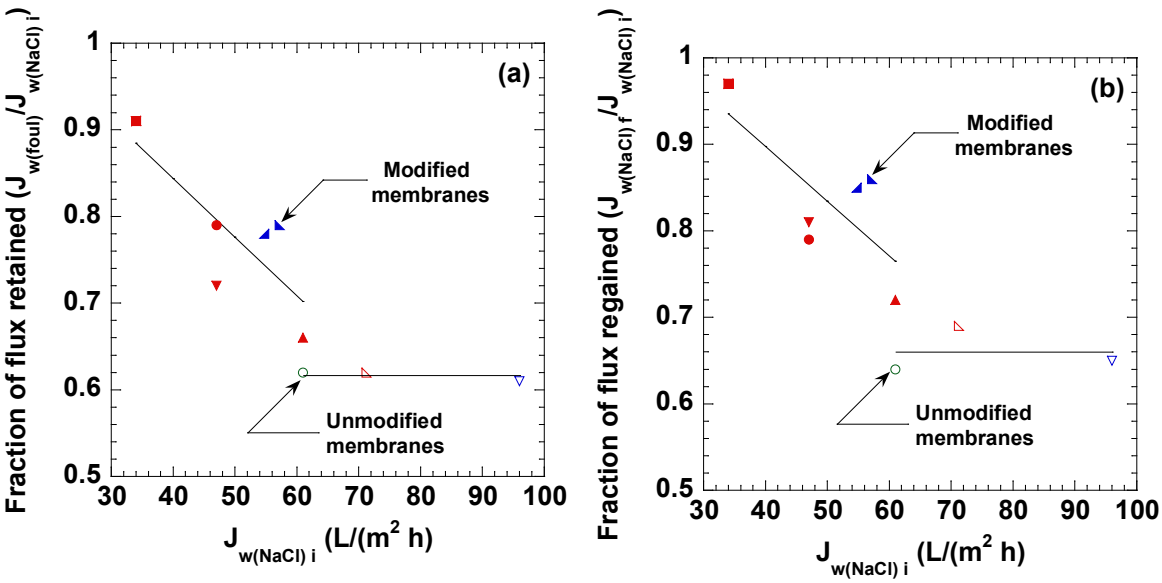

Figure A6. *(a) Fraction of flux retained after fouling in absence of intentionally added foulant and (b) fraction of flux regained after fouling and cleaning, as a function of initial water flux. Definition of symbols: ○ LE, ◺ XLE, ▽ NF90, ▲ 1% (w/w) MW 200 XLE, ▼ 15% (w/w) MW 200 XLE, ● 1% (w/w) MW 1000 XLE, ■ 15% (w/w) MW 1000 XLE, ◣ 1% (w/w) MW 1000 NF90, and ◢ 15% (w/w) MW 1000 NF90. Lines have been drawn through the modified and unmodified membrane data to guide the eye.*

7.3.1.1.1.1.1.1

Table A3 presents the initial NaCl rejection of each membrane ($R_{initial}$, measured at t = 1 hour), the NaCl rejection at t = 24 hours (R_{foul}), and the final NaCl rejection (R_{final}, measured after the cleaning procedure, at t = 30 hours). Rejection increased during the 24 hour experiment ($R_{foul} > R_{initial}$), and while the cleaning procedure did not restore the initial NaCl rejection, the final rejection was closest to the initial rejection for the membranes that recovered more of their initial water flux (e.g., 15% (w/w) MW 1000 XLE).

Table A3. NaCl rejection measured at t = 1 hr ($R_{initial}$), t = 24 hours (R_{foul}) and t = 30 hours (R_{final}) for fouling in the absence of intentionally added foulant.

Membrane	$R_{initial}$ (%)	R_{foul} (%)	R_{final} (%)
LE	99.2	99.7	99.6
XLE	99.1	99.7	99.6
1% (w/w) MW 200 XLE	99.1	99.6	99.5
15% (w/w) MW 200 XLE	99.4	99.7	99.7
1% (w/w) MW 1000 XLE	99.3	99.7	99.6
15% (w/w) MW 1000 XLE	99.5	99.8	99.6
NF90	97.4	98.9	99.0
1% (w/w) MW 1000 NF90	98.9	99.1	99.1
15% (w/w) MW 1000 NF90	99.0	99.2	99.3

A.4 References

[1] T.W. Del Pesco, Why fluorochemicals, Journal of the American Leather Chemists Association, 90 (1995) 108-113.

[2] D.-Y. Wi, I.W. Kim, J. Kim, Water repellent cotton fabrics prepared by PTFE RF sputtering, Fibers and Polymers, 10 (2009) 98-101.

[3] B. Baradie, M.S. Shoichet, Novel fluoro-terpolymers for coatings applications, Macromolecules, 38 (2005) 5560-5568.

[4] D. Mukherjee, A. Kulkarni, W.N. Gill, Chemical treatment for improved performance of reverse osmosis membranes, Desalination, 104 (1996) 239-249.

[5] A. Kulkarni, D. Mukherjee, W.N. Gill, Flux enhancement by hydrophilization of thin film composite reverse osmosis membranes, Journal of Membrane Science, 114 (1996) 39-50.

[6] R.G. Larson, T.J. Rehg, Spin Coating, in Liquid Film Coating: Scientific Principles and Their Technological Implications, S.F. Kistler, P.M. Schweizer (Eds.), Chapman & Hall, London, 1997.

[7] A.C. Sagle, E.M. Van Wagner, H. Ju, B.D. McCloskey, B.D. Freeman, M.M. Sharma, PEG-coated reverse osmosis membranes: desalination properties and fouling resistance, Journal of Membrane Science, 340 (2009) 92-108.

BIBLIOGRAPHY

A.W. Adamson, A.P. Gast, Physical Chemistry of Surfaces, 6th ed., John Wiley & Sons, Inc., New York, 1997.

E.V. Anslyn, D.A. Dougherty, Modern Physical Organic Chemistry, 10th ed., University Science Books, Sausalito, CA, 2006.

M. Asai, J.M. Floryan, Certain aspects of channel entrance flow, Physics of Fluids, 16 (2004) 1160-1163.

R.W. Baker, Membrane Technology and Applications, 2nd ed., John Wiley & Sons Ltd., West Sussex, 2004.

B. Baradie, M.S. Shoichet, Novel fluoro-terpolymers for coatings applications, Macromolecules, 38 (2005) 5560-5568.

S. Belfer, J. Gilron, O. Kedem, Characterization of commercial RO and UF modified and fouled membranes by means of ATR/FTIR, Desalination, 124 (1999) 175-180.

S. Belfer, J. Gilron, Y. Purinson, R. Fainshtain, N. Daltrophe, M. Priel, B. Tenzer, A. Toma, Effect of surface modification in preventing fouling of commercial SWRO membranes at the Eilat seawater desalination pilot plant, Desalination, 139 (2001) 169-176.

S. Belfer, Y. Purinson, R. Fainshtein, Y. Radchenko, O. Kedem, Surface modification of commercial composite polyamide reverse osmosis membranes, Journal of Membrane Science, 139 (1998) 175-181.

S. Belfer, Y. Purinson, O. Kedem, Surface modification of commercial polyamide reverse osmosis membranes by radical grafting: An ATR-FTIR study, Acta Polymerica, 49 (1998) 574-582.

P.R. Bevington, D.K. Robinson, Data Reduction and Error Analysis for the Physical Sciences, 2nd ed., McGraw Hill, New York, 1992.

R.B. Bird, W.E. Stewart, E.N. Lightfoot, Transport Phenomena, 2nd ed., John Wiley & Sons, Inc., Hoboken, New Jersey, 2002.

P.L.T. Brian, Concentration polarization in reverse osmosis desalination with variable flux and incomplete salt rejection, I & EC Fundamentals, 4 (1965) 439-445.

J.E. Cadotte, Interfacially Synthesized Reverse Osmosis Membrane, U.S. Patent 4,277,344, 1981.

J.E. Cadotte, R.J. Petersen, Thin-film composite reverse-osmosis membranes: origin, development, and recent advances, in Synthetic Membranes: Desalination, A.F. Turbak (Ed.), ACS Symposium Series, 153rd ed., Vol. 1, American Chemical Society, 1981, pp. 305-326.

J.E. Cadotte, R.J. Petersen, R.E. Larson, E.E. Erickson, A new thin-film composite seawater reverse osmosis membrane, Desalination, 32 (1980) 25-31.

M. Çakmakci, N. Kayaalp, I. Koyuncu, Desalination of produced water from oil production fields by membrane processes, Desalination, 222 (2008) 176-186.

H. Celio, Texas Materials Institute, The University of Texas at Austin, personal communication, 2009.

A.E. Childress, M. Elimelech, Effect of solution chemistry on the surface charge of polymeric reverse osmosis and nanofiltration membranes, Journal of Membrane Science, 119 (1996) 253-268.

H. Choi, K. Zhang, D.D. Dionysiou, D.B. Oerther, G.A. Sorial, Effect of permeate flux and tangential flow on membrane fouling for wastewater treatment, Separation and Purification Technology, 45 (2005) 68-78.

T.W. Del Pesco, Why fluorochemicals, Journal of the American Leather Chemists Association, 90 (1995) 108-113.

Dow Water & Process Solutions BW30-400 Product Specification, http://www.dow.com/liquidseps/prod/bw30_400.htm.

Dow Water & Process Solutions LE-400 Product Specification, http://www.dow.com/liquidseps/prod/le_400.htm.

Dow Water & Process Solutions NF90-400 Product Specification, http://www.dow.com/liquidseps/prod/nf90_400.htm.

Dow Water & Process Solutions SW30HR-380 Product Specification, http://www.dow.com/liquidseps/prod/sw30hr_380.htm.

Dow Water & Process Solutions XLE-440 Product Specification, http://www.dow.com/liquidseps/prod/xle_440.htm.

M. Elimelech, W.H. Chen, J.J. Waypa, Measuring the zeta (electrokinetic) potential of reverse osmosis membranes by a streaming potential analyzer, Desalination, 95 (1994) 269-286.

M. Elimelech, X. Zhu, A.E. Childress, S. Hong, Role of membrane surface morphology in colloidal fouling of cellulose acetate and composite aromatic polyamide reverse osmosis membranes, Journal of Membrane Science, 127 (1997) 101-109.

R.W. Fox, A.T. McDonald, P.J. Pritchard, Introduction to Fluid Mechanics, 6th ed., John Wiley and Sons, Hoboken, 2004.

B.D. Freeman, Basis of permeability/selectivity tradeoff relations in polymeric gas separation membranes, Macromolecules, 32 (1999) 375-380.

V. Freger, J. Gilron, S. Belfer, TFC polyamide membranes modified by grafting of hydrophilic polymers: an FT-IR/AFM/TEM study, Journal of Membrane Science, 209 (2002) 283-292.

C. Fritzmann, J. Löwenberg, T. Wintgens, T. Melin, State-of-the-art of reverse osmosis desalination, Desalination, 216 (2007) 1-76.

J. Gilron, S. Belfer, P. Vaisanen, M. Nystrom, Effects of surface modification on antifouling and performance properties of reverse osmosis membranes, Desalination, 140 (2001) 167-179.

D.K. Han, K.D. Park, K.-D. Ahn, S.Y. Jeong, Y.H. Kim, Preparation and surface characterization of PEO-grafted and heparin-immobilized polyeurethanes, Journal of Biomedical Materials Research: Applied Biomaterials, 23 (1989) 87-104.

J.M.S. Henis, M.K. Tripodi, Composite hollow fiber membranes for gas separation: the resistance model approach, Journal of Membrane Science, 8 (1981) 233-246.

E.M.V. Hoek, A.S. Kim, M. Elimelech, Influence of crossflow membrane filter geometry and shear rate on colloidal fouling in reverse osmosis and nanofiltration separations, Environmental Engineering Science, 19 (2002) 357-372.

G. Hurwitz, G.R. Guillen, E.M.V. Hoek, Probing polyamide membrane surface charge, zeta potential, wettability, and hydrophilicity with contact angle measurements, Journal of Membrane Science, 349 (2010) 349-357.

J.N. Israelachvili, Intermolecular and Surface Forces, 2nd ed., Academic Press, New York, 1991.

B.-H. Jeong, E.M.V. Hoek, Y. Yan, A. Subramani, X. Huang, G. Hurwitz, A.K. Ghosh, A. Jawor, Interfacial polymerization of thin film nanocomposites: a new concept for reverse osmosis membranes, Journal of Membrane Science, 294 (2007) 1-7.

D. Jiao, M.M. Sharma, Mechanism of cake buildup in crossflow filtration of colloidal suspensions, Journal of Colloid and Interface Science, 162 (1994) 454-462.

G. Kang, M. Liu, B. Lin, Y. Cao, Q. Yuan, A novel method of surface modification on thin-film composite reverse osmosis membrane by grafting poly(ethylene glycol), Polymer, 48 (2007) 1165-1170.

H.J. Kaper, H.J. Busscher, W. Norde, Characterization of poly(ethylene oxide) brushes on glass surfaces and adhesion of Staphylococcus epidermidis, Journal of Biomaterials Science Polymer Edition, 14 (2003) 313-324.

S. Kim, H. Ozaki, J. Kim, Effect of pH on the rejection of inorganic salts and organic compound using nanofiltration membrane, Korean Journal of Chemical Engineering, 23 (2006) 28-33.

P. Kingshott, H. Thissen, H.J. Griesser, Effects of cloud-point grafting, chain length, and density of PEG layers on competitive adsorption of ocular proteins, Biomaterials, 23 (2002) 2043-2056.

T. Koerner, H. Slebocka-Tilk, R.S. Brown, Experimental investigation of the primary and secondary deuterium kinetic isotope effects for epoxidation of alkenes and ethylene with m-chloroperoxybenzoic acid, Journal of Organic Chemistry, 64 (1999) 196-201.

W.J. Koros, G.K. Fleming, S.M. Jordan, T.H. Kim, H.H. Hoehn, Polymeric membrane materials for solution-diffusion based permeation separations, Progress in Polymer Science, 13 (1988) 339-401.

M.J. Kotelyanskii, N.J. Wagner, M.E. Paulaitis, Atomistic simulation of water and salt transport in the reverse osmosis membrane FT-30, Journal of Membrane Science, 139 (1998) 1-16.

R.A. Kudva, H. Keskkula, D.R. Paul, Compatibilization of nylon 6/ABS blends using glycidyl methacrylate/methyl methacrylate copolymers, Polymer, 39 (1998) 2447-2460.

A. Kulkarni, D. Mukherjee, W.N. Gill, Flux enhancement by hydrophilization of thin film composite reverse osmosis membranes, Journal of Membrane Science, 114 (1996) 39-50.

S.-Y. Kwak, S.G. Jung, Y.S. Yoon, D.W. Ihm, Details of surface features in aromatic polyamide reverse osmosis membranes characterized by scanning electron and atomic force microscopy, Journal of Polymer Science: Part B: Polymer Physics, 37 (1999) 1429-1440.

R.E. Larson, J.E. Cadotte, R.J. Petersen, Development of the FT-30 thin-film composite membrane for seawater desalting applications, NWSIA Journal, 8 (1981) 15-25.

R.G. Larson, T.J. Rehg, Spin Coating, in Liquid Film Coating: Scientific Principles and Their Technological Implications, S.F. Kistler, P.M. Schweizer (Eds.), Chapman & Hall, London, 1997.

D. Leckband, S. Sheth, A. Halperin, Grafted poly(ethylene oxide) brushes as nonfouling surface coatings, Journal of Biomaterials Science Polymer Edition, 10 (1999) 1125-1147.

J.H. Lee, H.B. Lee, J.D. Andrade, Blood compatibility of polyethylene oxide surfaces, Progress in Polymer Science, 20 (1995) 1043-1079.

S. Loeb, S. Sourirajan, Sea water demineralization by means of an osmotic membrane, in Advances in Chemistry Series, 38th ed., American Chemical Society, 1963, pp. 117-132.

J.S. Louie, I. Pinnau, I. Ciobanu, K.P. Ishida, A. Ng, M. Reinhard, Effects of polyether-polyamide block copolymer coating on performance and fouling of reverse osmosis membranes, Journal of Membrane Science, 280 (2006) 762-770.

U. Merten, H.K. Lonsdale, R.L. Riley, Boundary-layer effects in reverse osmosis, I & EC Fundamentals, 3 (1964) 210-213.

W.E. Mickols, Composite Membrane with Polyalkylene Oxide Modified Polyamide Surface, U.S. Patent 6,280,853 B1, 2001.

W.E. Mickols, Dow Water & Process Solutions, personal communication, 2008.

D. Mukherjee, A. Kulkarni, W.N. Gill, Chemical treatment for improved performance of reverse osmosis membranes, Desalination, 104 (1996) 239-249.

Nitto Denko Hydranautics CPA 2 Product Specification, http://www.membranes.com/docs/8inch/CPA2.pdf.

Nitto Denko Hydranautics ESPA 1 Product Specification, http://www.membranes.com/docs/8inch/ESPA1.pdf.

Nitto Denko Hydranautics ESPA 3 Product Specification, http://www.membranes.com/docs/8inch/ESPA3.pdf.

E. Ostuni, R.G. Chapman, R.E. Holmlin, S. Takayama, G.M. Whitesides, A survey of structure-property relationships of surfaces that resist the adsorption of protein, Langmuir, 17 (2001) 5605-5620.

Y.S. Park, J. Won, Y.S. Kang, Preparation of poly(ethylene glycol) brushes on polysulfone membranes for olefin/paraffin separation, Langmuir, 16 (2000) 9662-9665.

R.E. Parker, N.S. Isaacs, Mechanisms of epoxide reactions, Chemical Reviews, 59 (1959) 737-799.

D.R. Paul, Reformulation of the solution-diffusion theory of reverse osmosis, Journal of Membrane Science, 241 (2004) 371-386.

G. Pearce, S. Talo, K. Chida, A. Basha, A. Gulamhusein, Pretreatment options for large scale SWRO plants: case studies of UF trials at Kindasa, Saudi Arabia, and conventional pretreatment in Spain, Desalination, 167 (2004) 175-189.

R.J. Petersen, Composite reverse osmosis and nanofiltration membranes, Journal of Membrane Science, 83 (1993) 81-150.

R.F. Probstein, Physicochemical Hydrodynamics: An Introduction, 2nd ed., John Wiley & Sons, Inc., New York, 1994.

R. Rautenbach, R. Albrecht, Membrane Processes, John Wiley & Sons Ltd., West Sussex, 1989.

C.E. Reid, E.J. Breton, Water and ion flow across cellulosic membranes, Journal of Applied Polymer Science, 1 (1959) 133-143.

Review of the Desalination and Water Purification Technology Roadmap, The National Academies Press, Washington, D.C., 2005.

L.M. Robeson, Correlation of separation factor versus permeability for polymeric membranes, Journal of Membrane Science, 62 (1991) 165-185.

B.J. Rudie, T.A. Torgrimson, D.D. Spatz, Reverse-osmosis and ultrafiltration membrane compaction and fouling studies using ultrafiltration pretreatment, in Reverse Osmosis and Ultrafiltration, S. Sourirajan, T. Matsuura (Eds.), ACS Symposium Series, 281st ed., American Chemical Society, 1985, pp. 403-414.

A.C. Sagle, E.M. Van Wagner, H. Ju, B.D. McCloskey, B.D. Freeman, M.M. Sharma, PEG-coated reverse osmosis membranes: desalination properties and fouling resistance, Journal of Membrane Science, 340 (2009) 92-108.

R.F. Service, Desalination freshens up, Science, 313 (2006) 1088-1090.

T.K. Sherwood, P.L.T. Brian, R.E. Fisher, L. Dresner, Salt concentration at phase boundaries in desalination by reverse osmosis, I & EC Fundamentals, 4 (1965) 113-118.

V.L. Snoeyink, D. Jenkins, Water Chemistry, John Wiley & Sons, New York, 1980.

W. Stumm, Chemistry of the Solid-Water Interface: Processes at the Mineral-Water and Particle-Water Interface in Natural Systems, John Wiley & Sons, Inc., New York, 1992.

I. Sutzkover, D. Hasson, R. Semiat, Simple technique for measuring the concentration polarization level in a reverse osmosis system, Desalination, 131 (2000) 117-127.

C.Y. Tang, Y.-N. Kwon, J.O. Leckie, Fouling of reverse osmosis and nanofiltration membranes by humic acid - effects of solution composition and hydrodynamic conditions, Journal of Membrane Science, 290 (2007) 86-94.

E.M. Van Wagner, A.C. Sagle, M.M. Sharma, B.D. Freeman, Effect of crossflow testing conditions, including feed pH and continuous feed filtration, on commercial reverse osmosis membrane performance, Journal of Membrane Science, 345 (2009) 97-109.

J.A. Veil, M.G. Puder, D. Elcock, R.J. Redweik, A White Paper Describing Produced Water from Production of Crude Oil, Natural Gas, and Coal Bed Methane, Contract No. W-31-109-Eng-38; U.S. Department of Energy National Energy Technology Laboratory, Argonne National Laboratory, 2004.

D. Vial, G. Doussau, The use of microfiltration membranes for seawater pre-treatment prior to reverse osmosis membranes, Desalination, 153 (2002) 141-147.

E.M. Vrijenhoek, S. Hong, M. Elimelech, Influence of membrane surface properties on initial rate of colloidal fouling of reverse osmosis and nanofiltration membranes, Journal of Membrane Science, 188 (2001) 115-128.

L.G. Wade, Organic Chemistry, 4th ed., Prentice-Hall, Inc., Upper Saddle River, New Jersey, 1999.

F. Wang, V.V. Tarabara, Pore blocking mechanisms during early stages of membrane fouling by colloids, Journal of Colloid and Interface Science, 328 (2008) 464-469.

J.D. White, R.W. Skeean, G.L. Trammell, Lewis acid and photochemically mediated cyclization of olefinic beta-keto esters, Journal of Organic Chemistry, 50 (1985) 1939-1948.

D.-Y. Wi, I.W. Kim, J. Kim, Water repellent cotton fabrics prepared by PTFE RF sputtering, Fibers and Polymers, 10 (2009) 98-101.

J.G. Wijmans, R.W. Baker, The solution-diffusion model: a review, Journal of Membrane Science, 107 (1995) 1-21.

M.C. Wilbert, J. Pellegrino, A. Zydney, Bench-scale testing of surfactant-modified reverse osmosis/nanofiltration membranes, Desalination, 115 (1998) 15-32.

H. Yasuda, C.E. Lamaze, A. Schindler, Salt rejection by polymer membranes in reverse osmosis. II. ionic polymers, Journal of Polymer Science: Part A-2, 9 (1971) 1579-1590.

G.E. Zaikov, A.L. Iordanskii, V.S. Markin, Diffusion of Electrolytes in Polymers, VSP BV, Utrecht, 1988.

B. Zdyrko, V. Klep, I. Luzinov, Synthesis and surface morphology of high-density poly(ethylene glycol) grafted layers, Langmuir, 19 (2003) 10179-10187.

B. Zdyrko, S.K. Varshney, I. Luzinov, Effect of molecular weight on synthesis and surface morphology of high-density poly(ethylene glycol) grafted layers, Langmuir, 20 (2004) 6727-6735.

X. Zhu, M. Elimelech, Colloidal fouling of reverse osmosis membranes: measurements and fouling mechanisms, Environmental Science and Technology, 31 (1997) 3654-3662.

This page is intentionally left blank

DISTRIBUTION

Internal (Electronic Copy)

1	MS–0899	Technical Library, 9536
1	MS-0763	LDRD Office, 1911
1	MS–0735	J. Merson, 6730
1	MS-0754	M. Rigali, 6736
1	MS-0754	S. Altman, 6736
1	MS-0888	M. Hibbs, 6364
1	MS-0734	J. B. Kelley, 6375
1	MS-0734	E. Stechel, 6360
1	MS-0359	Y. Moreno, 1912

External (Electronic Copy)

Elizabeth M. Van Wagner
Department of Chemical Engineering
Center for Energy and Environmental Resources
University of Texas at Austin
elizavw@che.utexas.edu

Benny Freeman
Department of Chemical Engineering
Center for Energy and Environmental Resources
University of Texas at Austin
freeman@che.utexas.edu

Mukul M. Sharma
Department of Petroleum & Geosystems
Engineering, The University of Texas at Austin,
Austin, TX 78712
msharma@mail.utexas.edu

Michael A. Hickner
Department of Materials Science and Engineering
The Pennsylvania State University
hickner@matse.psu.edu

Sandia National Laboratories